# DEVELOPMENT OF THE COMBINED LOADING SHEAR TEST METHOD AND SHEAR STRAIN MEASUREMENT IN THE V-NOTCHED RAIL SHEAR TEST

by

Darren James Litz

A thesis submitted to the faculty of
The University of Utah
in partial fulfillment of the requirements for the degree of

Master of Science

Department of Mechanical Engineering

The University of Utah

December 2012

**The University of Utah Graduate School**

# STATEMENT OF THESIS APPROVAL

The thesis of **Darren James Litz**

has been approved by the following supervisory committee members:

| | | |
|---|---|---|
| **Daniel O. Adams** | , Chair | **1/3/2012** Date Approved |
| **Kenneth L. Devries** | , Member | **1/3/2012** Date Approved |
| **Rebecca M. Brannon** | , Member | **1/12/2012** Date Approved |

and by **Timothy A. Ameel** , Chair of the Department of **Mechanical Engineering**

and by Charles A. Wight, Dean of The Graduate School.

# ABSTRACT

Unique constraints are present when shear properties of orthotropic materials are desired, as they typically cannot be derived from tensile material properties like isotropic materials. Specific test specimen geometry, and in some instances specimen layup, are required in order to obtain valid shear property data. The V-Notched Rail Shear Test Method is one such test method developed to provide reliable shear test data for composite laminates. However, specimens made from suitably high strength materials will slip prior to failure providing invalid results. Previous work has been performed which improves on this test method by altering the specimen dimensions and fixture design in order to prevent slipping. Changes made to the fixture introduced another load path into the specimen, which can influence the stress state within the specimen. The current work looks at several aspects of the new Combined Loading Shear test fixture and how they affect the stress and strain state, as well as the measured shear strength. Photoelastic testing is performed to validate numerical models and to investigate the strain state in several different specimen layups as a result of the fixture changes.

Accurate shear strain measurement is required when determining the shear modulus of a material. Bonded strain gauges are often used when strain measurements are required; however, extensometers can provide the same functionality as strain gauges and have the advantage of being reusable. Extensometers are typically application specific and require careful consideration with regards to attachment and the region where extension is measured. The current study proposes a shear extensometer for a V-Notched Rail

Shear or Combined Loading Shear test specimen. A mechanics of materials model is used to calculate the shear strain in the specimen based on the relative displacement of a discrete set of points on the specimen face. Numerical simulations were performed to determine the points on the specimen face which would yield the most accurate measure of the in-plane shear modulus. A prototype device is tested using carbon/epoxy, glass/epoxy, and Kevlar/epoxy cross-ply laminates and the data from the extensometer are compared to data from bonded strain gauges to validate the extensometer.

# CONTENTS

ABSTRACT ..... iii

LIST OF TABLES ..... vii

1 THE V-NOTCHED COMBINED LOADING SHEAR TEST FOR FIBER REINFORCED COMPOSITE LAMINATES ..... 1

1.1 Introduction ..... 1
1.2 Numerical Modeling ..... 5
1.3 Numerical Results ..... 13
1.4 Mechanical Testing ..... 29
1.5 Results ..... 34
1.6 Conclusion ..... 57

2 DESIGN AND VALIDATION OF A SHEAR EXTENSOMETER FOR CROSS-PLY LAMINATES TESTED USING THE V-NOTCHED RAIL SHEAR TEST ..... 60

2.1 Introduction ..... 60
2.2 Analysis ..... 63
2.3 Mechanical Testing ..... 81
2.4 Conclusions ..... 94

3 DETERMINATION OF CLAMPING FORCES IN THE V-NOTCHED RAIL SHEAR AND V-NOTCHED COMBINED LOADING SHEAR TEST FIXTURES 96

3.1 Introduction ..... 96
3.2 Load Cell Design and Fabrication ..... 97
3.3 Calibration and Testing ..... 101
3.4 Conclusions ..... 108

4 THESIS CONCLUSIONS ..... 110

APPENDICES

A. PHOTOELASTIC RESULTS FROM THE V-NOTCHED RAIL SHEAR TEST ..... 113

B. COMBINED LOADING SHEAR FIXTURE DRAWINGS ..... 118

C. SHEAR STRAIN EXTENSOMETER DRAWINGS ..... 121

REFERENCES ..... 125

LIST OF TABLES

Table Page
1 Specimen material properties used in the numerical simulations. ..... 9

2 Specimen edge contact lengths used in the numerical study and depicted in Figure 9. 12

3 Loads at which the isochromatic and isoclinic contours were photographed for each laminate. ..... 33

4 Measured ultimate shear strength values for cross-ply laminates made from IM7/8552 pre-preg. ..... 36

5 Measured ultimate shear strength values for quasi-isotropic laminates made from IM7/8552 pre-preg. ..... 39

6 Measured ultimate shear strength values for $[\pm 45]_{ns}$ laminates made from IM7/8552 pre-preg. ..... 42

7 Maximum failure loads found using the Combined Loading Shear test fixture. ..... 42

8 Average measured ultimate shear strength of a $[0/90]_{4S}$ IM7/8552 carbon epoxy laminate. ..... 44

9 Numerical results showing the shear modulus supplied to the simulation, $G_{xy,Input}$, and the shear modulus calculated from Equation (7), $G_{xy,Calc}$ [10]. ..... 66

10 Lamina properties used in calculating the material properties of a $[0/90]_{ns}$ laminate. 71

11 Laminate properties for a $[0/90]_{ns}$ laminate used in the numerical simulations. ..... 72

12 Material properties of some common fiber/epoxy laminates and isotropic materials used in the numerical model. ..... 73

13 Measured extensometer point separation lengths. ..... 84

14 Shear modulus results for the IM7/8552 cross-ply laminate. ..... 89

15 Shear modulus results for the Kevlar/AR251 cross-ply laminates. ..... 90

16 Shear modulus results for the Glass/AF254 cross-ply laminates..... 91

17 Results showing the applied normal force, P, of a bolt for a given applied torque, T. ..... 107

# 1 THE V-NOTCHED COMBINED LOADING SHEAR TEST FOR FIBER REINFORCED COMPOSITE LAMINATES

## 1.1 Introduction

Methods for determining the shear strength of isotropic materials have been around for quite some time. Their testing procedures and specimen geometries are relatively simple when compared to procedures and geometries for fiber reinforced composite materials. Composites, by comparison, are capable of obtaining much higher shear strengths than metals which makes quantifying the strength of these materials difficult. Shear testing of composite materials poses a unique set of constraints when accurate material properties, namely the shear modulus and shear strength, are required. Many different shear testing method have been developed, often with a specific industry in mind. A general overview on the history of shear testing for composite laminates can be found in [1].

Currently, the most popular shear tests for composite laminates standardized by the American Society for Testing and Methods (ASTM) are the V-Notched Beam shear (D 5379) [2], which uses a 76 mm (3.0 in.) by 19 mm (0.75 in.) rectangular, center notched, specimen that is edge loaded in an asymmetric 4 point bend test (Figure 1), and the V-Notched Rail Shear test (D 7078) [3], which uses a larger 76 mm (3.0 in.) by 56 mm (2.2 in.) rectangular, center notched, specimen that is shear loaded through the specimen face (Figure 2). Both test methods provide reliable shear modulus and shear

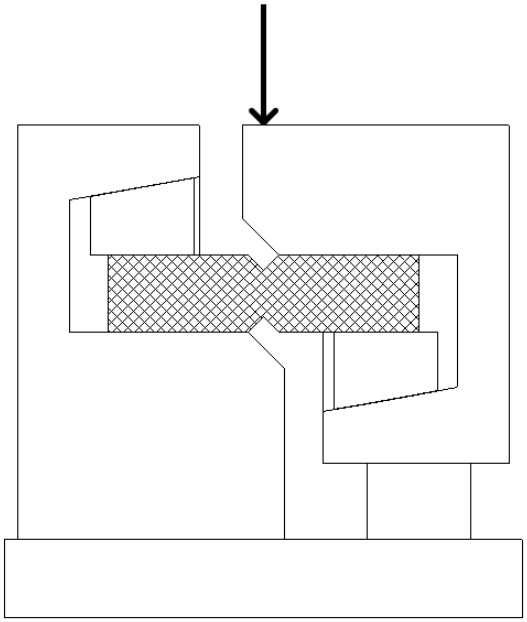

Figure 1: ASTM D 5379 test fixture and specimen.

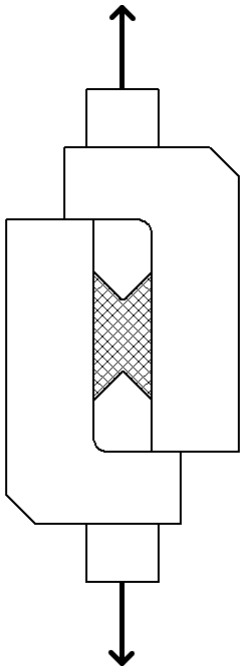

Figure 2: ASTM D 7078 test fixture and specimen.

strength measurements, however, both have limitations.

Due to its small test region, the V-Notched Beam Shear test is not well suited for woven fiber composites with coarse architectures. Specimens with large unit cells make results obtained using this test method questionable. High strength laminates also present problems as these specimens are susceptible to crushing at the inner loading points of the fixture before a gauge section failure occurs [4]. The V-Notched Rail Shear test was, in part, designed to overcome the limitations of the V-Notched Beam Shear test. In comparison to the V-Notched Beam Shear, the gauge section of the V-Notched Rail Shear test section is almost three times larger, which is beneficial when testing woven laminates with coarse fiber architecture. The rail shear fixture is also capable of testing laminates with much higher shear strengths than is possible with the V-Notched Beam Shear test method.

While the loading capabilities of the V-Notched Rail Shear test method is significantly improved over the V-Notched Beam Shear test method, the specimens can slip in the fixture before failure occurs [5]. In order to prevent the specimen from slipping more torque is usually applied to the fixture's clamping bolts, thereby increasing the normal force on the specimen face and the amount of force required for the specimen to slip. In some instances the amount of torque applied to the fixture's clamping bolts has caused permanent damage to the fixture. In other cases it will introduce a high stress in the area of the gauge section adjacent to the grips, which can cause a premature failure of the specimen, and invalidate the results of the test.

Work has been performed which combined the edge loading capability of the V-Notched Beam Shear method with the face loading and larger specimen geometry of the

V-Notched Rail Shear method in order to overcome the load limitations of both fixtures [5]. The components of a general Combined Loading Shear fixture are shown in Figure 3. This new fixture, which included an adjustable edge loader in addition to face loading grips, also utilized a larger specimen at 127 mm (5.0 in.) by 56 mm (2.2 in.), with the same notch dimensions as the V-Notched Rail Shear specimen. Shear strengths obtained using this new fixture were comparable to those obtained with the V-Notched Rail Shear fixture, and the loading capability of the Combined Loading Shear fixture was vastly improved over the V-Notched Rail Shear fixture. The current study looks at certain aspects of the fixture's design. A combination of numerical modeling and mechanical testing are performed to evaluate the effect of these changes and to ensure that results obtained using the new fixture design are comparable to those in the literature. The state of strain in the specimen gauge section is also investigated through photoelastic techniques using both

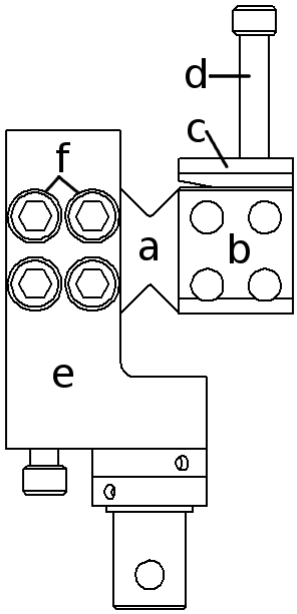


Figure 3: Depiction of the major components of a Combined Loading Shear fixture: specimen (a), face loader (b), edge loader (c), edge loader bolt (d), fixture half (e), face loader bolts (f). The right fixture half was omitted for clarity.

the proposed new fixture and the V-Notched Rail Shear fixture to verify that a desirable strain state is obtained.

## 1.2 Numerical Modeling

### 1.2.1 Introduction

Work performed by Abdallah and Gascoigne has shown that fixture design can significantly influence the state of strain in the specimen of edge loaded tests [6]. Because of this the influence of the edge loaders in Johnson's Combined Loading Shear fixture [5] are investigated here using the finite element method. Several finite element models were built to investigate different aspects of the proposed fixture design. The elements specifically investigated in this study include: the stress state in the gauge section as a result of changing the length of contact between the edge loaders and verification of the numerical model by emulating results obtainable through photoelasticity. The fixture that served as a basis for the solid models used in the numerical studies is shown in Figure 4 and Figure 5. The solid models were built in SolidWorks then imported into ANSYS Workbench 11.0. Where possible, the models utilized symmetry. The bolts used to apply loads to the face loaders, as well as their accommodating holes in the fixture halves were omitted to simplify the model. Drawings of the solid model used in numerical modeling are shown in Figure 6 and Figure 7. Previous work has shown that when modeling the stress state in the gauge section of the specimen an element size of 1.016 mm [0.040 in.] shows adequate refinement and convergence with regards to the maximum shear stress [5]. As such, the same element size and mesh refinement techniques used in [5] were also employed in these studies.

Four different material property sets representing two material systems were mod-

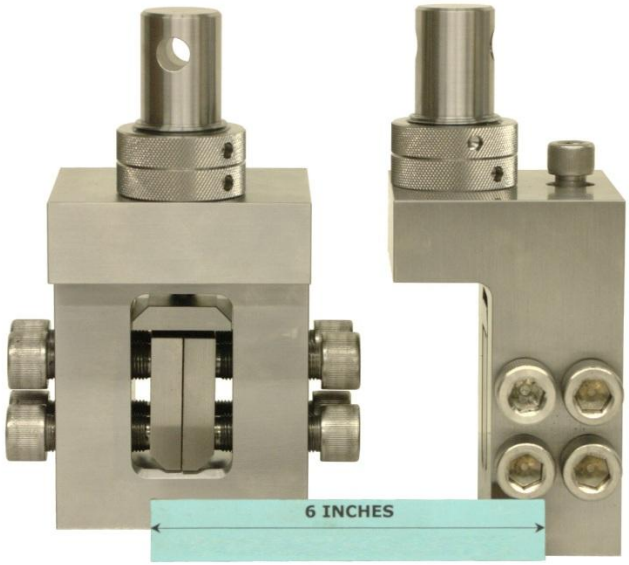


Figure 4: Side and front views of the Combined Loading Shear Fixture.


Figure 5: Front view of a fully assembled Combined Loading Shear test fixture.

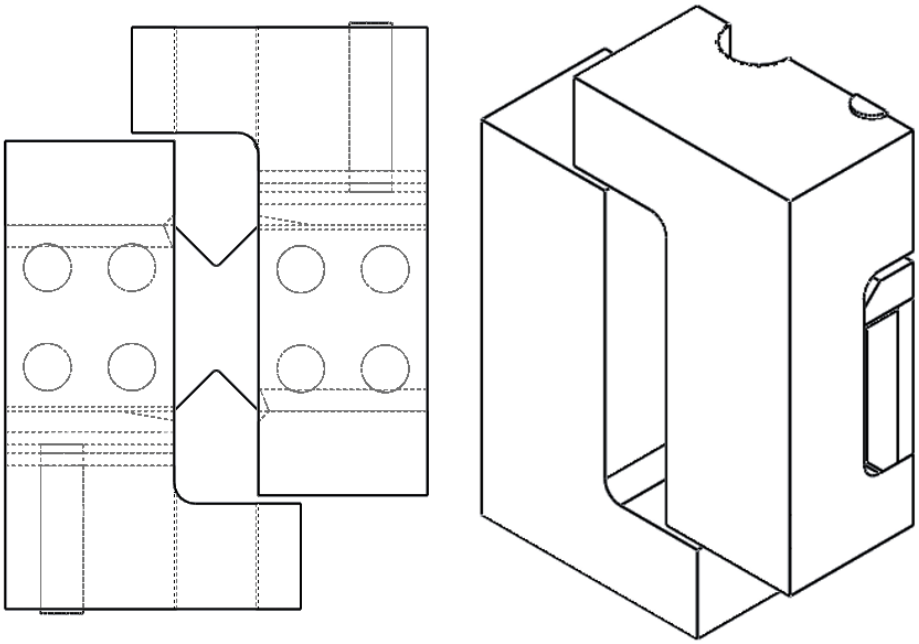

Figure 6: Depiction of the solid model used in the numerical simulations. Left: Front view of the fixture and test specimen with hidden edges shown. Right: Isometric view of the fixture.

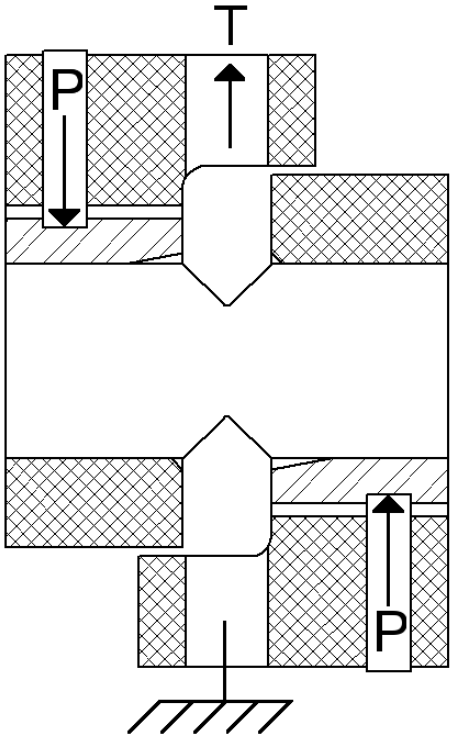


Figure 7: The back face of the solid model indicating the loads applied to the edge loaders (P), and the test load (T).

eled for the specimen geometry: an isotropic 6061 aluminum, and an IM7/8552 carbon epoxy system representative of a cross-ply $[0/90]_{ns}$, a quasi-isotropic $[0/\pm45/90]_{ns}$, and a $[\pm45]_{ns}$ laminate. All other constituents of the fixture were modeled using the properties of steel. The material properties are listed in Table 1. Each simulation utilized frictional contact between the specimen and the face loaders. Frictionless contact was applied between the specimen edges and the fixture. A no separation boundary condition was used for contact between the edge loaders and the fixture body. The contact between the edge loaders and the bolt were modeled as bonded. The edge loader bolt was modeled as bonded to the fixture body.

Three load steps were used: the first applied the clamping loads to the face loaders, the second applied the force to the edge loaders, and the third applied the tensile load to the fixture/specimen assembly. The loads applied to each clamping bolts were 33.36 kN (7.50 kip). This value was chosen based on the experiments performed in Section 0. The tensile load applied to the upper fixture was the value that would result in an average shear strain of 6 mε using the following equation:

$$T = G_{xy} \cdot \gamma \cdot t \cdot h \tag{1}$$

where $\gamma = 0.006$, $t$ is the specimen thickness, $h$ is the distance between the notches (31.53 mm (1.241 in.)), and $G_{xy}$ comes from Table 1. The in-plane shear and normal stress on the free surface of the specimen in each simulation were exported to a text file. A MATLAB program was written to read in the data and normalize the stresses to the average shear stress in the specimen, defined as:

Table 1: Specimen material properties used in the numerical simulations.

| Material | Layup | $E_x$ | | $E_y$ | | $E_z$ | | $G_{xy}$ | | $G_{xz}$ | | $G_{yz}$ | | $\nu_{xy}$ | $\nu_{xz}$ | $\nu_{yz}$ |
|---|---|---|---|---|---|---|---|---|---|---|---|---|---|---|---|---|
| | | [GPa] | [Msi] | [GPa] | [Msi] | [GPa] | [Msi] | [GPa] | [Msi] | [GPa] | [Msi] | [GPa] | [Msi] | | | |
| IM7/8552 | $[0/90]_{ns}$ | 88.3 | 12.80 | 88.3 | 12.80 | 13.5 | 1.960 | 4.96 | 0.719 | 4.21 | 0.611 | 4.21 | 0.611 | 0.041 | 0.410 | 0.410 |
| | $[\pm45]_{ns}$ | 17.9 | 2.601 | 17.9 | 2.601 | 13.5 | 1.960 | 42.40 | 6.150 | 4.21 | 0.611 | 4.21 | 0.611 | 0.810 | 0.080 | 0.080 |
| | $[0/\pm45/90]_{ns}$ | 62.6 | 9.079 | 62.6 | 9.079 | 13.5 | 1.960 | 23.72 | 3.440 | 4.21 | 0.611 | 4.21 | 0.611 | 0.320 | 0.290 | 0.290 |
| Al 6061 | | | 68.90 | | | | 9.993 | | 25.90 | | | | 3.757 | | 0.330 | |
| Steel | | | 200 | | | | 29.00 | | 75.19 | | | | 11.15 | | 0.300 | |

* Value was derived based on isotropic material properties and was not supplied to the model.

$$\tau_{avg} = \frac{T}{t \cdot h} \tag{2}$$

where *T*, *t*, and *h* are the same values used in Equation (2). Contour plots of the normalized data were then created in Grapher 8.0.

### 1.2.2 Edge Loader Length Variation

In the numerical work performed in [5] the fixture was initially in contact with the entire top and bottom edges of the gripped region of the specimen. It is proposed that by adjusting the length of contact between these two entities a more desirable stress state can be obtained. It has also been shown by Adams and Walrath that the inner loading points in an asymmetrical beam shear specimen can produce undesirable normal stresses that intrude into the gauge section [4,7]. Additionally, V-notched beam shear specimens have been known to crush at the inner loading points during testing [4]. Looking at Figure 8 it can be seen why these phenomena occur. The loads acting at a distance *a*/2 from the cen-

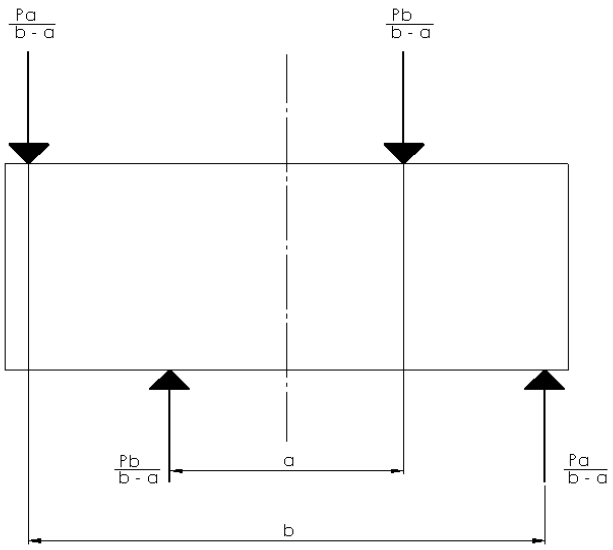


Figure 8: Depiction of a four-point asymmetrical bend test setup.

terline are higher in magnitude than those acting at a distance $b/2$ from the centerline. Increasing $b$, or decreasing $a$, results in an increase in load at the inner loading points, which in turn, increases the likelihood of the specimen crushing at the point of load application, and normal stresses increasing their presence in the gauge section. In order to overcome this in the V-notched beam shear method, the loading points were moved further away from the specimen centerline. It is believed that the same benefit could be realized by moving the inner loading point in the Combined Loading Shear test away from the gauge section. However, moving the contact point too far would likely decrease the fixture's ability to prevent the specimen from slipping. Four edge loading configurations were studied. A generic diagram of the configuration of the edge loaders is shown in Figure 9 and the values used for the contact lengths A and B are listed in Table 2.

Previous numerical work has also shown that thicker specimen geometries result in a less desirable stress state than thinner geometries [5]. For this reason only a relatively thick specimen (12.7 mm (0.50 in.)) was modeled in this study. Additionally, no edge load was applied. This is representative of tightening the bolt until the edge loader just makes contact with the specimen edge. For each model and laminate the specimen free-surface in-plane shear and normal stresses are presented in Section 1.3.1.

### 1.2.3 Verification of Numerical Model

In Section 1.5.2.3 three different layups were tested using photoelastic techniques. In order to verify the numerical results presented in this study models were built using the specimen thickness of the $[0/90]_{4S}$, $[\pm45]_{5S}$, and $[0/\pm45/90]_{4S}$ laminates used in Section 1.5.2.3. Each model utilized the edge load lengths of Model 3 listed in Table 2. The edge loaders in these numerical simulations were modeled as if no torque was applied to the

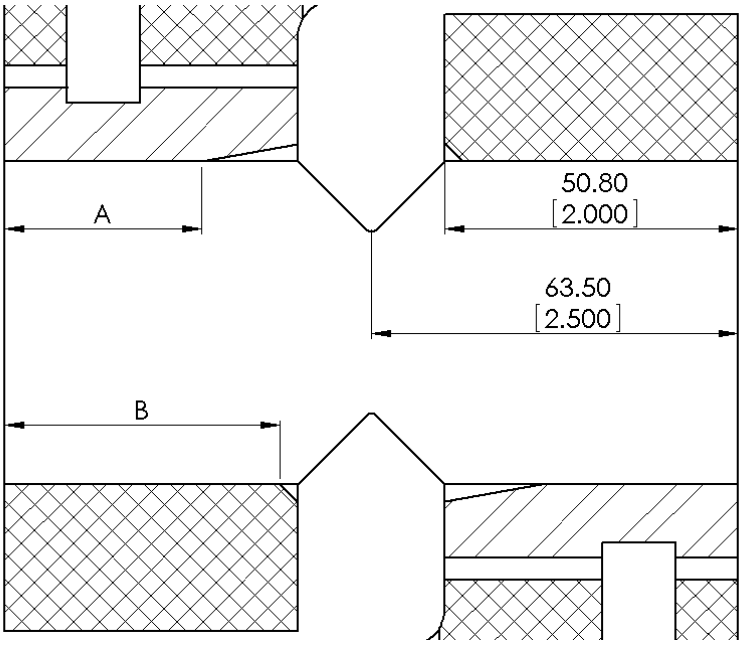


Figure 9: Diagram of the edge loader dimensions that were varied. The non-hatched region is the specimen, hatched region is the edge loaders, and the cross hatched region is the fixture. Dimensions are in mm [in.].

Table 2: Specimen edge contact lengths used in the numerical study and depicted in Figure 9.

| Model | A | | B | |
|---|---|---|---|---|
| | [mm] | [in.] | [mm] | [in.] |
| 1 | 50.80 | 2.000 | 50.80 | 2.000 |
| 2 | 50.80 | 2.000 | 47.63 | 1.875 |
| 3 | 34.11 | 1.343 | 47.63 | 1.875 |
| 4 | 25.40 | 1.000 | 47.63 | 1.875 |

edge loader bolts. The photoelastic testing measured the difference in the magnitudes of the principal strains as well as the area in which the principal strains were oriented at 45°. In each model the in-plane strains, $\varepsilon_x$, $\varepsilon_y$, and $\gamma_{xy}$, on the specimen free surface were exported to text files then manipulated in MATLAB to determine the maximum shear strain, $\gamma_{max} = \varepsilon_1 - \varepsilon_2$, and principal direction at each node. The principal strain can be determined by solving the Eigen value problem

$$|\boldsymbol{\varepsilon} - \lambda \boldsymbol{I}| = 0 \tag{3}$$

where $\boldsymbol{\varepsilon}$ is the 2D strain tensor:

$$\boldsymbol{\varepsilon} = \begin{bmatrix} \varepsilon_x & \frac{\gamma_{xy}}{2} \\ \frac{\gamma_{xy}}{2} & \varepsilon_y \end{bmatrix} \tag{4}$$

$\lambda$ is the Eigen values for the system, and $\boldsymbol{I}$ is the 2x2 identity matrix. The solution to Equation (3), along with the principal directions, were calculated using a built in MATLAB function. The nodal values were output to a text file and contour plots of $\gamma_{max}$ and the 45° principal strain were created using Grapher 8.0.

The results of this section are deferred until Section 1.5.2.3 in order to expedite a direct comparison with experimental results.

## 1.3 Numerical Results

### 1.3.1 Edge Loader Length Variation

In this section the in-plane shear stress, axial normal stress, and transverse normal stress contours are shown for each edge length configuration listed in Table 2. The axial direction is taken to be coincident with the direction of the applied load while the trans-

verse direction is perpendicular. Each stress contour is normalized by the average shear stress defined by Equation (2). For an ideal case, the test region of the specimen should have a normalized shear stress value of 1 while both the normalized axial and transverse normal stress should have a value of 0.

#### 1.3.1.1 Model 1 Results

The normalized in-plane shear, transverse normal and axial normal stress contours for the first edge loader configuration listed in Table 2 are depicted in Figure 10 - Figure 12. The cross-ply results are shown in Figure 10, the quasi-isotropic in Figure 11, and the $[\pm 45]_{ns}$ in Figure 12.

#### 1.3.1.2 Model 2 Results

The in-plane shear, transverse normal and axial normal stress contours, normalized to the average shear stress, for the second edge loader configuration listed in Table 2 are depicted in Figure 13 - Figure 15. The cross-ply results are shown in Figure 13, the quasi-isotropic in Figure 14, and the $[\pm 45]_{ns}$ in Figure 15.

#### 1.3.1.3 Model 3 Results

The in-plane shear, transverse normal and axial normal stress contours, normalized to the average shear stress, for the third edge loader configuration listed in Table 2 are depicted in Figure 16 - Figure 18. The cross-ply results are shown in Figure 16, the quasi-isotropic in Figure 17, and the $[\pm 45]_{ns}$ in Figure 18.

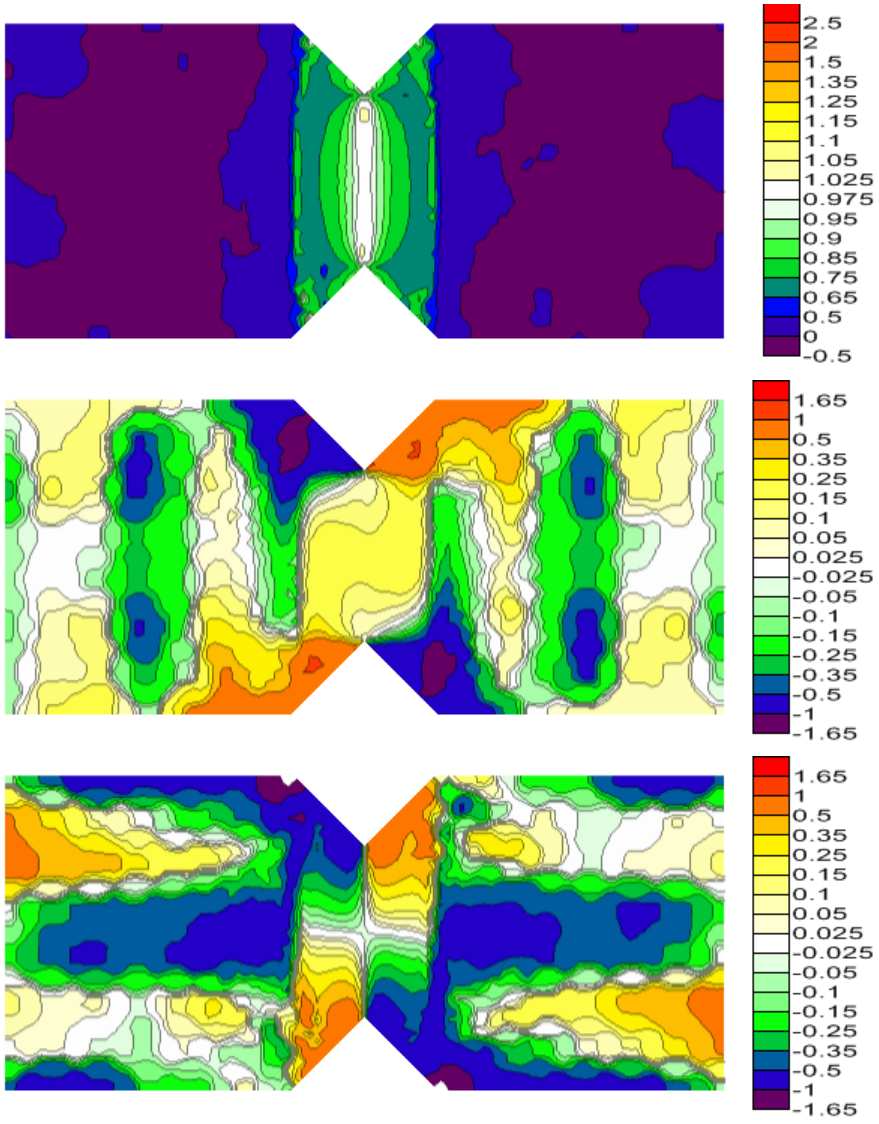


Figure 10: Normalized shear (top), transverse normal (middle), and axial normal (bottom) stress contours for a $[0/90]_{ns}$ laminate and the edge loading lengths for Model 1 in Table 2.

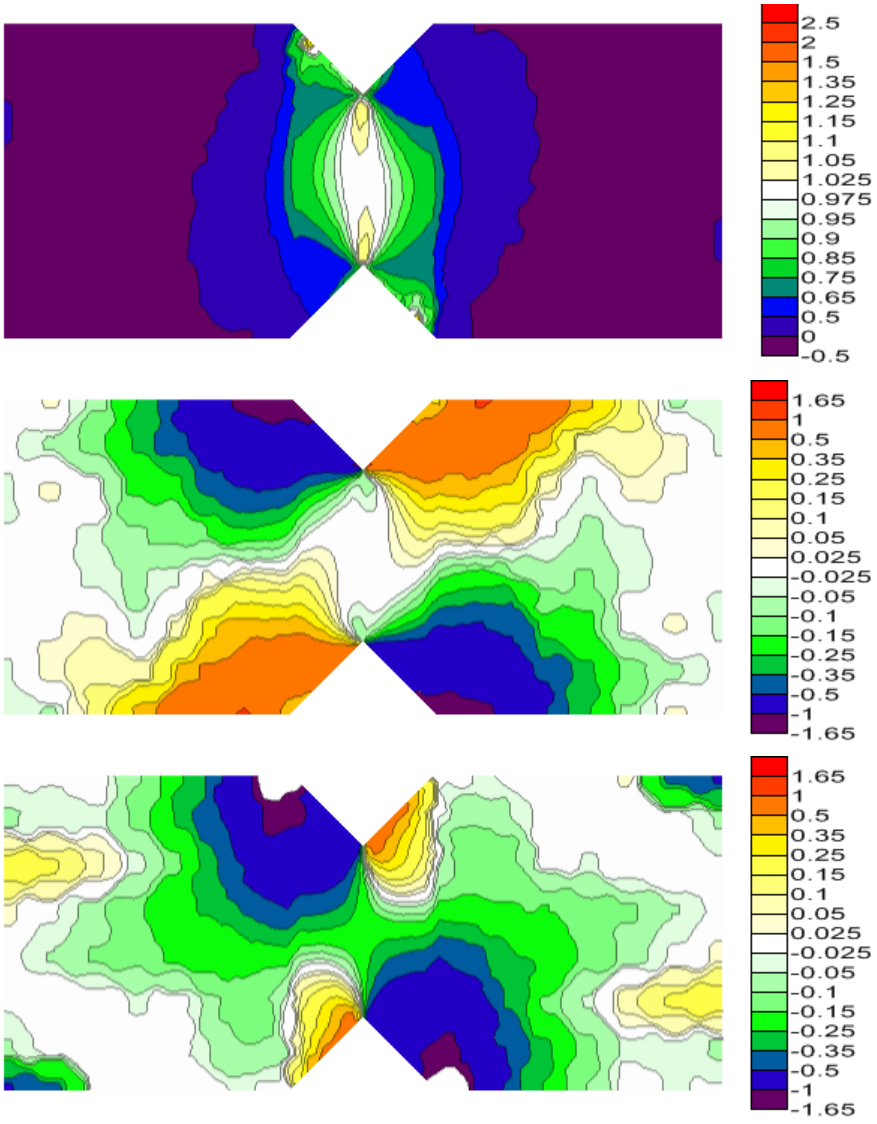


Figure 11: Normalized shear (top), transverse normal (middle), and axial normal (bottom) stress contours for a $[0/\pm45/90]_{ns}$ laminate and the edge loading lengths for Model 1 in Table 2.

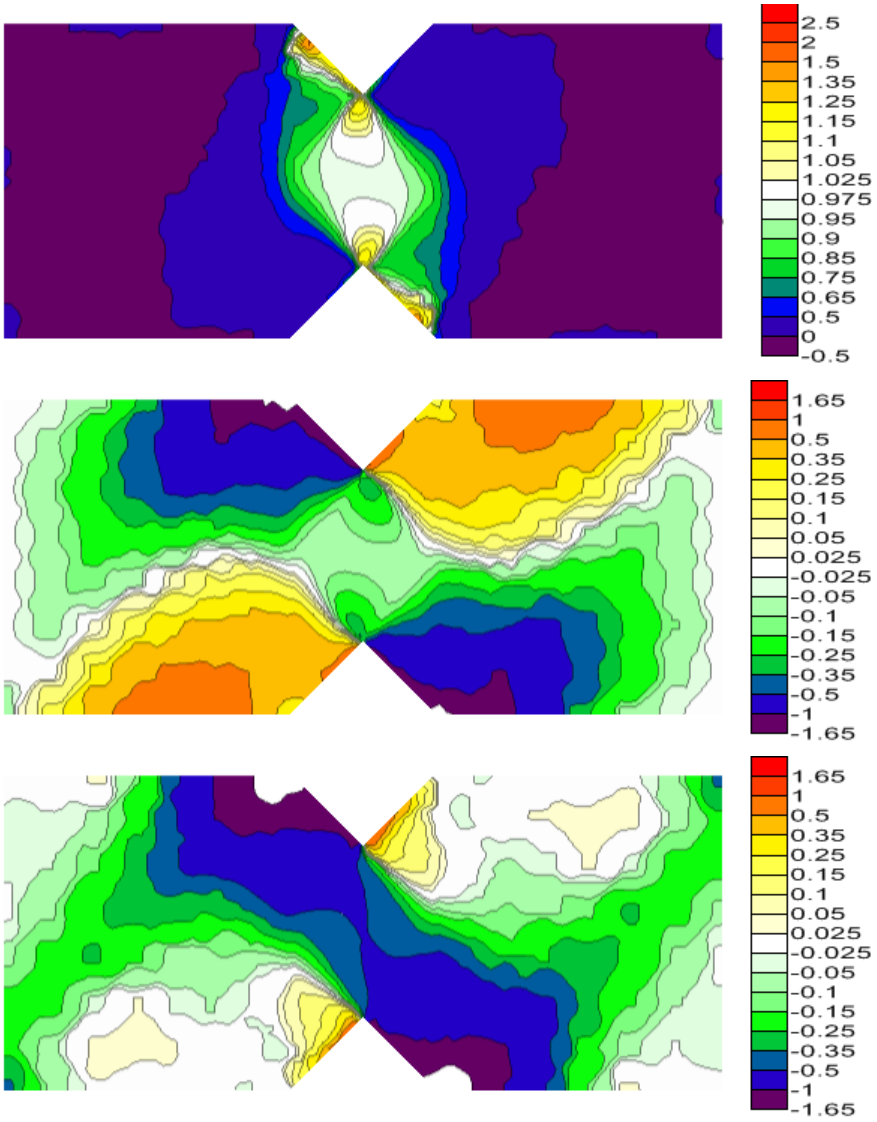


Figure 12: Normalized shear (top), transverse normal (middle), and axial normal (bottom) stress contours for a $[\pm 45]_{ns}$ laminate and the edge loading lengths for Model 1 in Table 2.

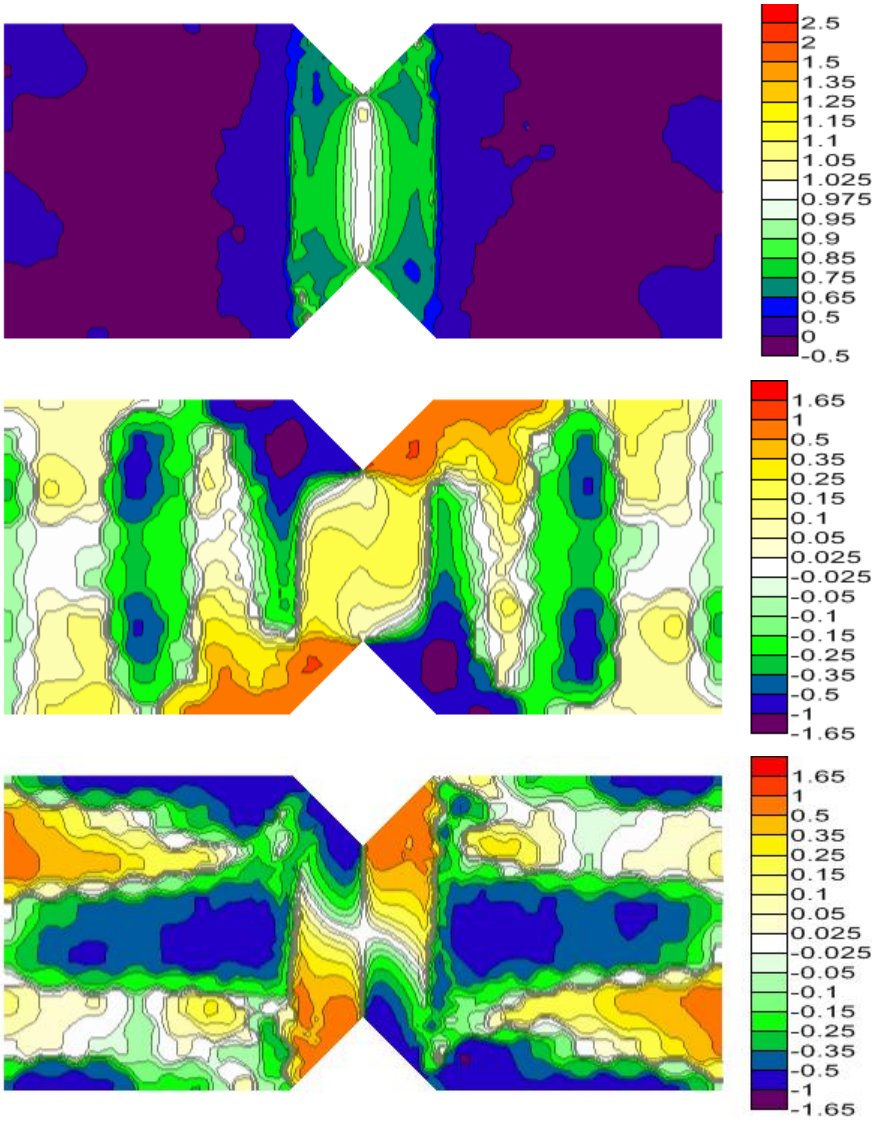


Figure 13: Normalized shear (top), transverse normal (middle), and axial normal (bottom) stress contours for a $[0/90]_{ns}$ laminate and the edge loading lengths for Model 2 in Table 2.

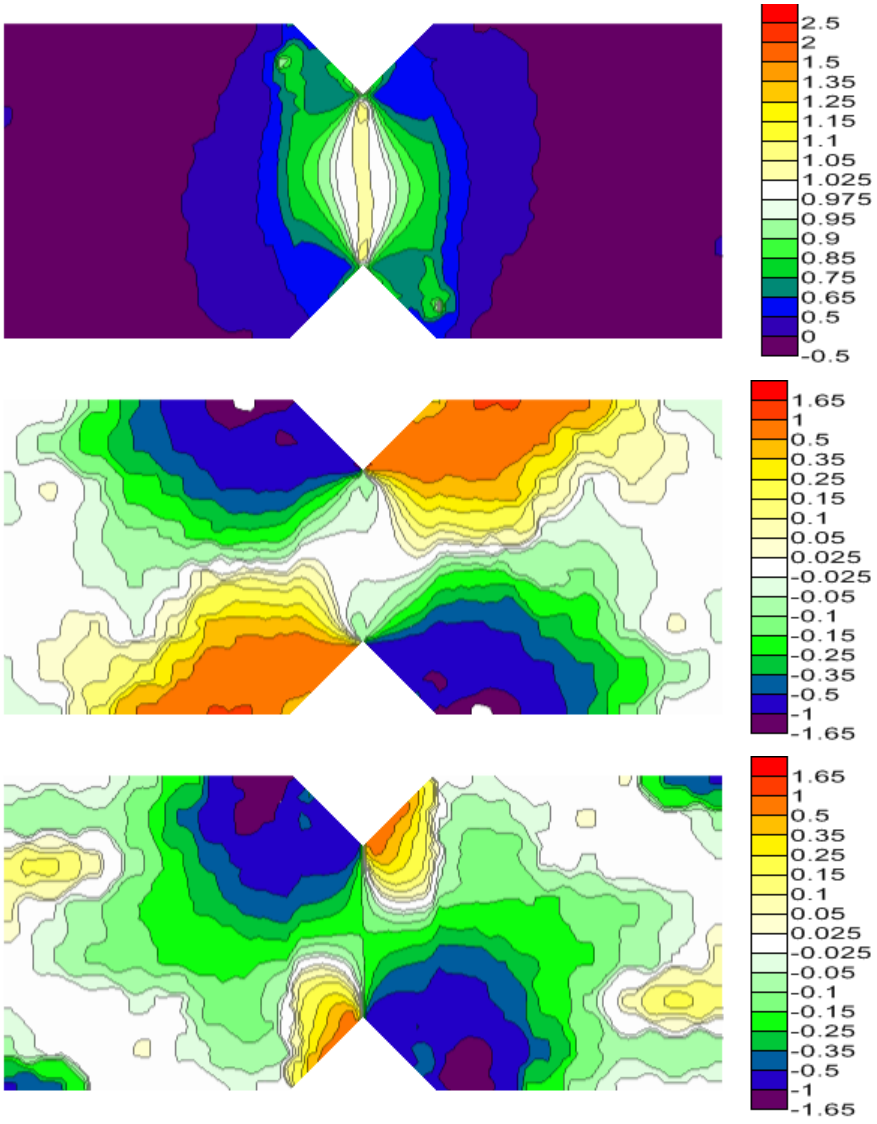


Figure 14: Normalized shear (top), transverse normal (middle), and axial normal (bottom) stress contours for a $[0/\pm45/90]_{ns}$ laminate and the edge loading lengths for Model 2 in Table 2.

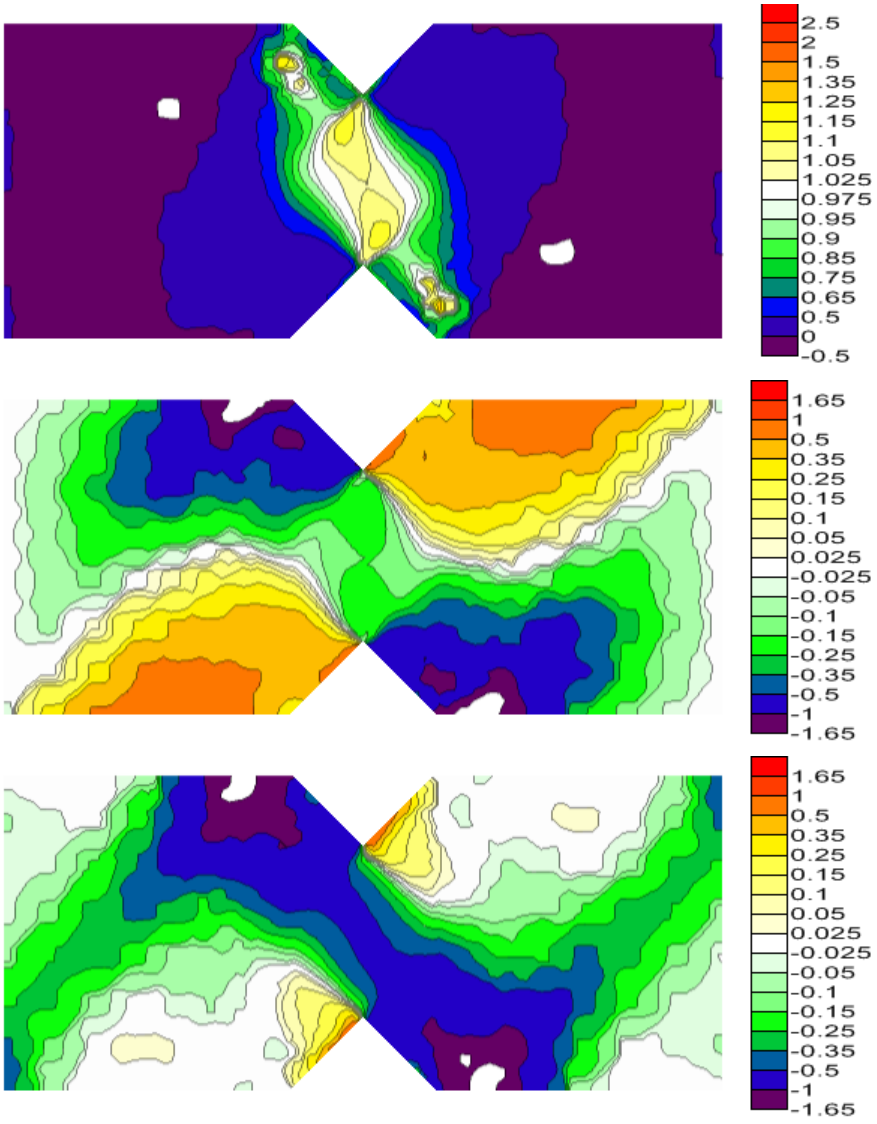


Figure 15: Normalized shear (top), transverse normal (middle), and axial normal (bottom) stress contours for a $[\pm 45]_{ns}$ laminate and the edge loading lengths for Model 2 in Table 2

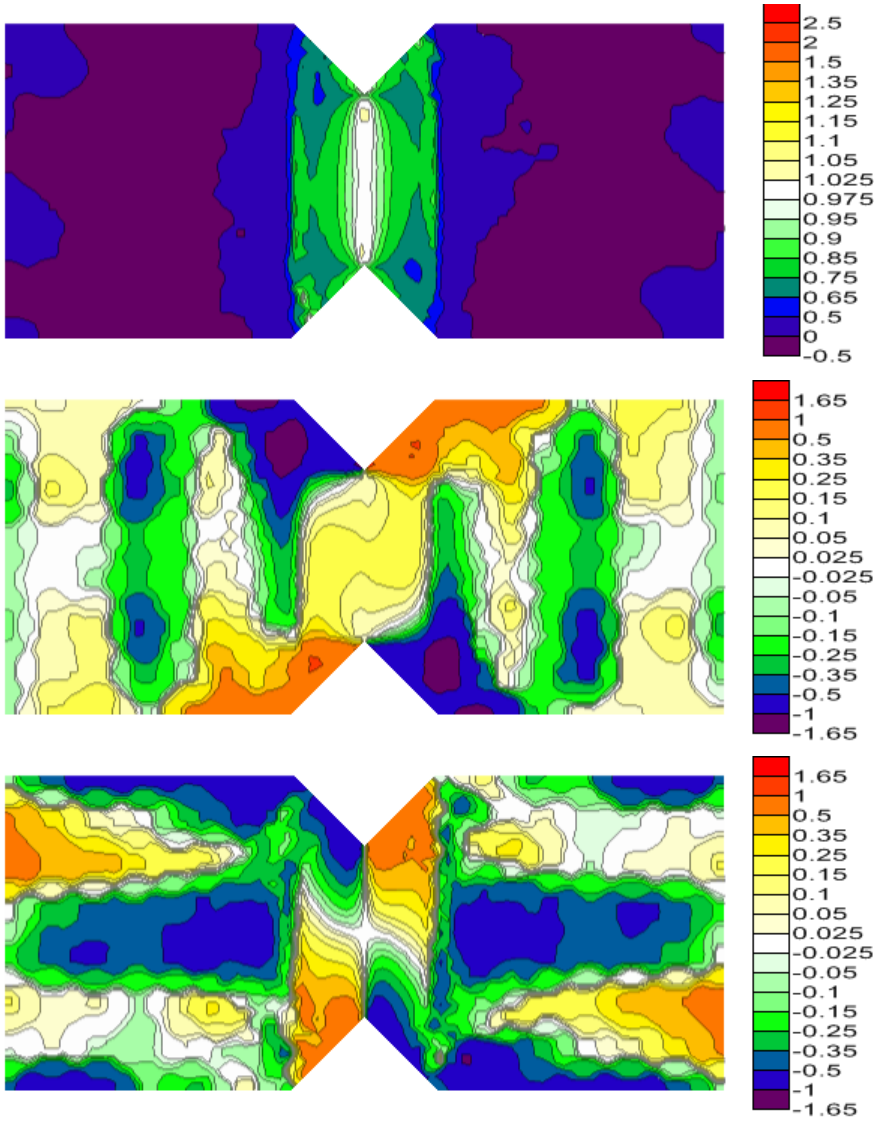


Figure 16: Normalized shear (top), transverse normal (middle), and axial normal (bottom) stress contours for a $[0/90]_{ns}$ laminate and the edge loading lengths for Model 3 in Table 2.

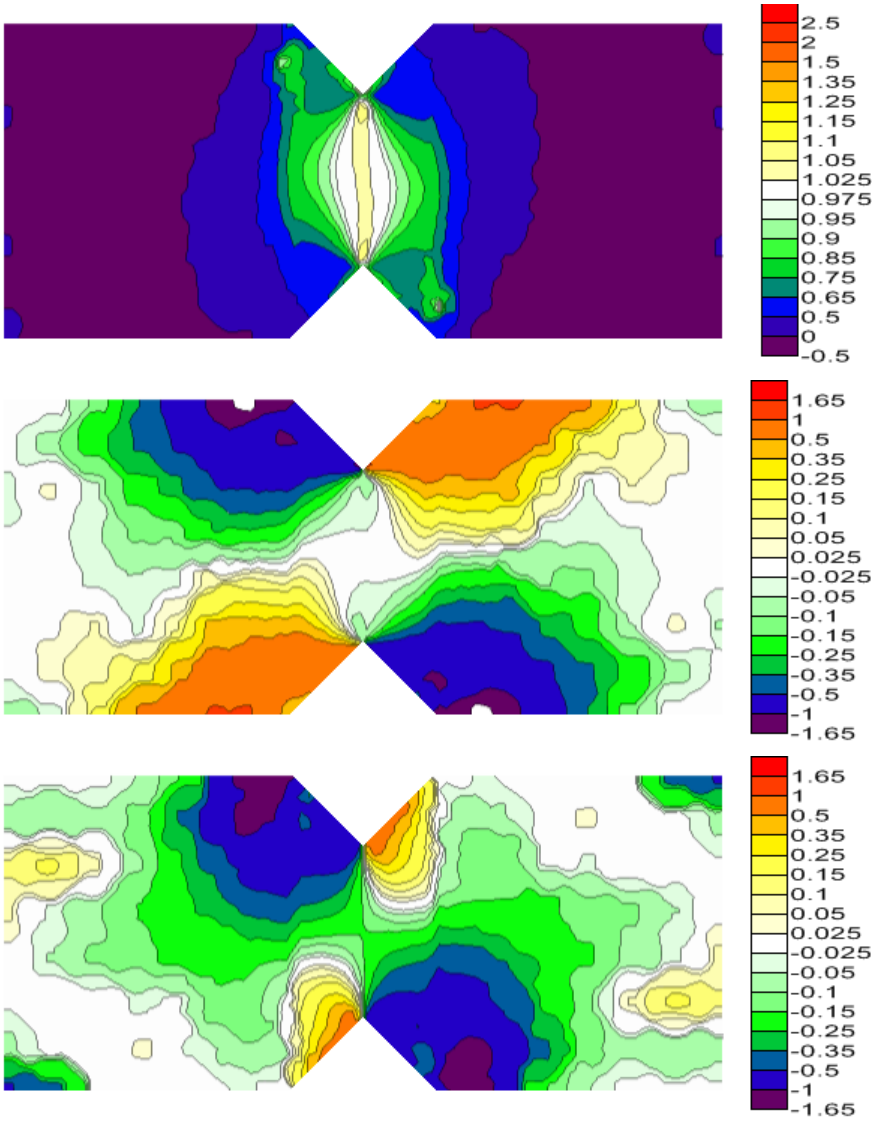


Figure 17: Normalized shear (top), transverse normal (middle), and axial normal (bottom) stress contours for a $[0/\pm45/90]_{ns}$ laminate and the edge loading lengths for Model 3 in Table 2.

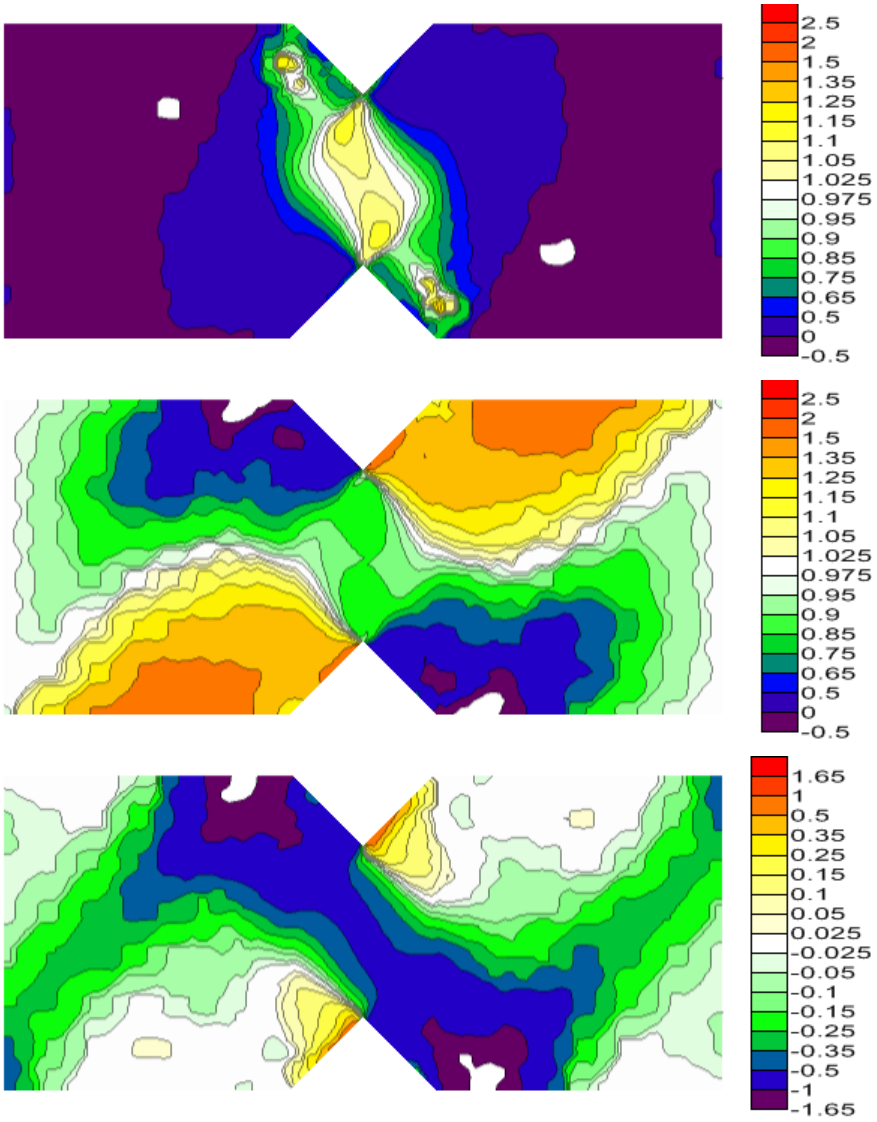


Figure 18: Normalized shear (top), transverse normal (middle), and axial normal (bottom) stress contours for a $[\pm 45]_{ns}$ laminate and the edge loading lengths for Model 3 in Table 2.

1.3.1.4 Model 4 Results

The in-plane shear, transverse normal and axial normal stress contours, normalized to the average shear stress, for the fourth edge loader configuration listed in Table 2 are depicted in Figure 19 - Figure 21. The cross-ply results are shown in Figure 19, the quasi-isotropic in Figure 20, and the $[\pm 45]_{ns}$ in Figure 21.

1.3.1.5 Observations on Edge Contact Length

Looking at the $[0/90]_{ns}$ laminates, the normalized in-plane shear stress, $\tau_{xy}/\ \tau_{avg}$, is relatively unaffected by changes in the edge contact length. In each configuration, the test region has a normalized value close to the average shear stress. The normalized transverse normal stress, $\sigma_x/\tau_{avg}$, for all four edge configurations show values that are between 15% and 25% of the average shear stress. A small decrease in the transverse normal stress is noticed between the notches when the contact length B is decreased from 50.80 mm (2.000 in.) to 34.11 mm (1.875 in.). The normalized axial normal stress, $\sigma_y/\tau_{avg}$, between the notches also show a small improvement when length B is decreased. However, as length A is decreased, both the normalized transverse and axial normal stresses show little or no change in stress state. From these models is seen that the adjustment of the inner loading point, B, shows the most influence.

Looking at the quasi-isotropic laminate ($[0/\pm 45/90]_{ns}$), the predicted stress states show the most change when the inner loading point is moved outward. Decreasing length B results in the shear stress increasing to 2.5% to 5% above the average between the notches. The normalized transverse normal stresses show a slight increase in the area of compressive stresses ranging from -2.5% to -5%, and the normalized axial normal stresses also show an improvement when decreasing B, as the area of compressive stress

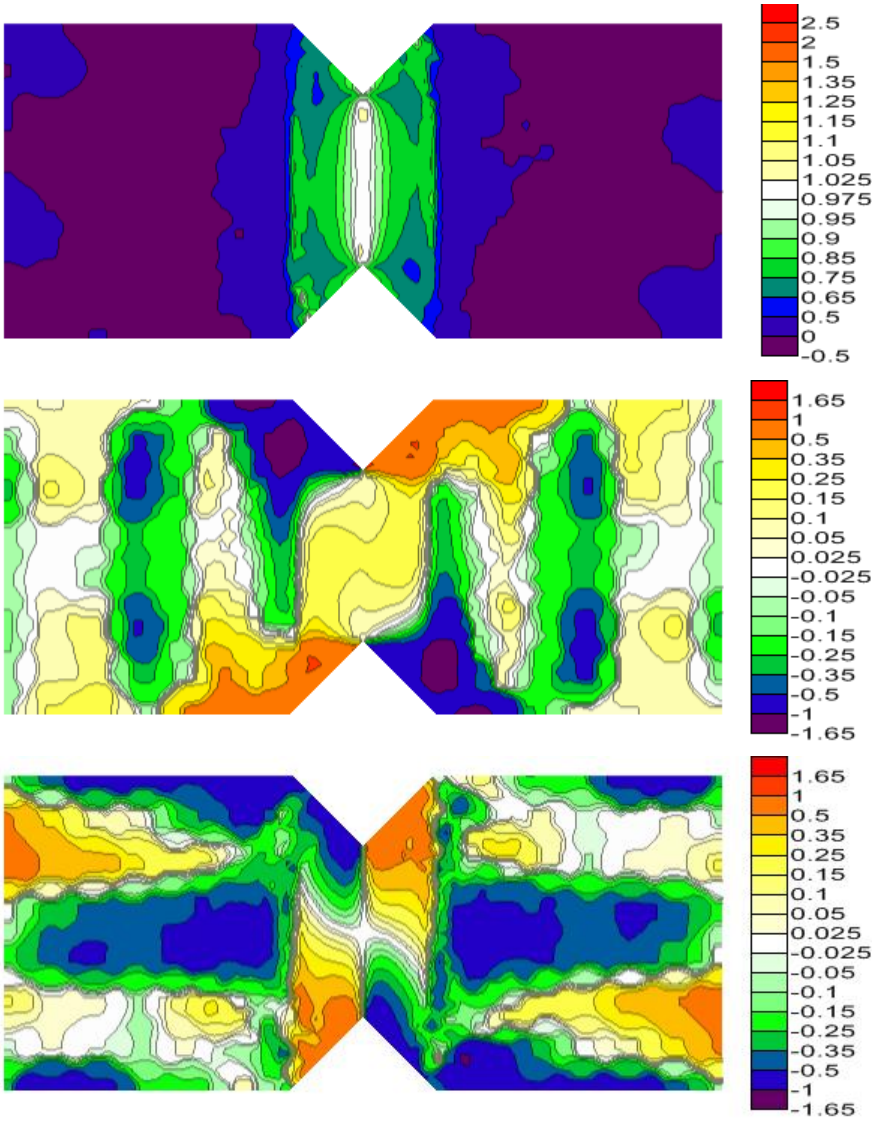


Figure 19: Normalized shear (top), transverse normal (middle), and axial normal (bottom) stress contours for a $[0/90]_{ns}$ laminate and the edge loading lengths for Model 4 in Table 2.

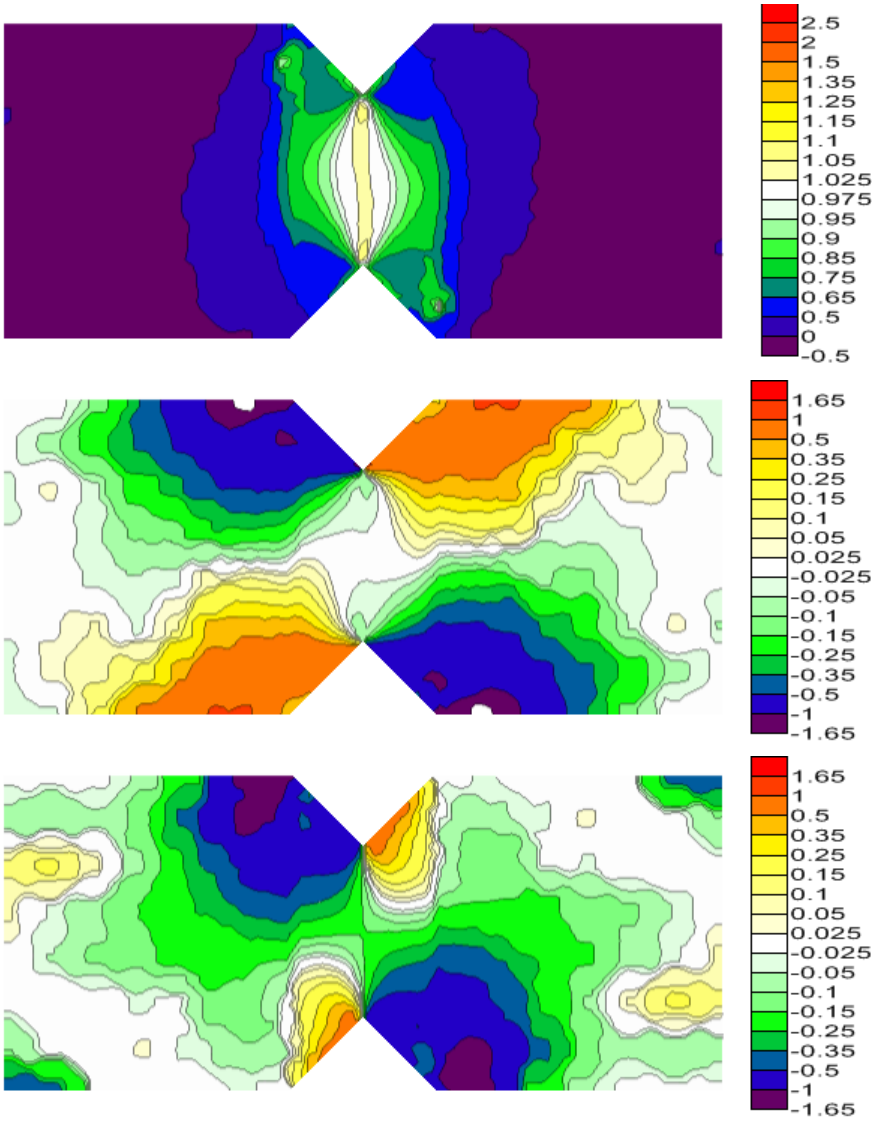


Figure 20: Normalized shear (top), transverse normal (middle), and axial normal (bottom) stress contours for a $[0/\pm45/90]_{ns}$ laminate and the edge loading lengths for Model 4 in Table 2.

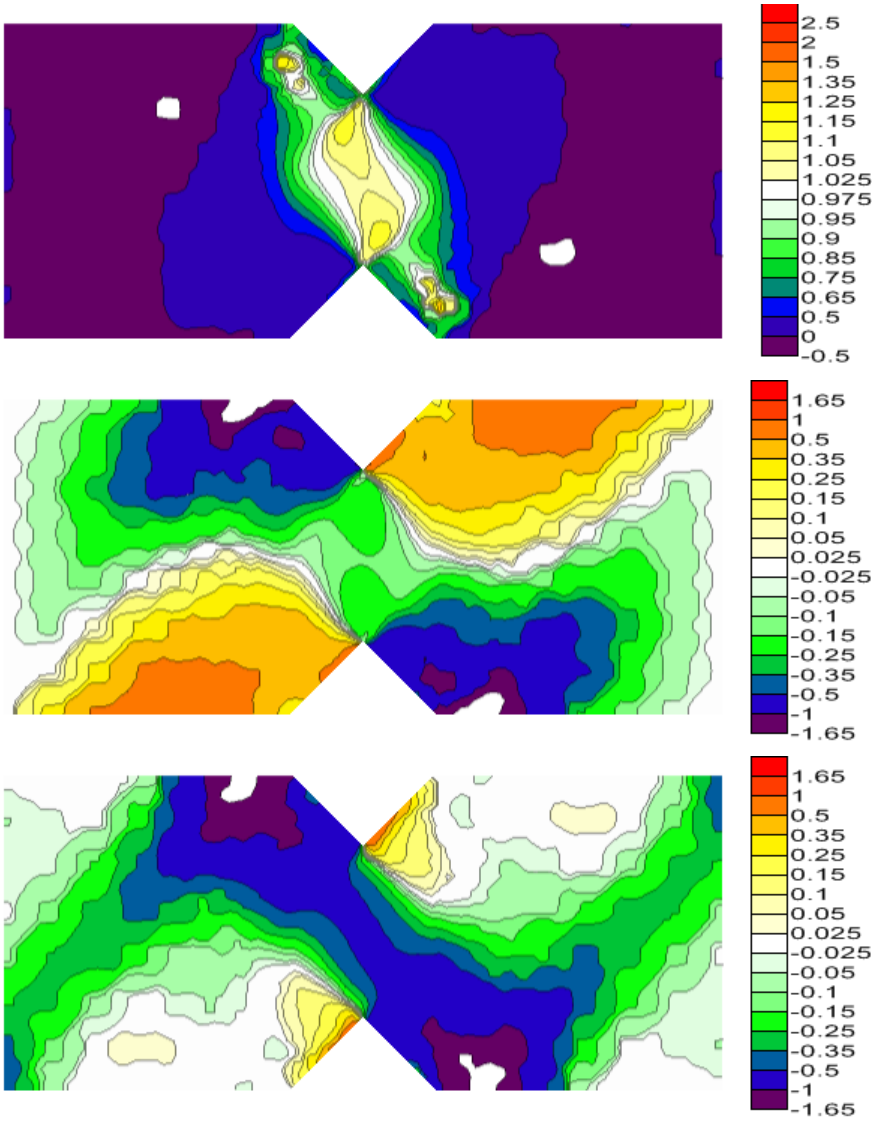


Figure 21: Normalized shear (top), transverse normal (middle), and axial normal (bottom) stress contours for a $[\pm 45]_{ns}$ laminate and the edge loading lengths for Model 4 in Table 2.

in the range of -15% to -25% is smaller for Models 2 – 4 than for Model 1. Changes to length A are less significant than the change to length B, and is evident when comparing the contour plots of Models 2 – 4.

The $[\pm 45]_{ns}$ laminates show appreciable differences in stress states with changes in the contact length between the specimen and fixture. The most influential change, again, is the inner loading point. The foremost difference to this change is in the normalized shear stress state, which changes from having a value which takes on a range of values between +25% and -2.5% of the average shear stress, in the region between the notches, to one which is approximately 5% – 10% higher than the average shear stress in the same region. A slight improvement is also achieved by decreasing length A from 50.80 mm (2.000 in.) to 34.11 mm (1.343 in.). The shear stress state does not improve, however, by decreasing A to 25.40 mm (1.000 in.). The normalized transverse normal stresses, $\sigma_x/\tau_{avg}$, also show a change in the stress gradient across the centerline of the specimen. In Model 1, these stresses along the centerline of the specimen vary from -35% to -2.5% of the average shear stress, whereas for Models 2 – 3, the normalized transvers normal stress along the centerline are between -25% and -15%. Model 4 is similar to models 2 and 3; however, there is a small region near the center of the specimen that is within -10% to -15% of the average shear stress. The normalized axial normal stresses, $\sigma_y/\tau_{avg}$, for each model show a band of compressive stress which is approximately 35 – 50% of the average shear stress. For Models 2 – 4 the band is oriented at approximately 135°, while for Model 1 it is oriented at approximately 92°. The smaller band angle for Model 1 also shows that more of the area between the notches is subjected to higher compressive axial normal stress than for Models 2 – 4.

It is also predicted that in the stress states for Model 1 the normalized axial normal stresses show a large compressive stress where the notches meet the loaded edges. This point is where the specimen meets the fixture and is the inner loading point for the asymmetrical four-point bend configuration shown in Figure 8. By moving the inner loading point away from the gauge section the magnitude of the axial stress decreases for the cross-ply and quasi-isotropic laminate. For these laminates, this modification should reduce the likelihood of crushing the specimen edges. This improvement may not be seen for $[\pm 45]_{ns}$ laminates as the high axial compressive stresses simply move outward to the new location of the inner loading point.

## 1.4 Mechanical Testing

### 1.4.1 Specimen Preparation

The material system used in this study was IM7/8552 unidirectional carbon/epoxy pre-preg tape from Hexcel Corporation. The following laminates were manufactured: $[0/90]_{2S}$, $[0/90]_{4S}$, $[0/90]_{5S}$, $[\pm 45]_{3S}$, $[\pm 45]_{4S}$, $[\pm 45]_{5S}$, $[0/\pm 60]_{3S}$, $[0/\pm 45/90]_{3S}$, and $[0/\pm 45/90]_{4S}$. The laminates were manufactured using a well-and-plunger mold in a Carver heated hydraulic press. Each pre-preg layer was placed into the mold according to the layup stacking order, then the top plate of the mold (plunger) was placed on top of the laminate and the entire mold was inserted into the press. The mold was loaded to approximately 105 kPa (15 psig) and the temperature of the platens set to 107.2 °C (225 °F). Once the temperature of the platens had reached equilibrium (approximately 17-21 minutes) the temperature and pressure were held for approximately 40 minutes, after which time the pressure was increased to 698 kPa (100 psig) and the temperature increased to 176.7 °C (350 °F). After the temperature of the platens had reached equilibri-

um (17-22 minutes) the pressure and temperature were maintained for 120 minutes, after which the pressure was removed and the mold was allowed to cool to ambient temperature. The laminate was then removed from the mold and labeled. The finished laminates measured 305 mm (12 in.) by 305 mm (12 in.) and the average cured ply thickness was 0.316 mm (0.0124 in.).

The specimens were rough cut from the laminate to the dimensions shown in Figure 22 in an OMAX abrasive waterjet machine. The edges that would be in contact with the edge loaders of the fixture were then machined using a sanding drum fixed in a 3-axis milling machine in order to ensure their perpendicularity to the specimen face. After machining the edges, each specimen was measured.

For the photoelastic tests a PS-1D photoelastic sheet and PC-1 two part adhesive from Vishay Measurements Group were used. The sheet had a nominal thickness of 0.53 mm (0.021 in.) a K factor of 0.15 and a fringe value of 3600. Each full fringe order is expressed as a red-blue color transition. A rectangular strip, nominally 23 mm (0.9 in.)

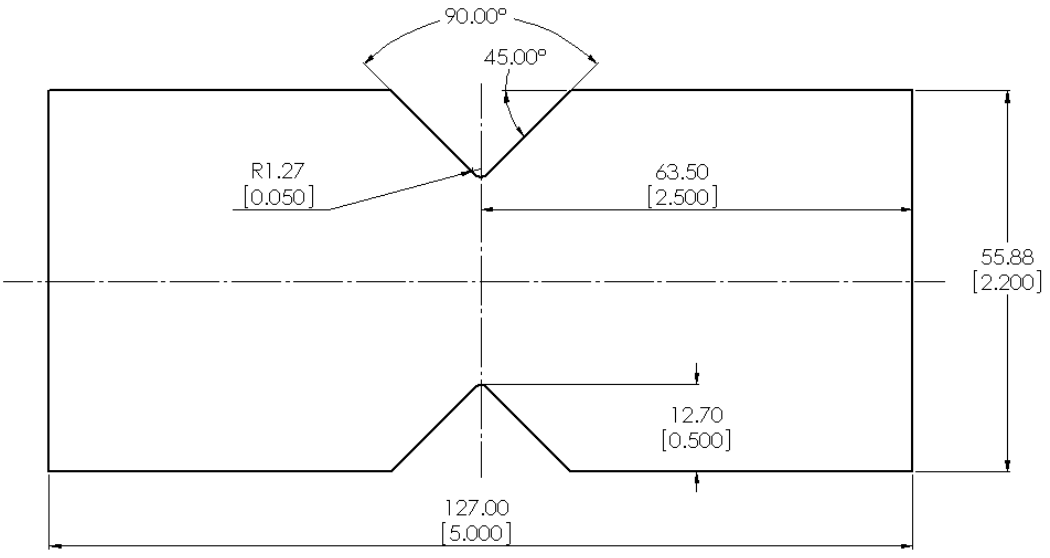


Figure 22: Target dimensions for the Combined Loading Shear specimen in mm [in.].

wide, was cut from the sheet for each specimen. Notches were then cut into each strip to roughly match those of the specimen, with a 2-3 mm (0.8 -0.12 in.) overhang. After bonding the photoelastic sheets to each specimen, and allowing the adhesive to fully cure, the excess photoelastic material was removed using small files until it matched the contour of the specimen notch. Three different layups were investigated: $[0/90]_{4S}$, $[\pm45]_{5S}$, and $[0/\pm45/90]_{4S}$.

### 1.4.2 Test Fixture

One of the primary drivers behind this study was to arrive at a suitable test fixture design that will yield shear modulus and shear strength values of composite laminates that are consistent with those found in the literature, and be capable of testing higher strength laminates than is possible with the current D 7078 test fixture. Through numerical simulations presented in Section 1.2 the dimensions of the Combined Loading Shear test fixture were determined.

The fixture used for experimental testing is shown in Figure 4 and Figure 5. The dimensions of the individual fixture components are shown in Appendix B. The fixture is designed to operate in tension only. The fixture incorporates many of the features described in Sections 1.2.2. The chamfer on the body of the fixture effectively moves the inner loading points away from the gauge section, which resulted in decreasing the axial normal compressive stresses at the inner loading point. The fixture halves, face loaders and edge loaders were all machined from 17-4PH stainless steel.

### 1.4.3 Testing Procedure

Three series of tests were performed with the new fixture. The objective of the first set of tests was to determine whether the proposed new fixture would produce ultimate shear strength values similar to those published in the literature when no pre-applied specimen edge load was used. All of the laminates listed in Section 1.4.1 were used in these shear strength tests. The second set of tests was to determine if preloading the specimen edge would affect the measured ultimate shear strength. For this study only the $[0/90]_{4S}$ laminate was used. A cross-ply laminate was chosen because the finite element model predicted that the shear stresses for this layup are highly influenced by the edge preload. The third set of tests involved performing a photoelastic analysis on a $[0/90]_{4S}$, $[0/\pm45/90]_{4S}$, and $[\pm45]_{5S}$ specimen in order to obtain the strain field in the test section of the specimen.

Assembly of the Combined Loading Shear test fixture was performed in a manner similar to the fixture for ASTM D7078 [3]. The specimen was inserted into one half of the test fixture using an alignment jig to center the notches between the fixture halves. The edge loader bolt was then tightened to ensure the specimen edges were in contact with the fixture and the edge loader. The bolts for the face loaders were then adjusted to align the centerline of the specimen with the centerline of the fixture half and then tightened in five torque stages to a final torque of 65 N·m (48 lbf·ft). The second fixture half was then installed using the same methods. The edge loader bolts for both fixture halves were then loosened and retightened in order to bring the edge loaders into contact with the specimen, and ensure that there was no preload applied to the specimen edges. For the edge load study, the edge loader bolts where then torqued to the appropriate value.

For shear strength measurements, an Instron A212-201 222 kN (50 kip) load cell was used to measure the load while a National Instruments SCXI-1520 strain module was used to monitor the load cell output using a program developed in LabView. A crosshead speed of 1.27 mm/min (0.05 in./min) was used. Each test proceeded until a significant drop in load occurred. Shear stress – crosshead displacement plots were then created from the test data and are presented in Section 1.5.1.

For the photoelastic testing, a United 89 kN (20 kip) load cell was used to measure the loads. Datum 3.0 was used to control the load frame. The testing speed was 1.27 mm/min (0.050 in./min). Datum was programmed to stop at specific loads in order to photograph the isoclinic and isochromatic fringes. The loads used are shown in Table 3. Only the ±45° isoclinics, along with the isochromatic fringes were recorded as they are of primary concern for shear testing. Two edge loader torques were investigated with each specimen: no edge load or 'finger tight', and 40 N·m (29.5 lbf·ft). Even though the same specimen was used for both edge load torque values, the specimen was reinstalled in the fixture as though it were a new test for each edge load.

Table 3: Loads at which the isochromatic and isoclinic contours were photographed for each laminate.

| Layup | Load Steps kN [lbf] | | |
|---|---|---|---|
| $[0/90]_{4S}$ | 2.00 [450] | 4.00 [900] | 6.01 [1350] |
| $[\pm 45]_{5S}$ | 17.8 [4000] | 28.9 [6500] | 40.0 [9000] |
| $[0/\pm 45/90]_{4S}$ | 19.6 [4400] | 25.8 [5800] | 32.0 [7200] |

A Measurements Group 031-A polariscope was used to view the photoelastic fringes. A Nikon D3000 digital camera and a Sigma EX 105 mm DG Macro lens were used to photograph the resulting fringe contours. The camera settings used were: aperture $f2.8$, shutter speed 1/10 s, ISO 800, and incandescent white balance. The images were opened in UFRaw and edited in GIMP before saving in an uncompressed Windows Bitmap format. The exposure values, EV, of the isochromatic images were increased to +3.25 in order to differentiate the isoclinics from low exposure areas. This was not done to the isochromatic images as this would generally over expose the image. Both the polariscope and the camera were mounted to a tripod. An angle gauge was used to ensure the alignment of the tripod mounting boss.

## 1.5 Results

### 1.5.1 Shear Strength Results

#### 1.5.1.1 Cross-ply Laminates

The shear stress – displacement plots for the $[0/90]_{2S}$, $[0/90]_{4S}$, and $[0/90]_{5S}$ laminates are shown in Figure 23, Figure 24, and Figure 25, respectively. The cross-ply specimens showed a distinct characteristic not exhibited by either the quasi-isotropic or the $[\pm45]_{ns}$ laminates. The response of the material was linear until approximately 96.5 MPa (14.0 ksi), at which point the stiffness changed showing a significant nonlinear behavior. The thinnest laminate, in some instances, exhibited a slope of approximately zero at elevated loading. This result may be attributable to specimen instability, as both of the thicker specimens did not exhibit this behavior.

The ultimate shear strengths for the cross-ply laminates tested are shown in Table 4. These values are only slightly larger than those reported in [5], and the coefficients of

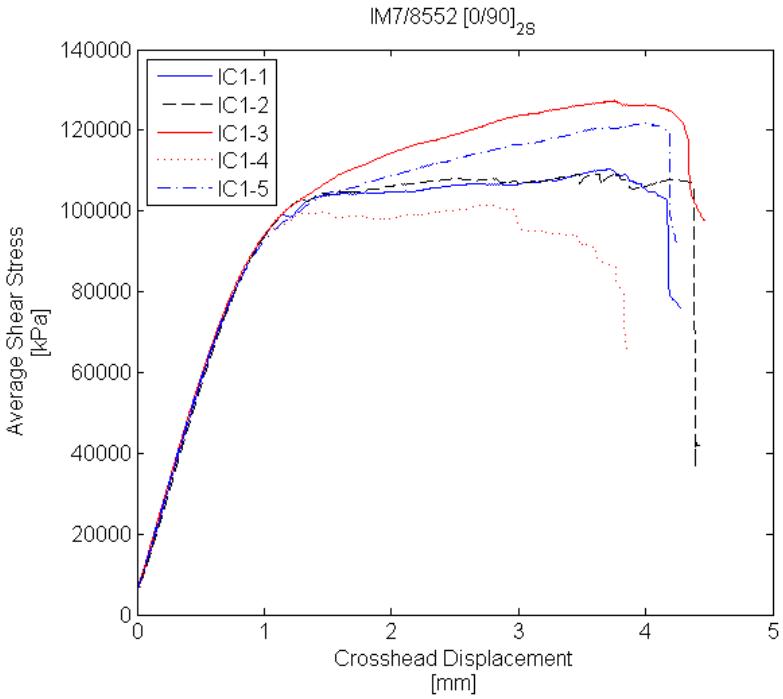


Figure 23: Stress/displacement response for a $[0/90]_{2S}$ IM7/8552 carbon/epoxy laminate.

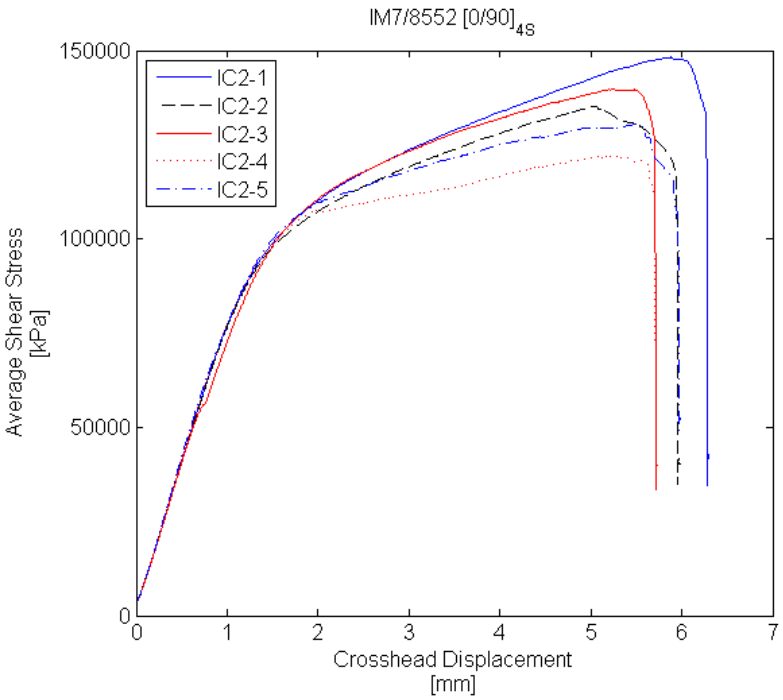


Figure 24: Stress/displacement response of a $[0/90]_{4S}$ IM7/8552 carbon/epoxy laminate

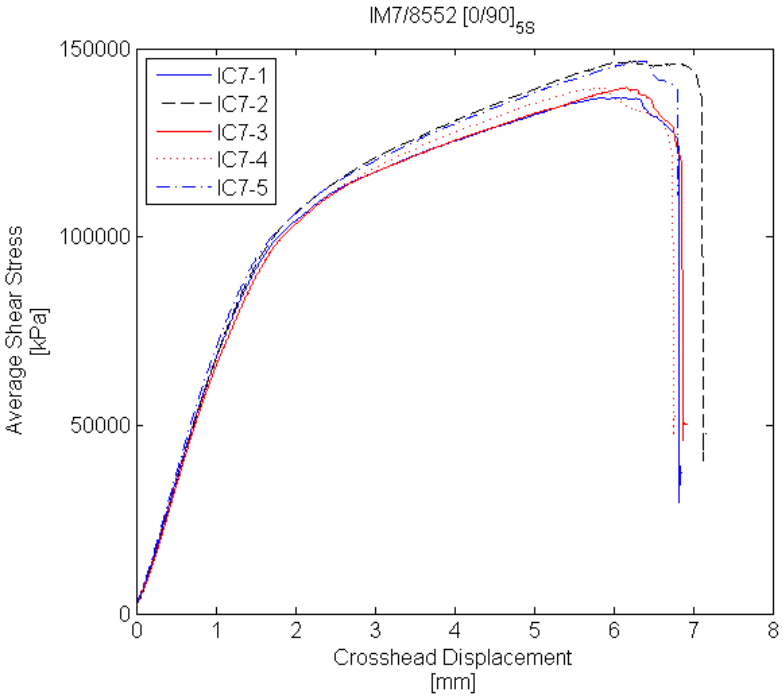


Figure 25: Stress/displacement response of a $[0/90]_{5S}$ IM7/8552 carbon/epoxy laminate.

Table 4: Measured ultimate shear strength values for cross-ply laminates made from IM7/8552 pre-preg.

| | Average $\tau_{max}$ | | COV |
|---|---|---|---|
| Laminate | [MPa] | [ksi] | [%] |
| $[0/90]_{2S}$ | 114 | 16.5 | 9.07 |
| $[0/90]_{4S}$ | 135 | 19.6 | 7.25 |
| $[0/90]_{5S}$ | 142 | 20.6 | 3.09 |

variation are generally lower for the new Combined Loading Shear fixture. Failure patterns were also generally the same as those in [5].

1.5.1.2 Quasi-Isotropic Laminates

The shear stress – displacement plots for the $[0/\pm60]_{3S}$, $[0/\pm45/90]_{3S}$, and $[0/\pm45/90]_{4S}$ laminates are shown in Figure 26, Figure 27, and Figure 28, respectively, and the ultimate shear strength values are listed in Table 5. Unlike the cross-ply laminates, it is seen that both the $[0/\pm60]_{ns}$ and $[0/\pm45/90]_{ns}$ quasi-isotropic laminates demonstrate a linear response until failure. The ultimate shear stresses for the common laminates listed in Table 5 are slightly larger than those in [5] and the variation is generally lower for the new fixture. While the coefficient of variation for the ultimate strength of the $[0/\pm60]_{3S}$ is significantly low, it is likely due to the limited number of samples tested and should not be interpreted to imply that the strength of this layup is statistically less

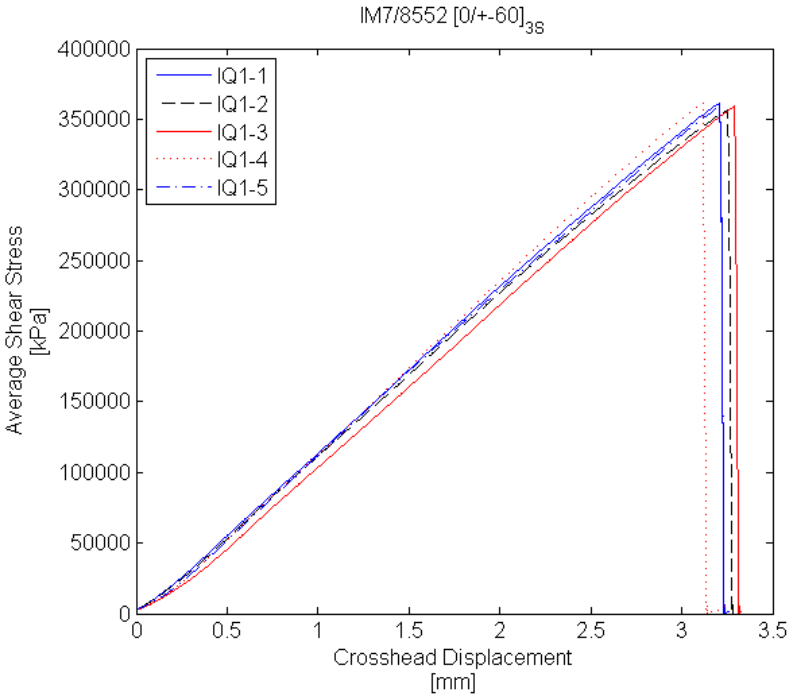


Figure 26: Stress/displacement response of a $[0/\pm60]_{3S}$ IM7/8552 carbon/epoxy laminate.

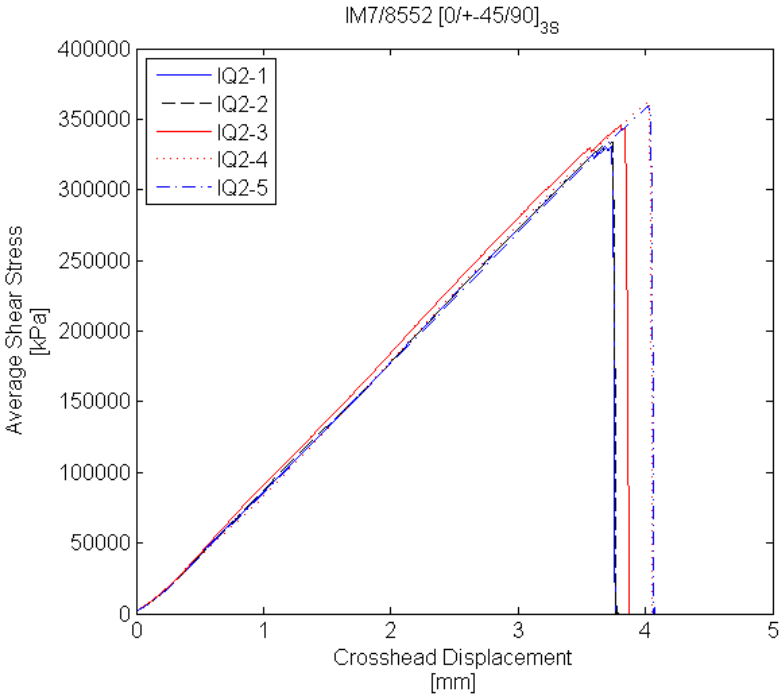


Figure 27: Stress/displacement response of a $[0/\pm45/90]_{3S}$ IM7/8552 carbon/epoxy laminate.

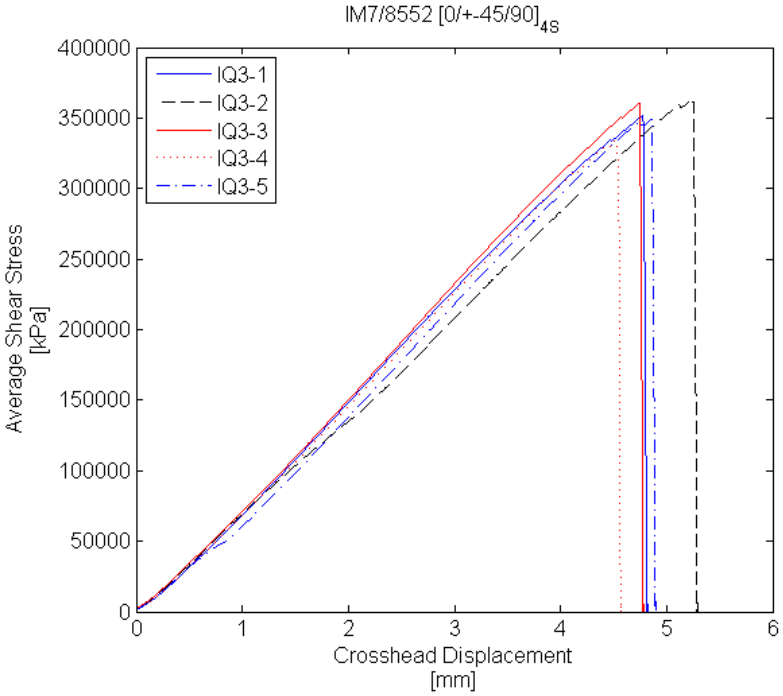


Figure 28: Stress/displacement response of a $[0/\pm45/90]_{4S}$ IM7/8552 carbon/epoxy laminate.

Table 5: Measured ultimate shear strength values for quasi-isotropic laminates made from IM7/8552 pre-preg.

| Laminate | Average $\tau_{max}$ [MPa] | [ksi] | COV [%] |
|---|---|---|---|
| $[0/\pm60]_{3S}$ | 359 | 52.1 | 0.58 |
| $[0/\pm45/90]_{3S}$ | 346 | 50.2 | 4.17 |
| $[0/\pm45/90]_{4S}$ | 351 | 50.9 | 3.27 |

varied than other quasi-isotropic layups. The strength values obtained using this fixture also show a smaller variation between laminate thicknesses than the fixture used by Johnson [5].

1.5.1.3 $[\pm45]_{ns}$ Laminates

The shear stress – displacement plots for the $[\pm45]_{3S}$, $[\pm45]_{4S}$, and $[\pm45]_{5S}$ laminates are shown in Figure 29, Figure 30, and Figure 31, respectively. The response of these laminates is generally linear to failure, similar to the quasi-isotropic laminates. Additionally, the $[\pm45]_{ns}$ specimens generally exhibited a tendency to slip slightly within the grips. When comparing the gripped region of the specimen face of these specimens to those of the cross-ply or quasi-isotropic, it is readily apparent from the abrasions left by the face loaders that the regions nearest the gauge section moved relative to the grips. In each specimen that showed signs of slipping, the region that displayed the most relative displacement was always adjacent to the gauge section. This behavior was also observed by Johnson [5], and because his fixture made contact with the specimen immediately adjacent to the notch it is believed that moving the inner loading point closer to the notch will not limit the amount of specimen slipping.

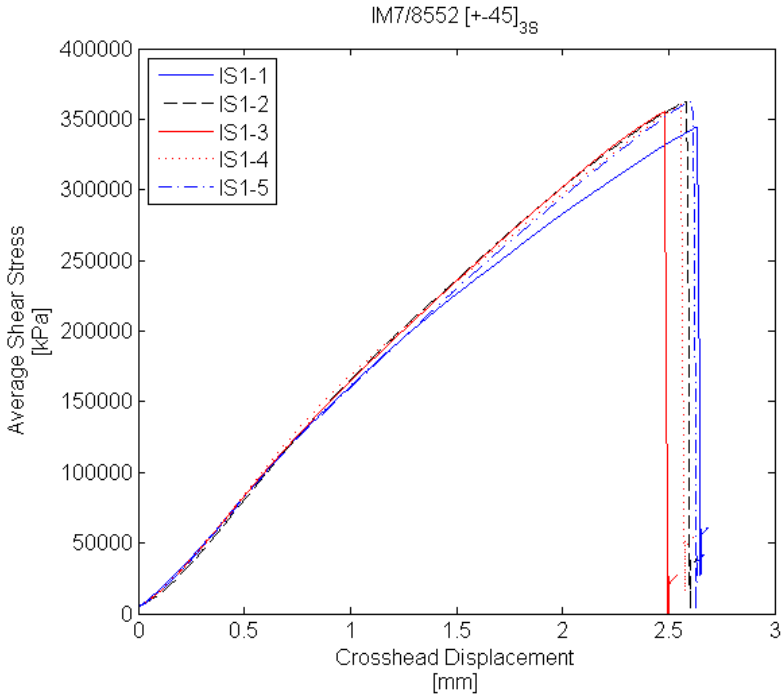


Figure 29: Stress/displacement response of a $[\pm 45]_{3S}$ IM7/8552 carbon/epoxy laminate.

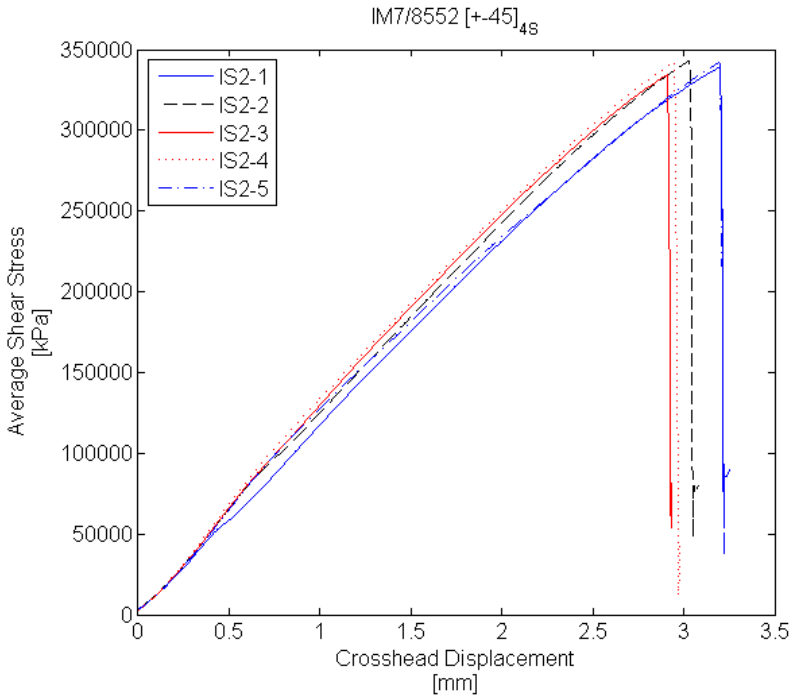


Figure 30: Stress/displacement response of a $[\pm 45]_{4S}$ IM7/8552 carbon/epoxy laminate.

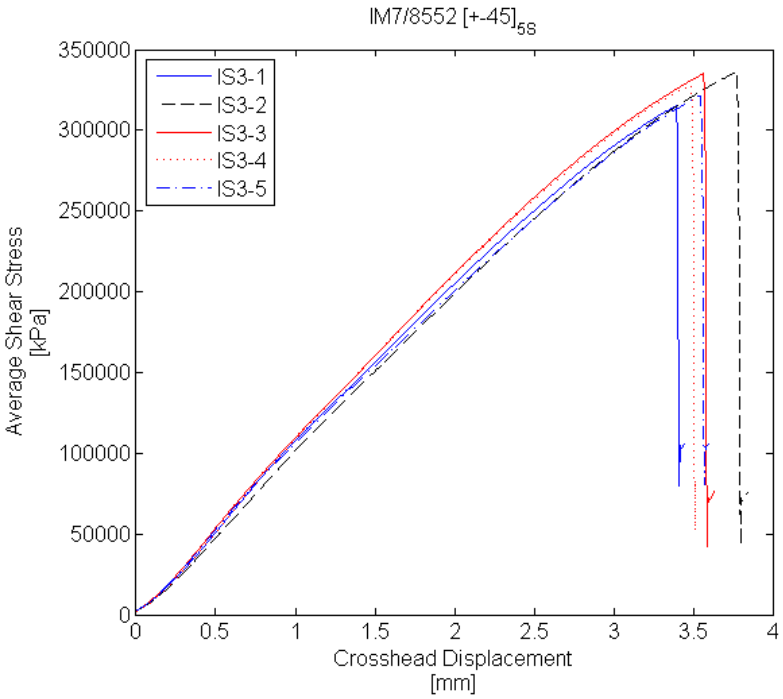


Figure 31: Stress/displacement response of a $[\pm 45]_{5S}$ IM7/8552 carbon/epoxy laminate.

The ultimate shear strengths measured using the Combined Loading Shear test are listed in Table 6. In general the measured shear strengths are slightly lower than those reported in [5] and showed the same general trend of decreasing in strength with increasing specimen thickness. The variations within each specimen group are low.

1.5.1.4 Failure Loads

The maximum measured tensile load for each layup tested in Section 1.5.1.1, 1.5.1.2, and 1.5.1.3 are shown in Table 7. The largest test load experienced by the Combined Loading Shear test fixture was 112 kN (25.3 kip) from a $[0/\pm 45/90]_{4S}$ specimen. This load is more than double the load at which slipping occurred in [5].

Table 6: Measured ultimate shear strength values for $[\pm 45]_{ns}$ laminates made from IM7/8552 pre-preg.

| Laminate | Average $\tau_{max}$ [MPa] | Average $\tau_{max}$ [ksi] | COV [%] |
|---|---|---|---|
| $[\pm 45]_{3S}$ | 357 | 51.8 | 2.15 |
| $[\pm 45]_{4S}$ | 340 | 49.3 | 1.04 |
| $[\pm 45]_{5S}$ | 327 | 47.5 | 2.78 |

Table 7: Maximum failure loads found using the Combined Loading Shear test fixture.

| Laminate | Max Load [kN] | Max Load [kip] |
|---|---|---|
| $[0/90]_{2S}$ | 9.75 | 2.19 |
| $[0/90]_{4S}$ | 23.1 | 5.20 |
| $[0/90]_{5S}$ | 28.7 | 6.45 |
| $[0/\pm 60]_{3S}$ | 63.8 | 14.3 |
| $[0/\pm 45/90]_{3S}$ | 86.0 | 19.3 |
| $[0/\pm 45/90]_{4S}$ | 112 | 25.3 |
| $[\pm 45]_{3S}$ | 42.1 | 9.47 |
| $[\pm 45]_{4S}$ | 53.7 | 12.1 |
| $[\pm 45]_{5S}$ | 66.7 | 15.0 |

### 1.5.2 Edge Load Variation

#### 1.5.2.1 Shear Strength

The shear stress - displacement plots for the 10 N·m, 40 N·m, and 65 N·m edge loader bolt torque are shown in Figure 32, Figure 33, and Figure 34, respectively. The ultimate shear strengths are listed in Table 8. By increasing the torque applied to the edge loader from finger tight to 10 N·m (7.4 lbf·ft) the average ultimate shear strength in-

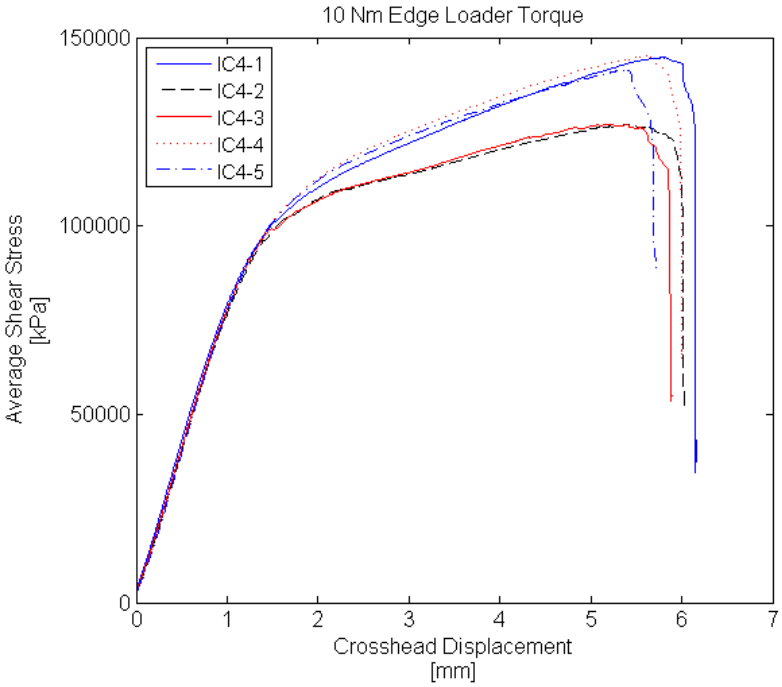


Figure 32: Stress/displacement response of a $[0/90]_{4S}$ IM7/8552 carbon/epoxy laminate when using an applied torque of 10 N·m on the edge loader bolt.

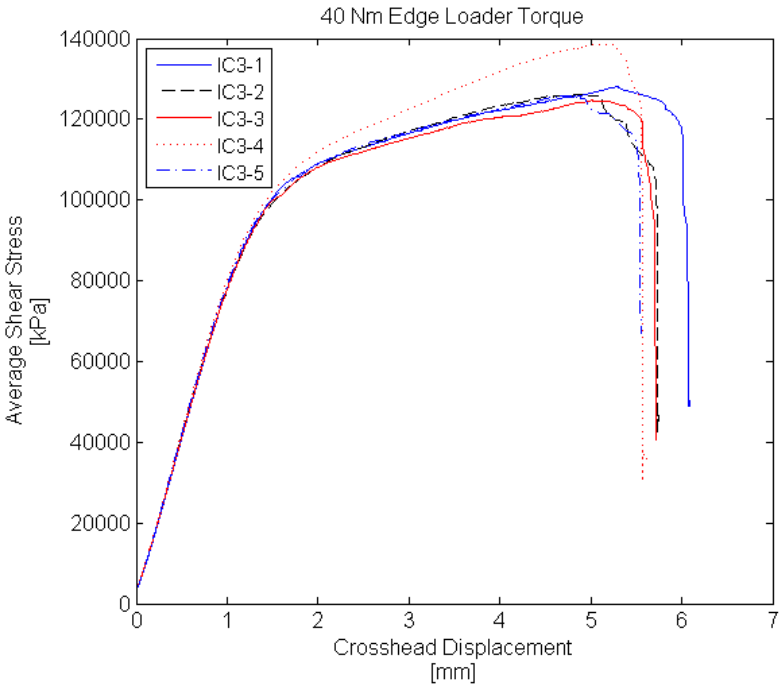


Figure 33: Stress/displacement response of a $[0/90]_{4S}$ IM7/8552 carbon/epoxy laminate when using an applied torque of 40 N·m on the edge loader bolt.

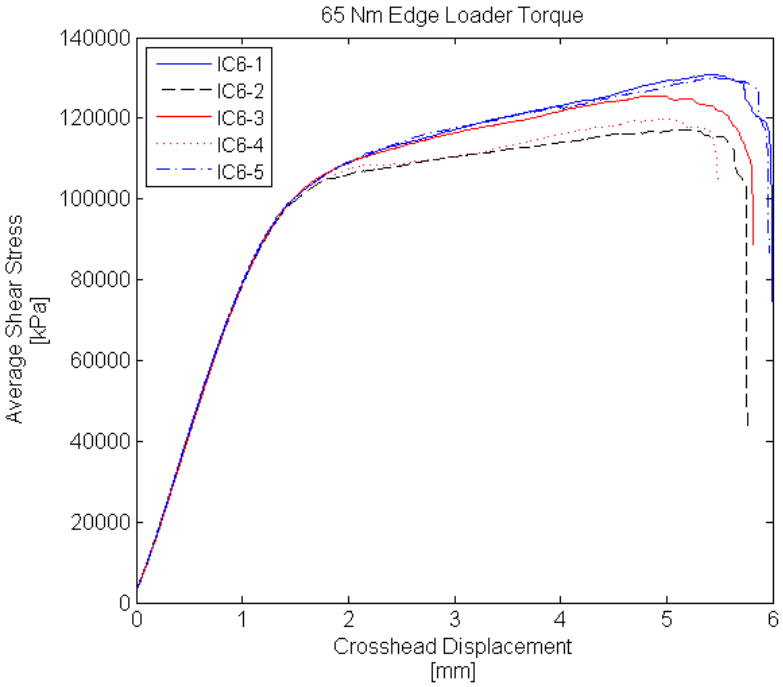


Figure 34: Stress/displacement response of a $[0/90]_{4S}$ IM7/8552 carbon/epoxy laminate when using an applied torque of 65 N·m on the edge loader bolt.

Table 8: Average measured ultimate shear strength of a $[0/90]_{4S}$ IM7/8552 carbon epoxy laminate.

| Edge Torque | | Average $\tau_{max}$ | | COV |
|---|---|---|---|---|
| [N·m] | [lbf·ft] | [MPa] | [ksi] | [%] |
| 0 | 0.0 | 135 | 19.6 | 7.26 |
| 10 | 7.4 | 137 | 19.9 | 6.77 |
| 20 | 15 | 127 | 18.4 | 5.46 |
| 40 | 30 | 129 | 18.7 | 4.39 |
| 65 | 48 | 125 | 18.1 | 4.87 |

creased by 1.4 % while the variation in strength decreased by 6.7 %. Comparing Figure 24 to Figure 32, the shear stress – displacement response of the specimens tested with a 10 N·m (7.4 lbf·ft) torque applied to the edge loader bolt showed less scatter in the non-linear region than the specimens tested with no torque applied to the edge loader bolts. Specimens tested using a higher torque had a higher tendency to exhibit an unstable stress – displacement response after approximately 96.5 MPa (14.0 ksi). In general, the apparent shear strength decreased as the edge loader bolt torque was increased, while the corresponding variation in the apparent shear strength decreased. From the values listed in Table 8, the difference between the maximum and minimum apparent shear strength is 9.4%. It was also observed that the lowest measured shear strength was produced using an edge torque of 65 N·m, while the highest was measured using no edge torque.

1.5.2.2 Validation of Numerical Model

The numerical results simulating a photoelastic analysis (maximum shear strain, $\gamma_{max}$, and orientation of the principal strains) for the cross-ply, quasi-isotropic, and $[\pm 45]_{5S}$ laminates are shown in Figure 35, Figure 36, and Figure 37, respectively. The results predict that only the cross-ply laminate will have a highly uniform shear strain state along the specimen centerline. Based on the strain principal angle, most of the specimen free surface will be in a state of shear. The maximum shear strains are fairly uniform throughout the test region with the highest strains occurring along the specimen centerline. There are strain concentrations near the notch tips; however, the strain gradient along the specimen centerline is small.

The maximum shear strains for the quasi-isotropic laminate likewise have a fairly uniform distribution within the test section and a small strain gradient between the notch

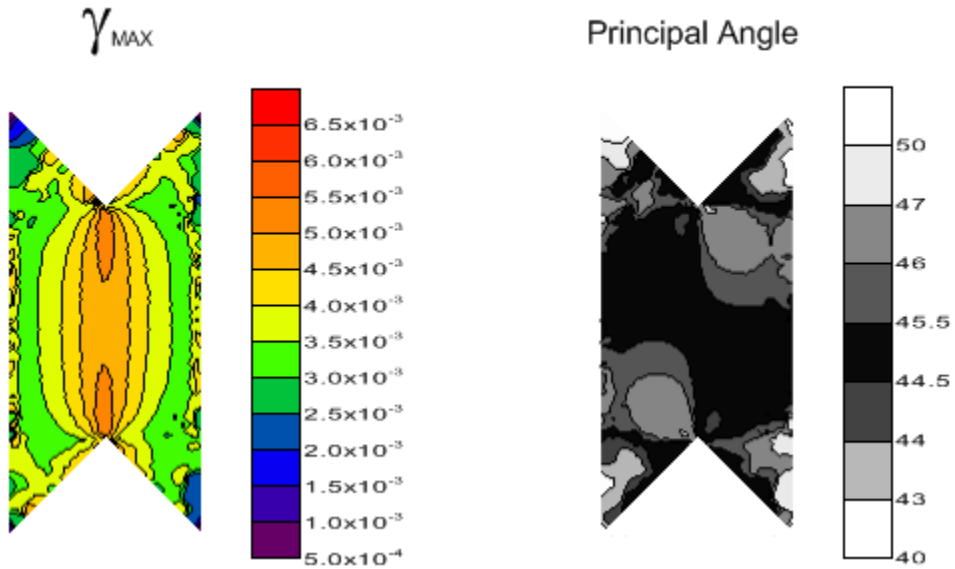


Figure 35: Maximum shear strain and principal strain angle contour plots for the cross-ply laminate.

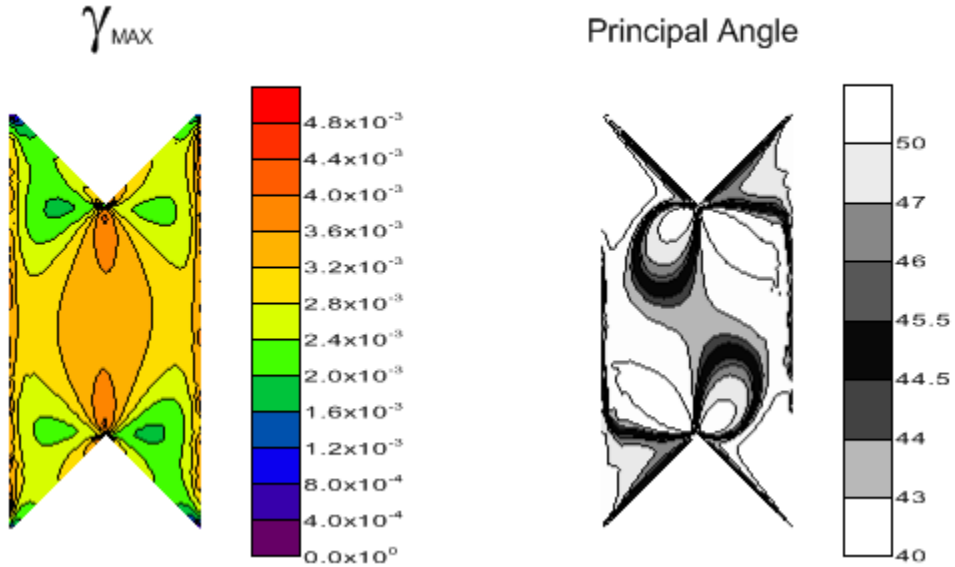


Figure 36: Maximum shear strain and principal strain angle contour plots for the quasi-isotropic laminate.

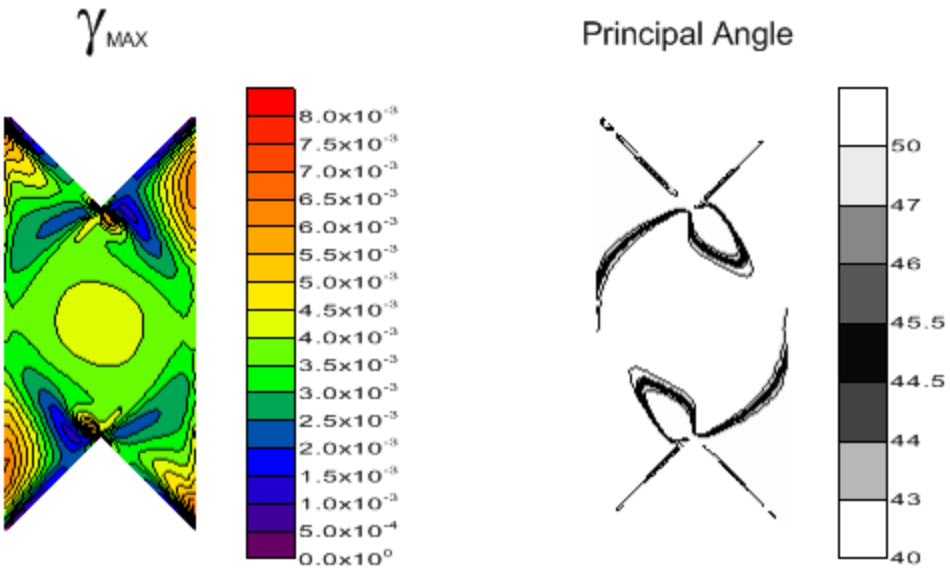


Figure 37: Maximum shear strain and principal strain angle contour plots for the $[\pm 45]_{5S}$ laminate.

es. The orientations of the principal strains, however, are not at ±45°. From Figure 36 it is predicted that the principal strains between the notches comes within 2° of being a shear strain state. Unlike the cross-ply results there is a much smaller region within the test section where the principal strains are oriented within 5° of being a shear strain state.

The strain state of the $[\pm 45]_{5S}$, shown in Figure 37, is predicted to be much less uniform than either the cross-ply or the quasi-isotropic. The maximum shear strain has a larger strain gradient between the notches. Additionally, the principal strains oriented at ±45° occupy a much smaller region than the other two laminates, and the strain state in the region between the notches is not the preferred state of shear. Based on this result, the $[\pm 45]_{ns}$ laminate is not suitable for shear testing.

1.5.2.3 Photoelastic Testing

Only images taken at the second and third load steps listed in Table 3 are emphasized in this section. During some tests, certain sections of the photoelastic film debond-

ed from the specimen. The debonds always occurred at the notch edges away from the center of the specimen. In the isochromatic images these areas have been blacked out, while in the isoclinic images, they are highlighted in white. The contours for the cross-ply laminates are shown in Figure 38 and Figure 39, the quasi-isotropic images are shown in Figure 40 and Figure 41, and the $[\pm 45]_{5S}$ images are shown in Figure 42, Figure 43, and Figure 44. Each image contains the isochromatic and the ±45° isoclinic contours. In the images containing two sets of isochromatic and isoclinic contours, the test that utilized a larger edge load value is located immediately below the results of the test utilizing the lower edge load.

Comparing the images of the second load step for each laminate to their respective numerical predictions in Section 1.5.2.2 it is seen that the both the cross-ply and quasi-isotropic laminates are in good agreement. Agreement for the $[\pm 45]_{5S}$ laminate, however, only occurs at the first load step. Above the first load step, when no edge load is applied, the orientation of the principal strains changes significantly, indicating that the specimen has slipped within the grips or another significant deformation has occurred within the specimen/fixture assembly. This same behavior is not seen when a significant edge load is applied, as the principal strain maintain their orientation throughout the load steps used.

Looking carefully at the isochromatics for each laminate shows that the maximum shear strain, $\gamma_{max} = |\varepsilon_1 - \varepsilon_2|$, increased when the torque applied to the edge loader bolt increased. The $[\pm 45]_{5S}$ laminate shows the greatest difference in the measured maximum shear strain between the two edge loader torque values. Each laminate also shows a difference in the isoclinics when the edge load was increased.

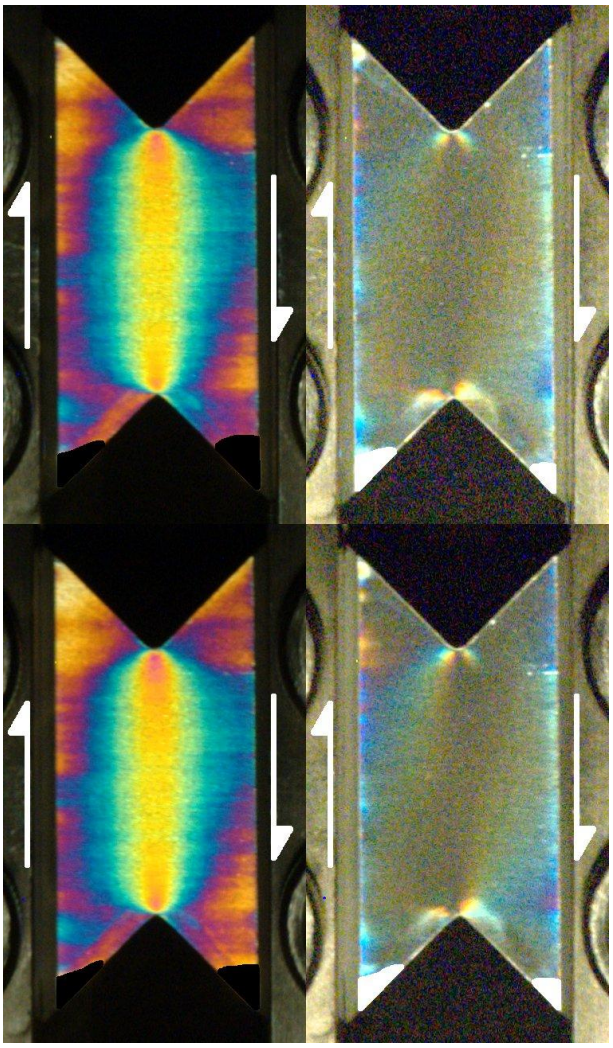

Figure 38: Isochromatic contours (left) and 45° isoclinic (right) for the $[0/90]_{4S}$ laminate at the second load value. The top images are at no edge load and the bottom images are at 40 N·m edge loader torque.

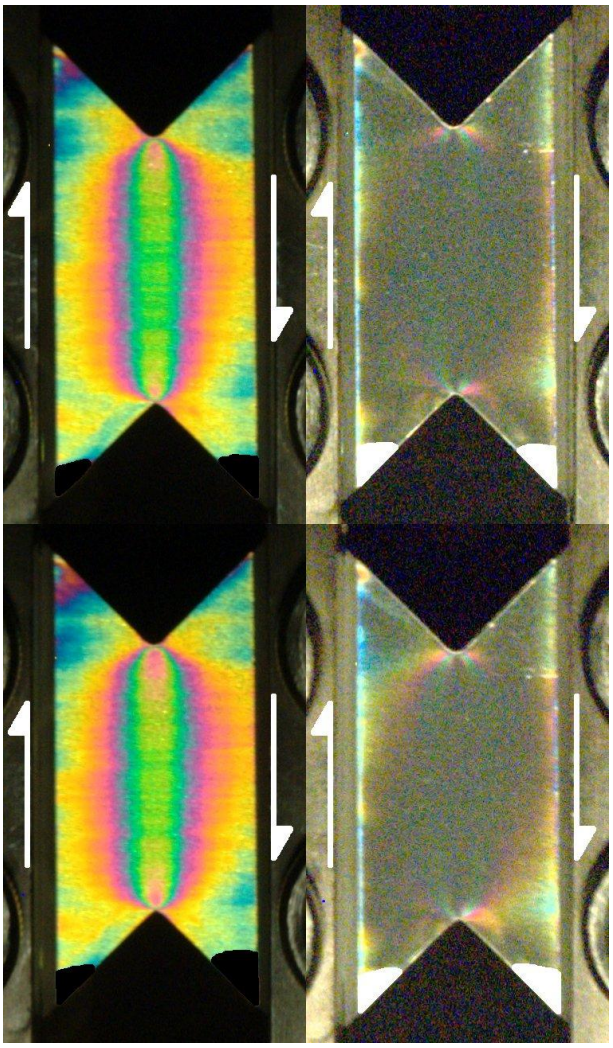

Figure 39: Isochromatic contours (left) and 45° isoclinic (right) for the [0/90]4S laminate at the third load value. The top images are at no edge load and the bottom images are at 40 N·m edge loader torque.

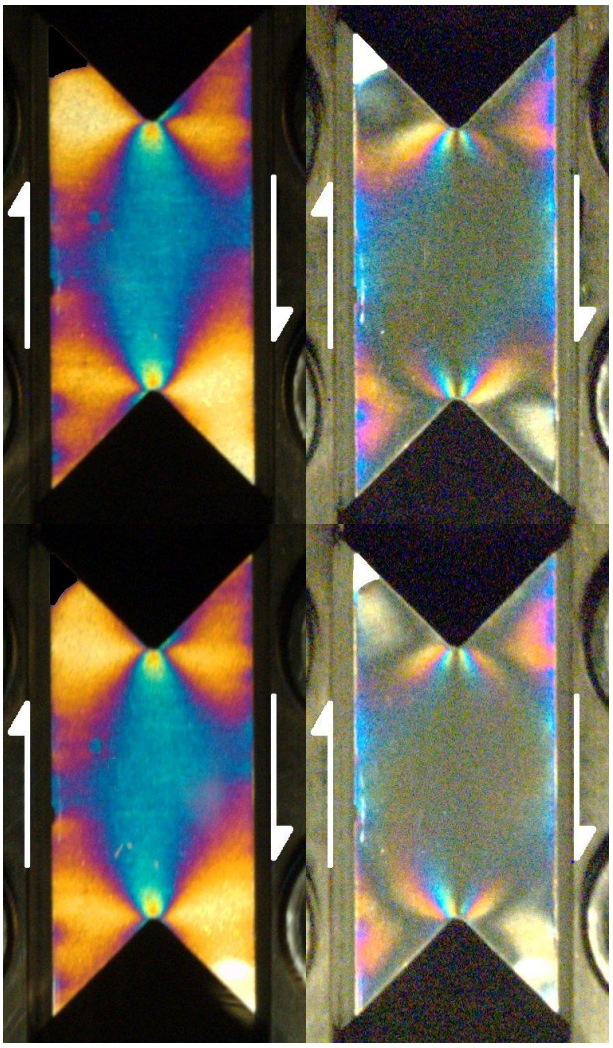

Figure 40: Isochromatic contours (left) and 45° isoclinic (right) for the $[0/\pm45/90]_{4S}$ laminate at the second load value. The top images are at no edge load and the bottom images are at 40 N·m edge loader torque.

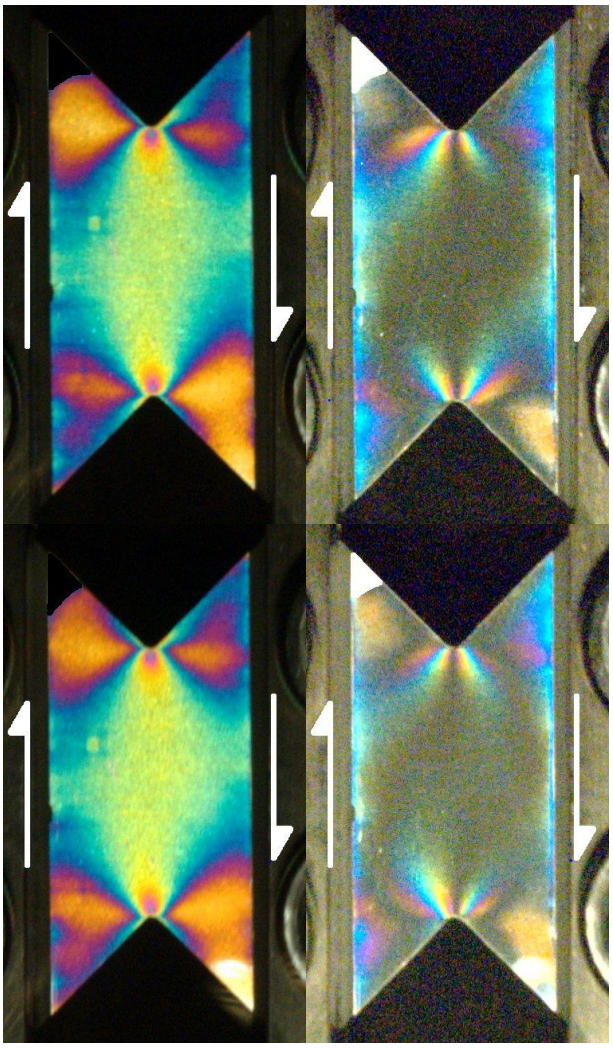

Figure 41: Isochromatic contours (left) and 45° isoclinic (right) for the $[0/\pm45/90]_{4S}$ laminate at the third load value. The top images are at no edge load and the bottom images are at 40 N·m edge loader torque.

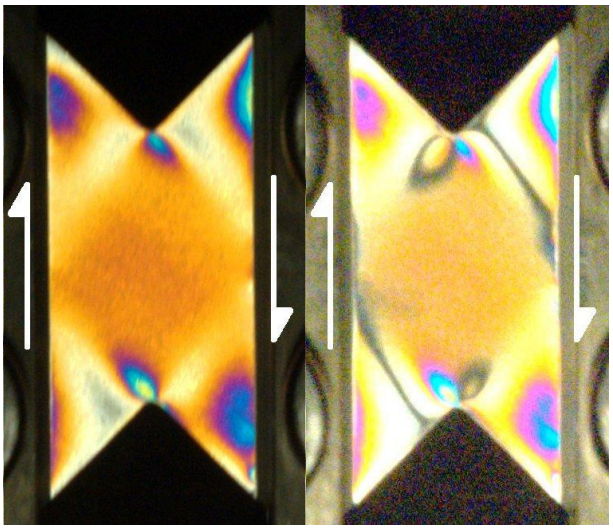

Figure 42: Isochromatic contours (left) and 45° isoclinic (right) for the $[\pm 45]_{5S}$ laminate at the first load value and no applied edge load.

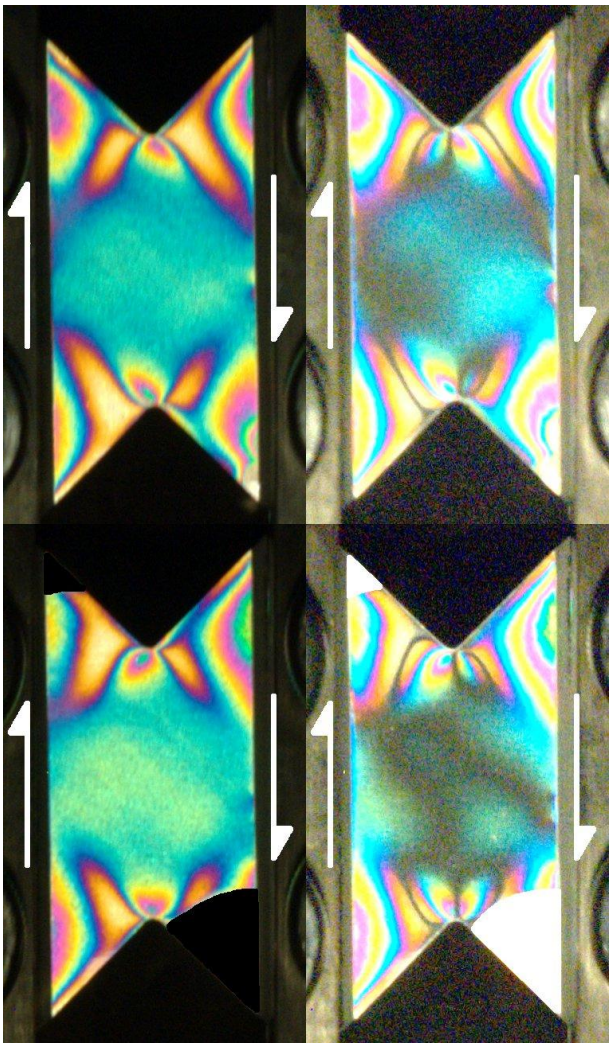

Figure 43: Isochromatic contours (left) and 45° isoclinic (right) for the $[\pm 45]_{5S}$ laminate at the second load value. The top images are at no edge load and the bottom images are at 40 N·m edge loader torque.

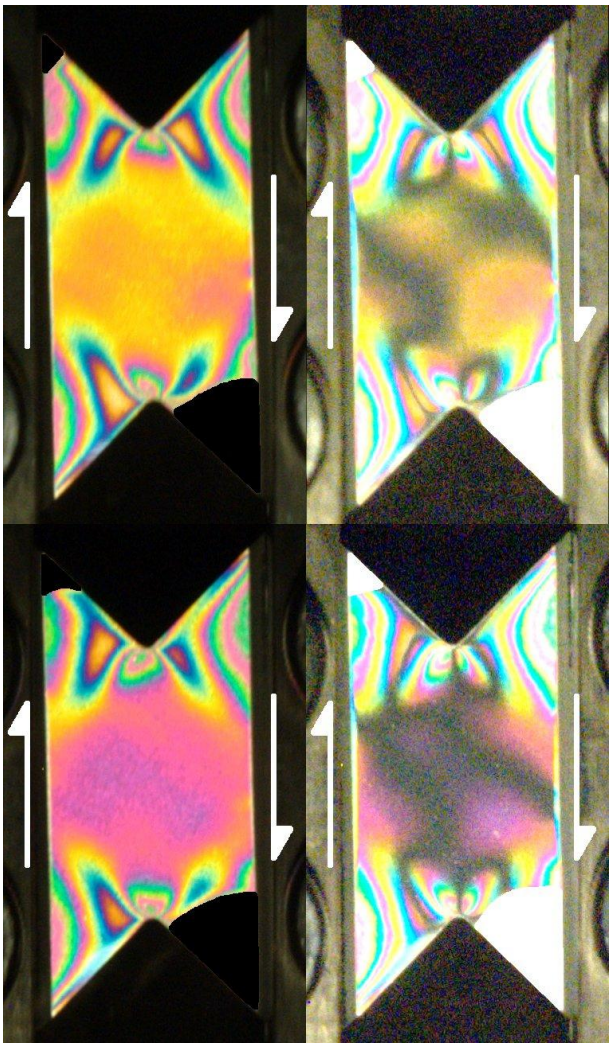

Figure 44: Isochromatic contours (left) and 45° isoclinic (right) for the $[\pm 45]_{5S}$ laminate at the third load value. The top images are at no edge load and the bottom images are at 40 N·m edge loader torque.

The cross-ply laminates do not show a large difference in the isochromatics, however, looking at the area near the notch tip shows a larger area of higher shear strain at 40 N·m (30 lbf·ft) torque than at finger tight conditions. The isoclinics at both edge load values encompass almost the entire gauge section. Because of this the isochromatics can be directly compared to the normalized shear stress contours for cross-ply laminates in [1]. The most critical area is the region between the notches, and both edge load values have a ±45° isoclinic along the specimen centerline.

The quasi-isotropic laminate has a much smaller region of preferred shear strain compared to the cross-ply, as evident by the isoclinics in Figure 40 and Figure 41. The isoclinics for this layup are distinct. In the test using a 'finger tight' edge load the isoclinics form crescents at the upper right and lower left of the test section centerline, and follow the faces of the notch flanks. At both load levels the specimen centerline attains the preferred shear strain state, and, apart from the regions near the notches, the strains along the centerline are highly uniform. The 40 N·m (30 lbf·ft) test shows a response somewhat similar to the test with no applied edge load; however, the isochromatics show a slightly higher fringe value between the notches in the 40 N·m (30 lbf·ft) test than in the test with no edge load. There are also differences in the shape of the isoclincs, which are more noticeable in Figure 41. Comparing the center of the isoclinic from the specimen tested with no edge load to the 40 N·m (30 lbf·ft) isoclinic in Figure 41, it is seen that the center of the 40 N·m (30 lbf·ft) test is slightly lighter in color indicating that the region has not obtained the preferred shear state. However, the difference is small and a lower edge loader bolt torque should provide a strain state sufficiently close to the strain state shown in Figure 40.

The isochromatic and isoclinc contours for the $[\pm 45]_{5S}$ laminate at the first load step are shown in Figure 42, while the second and third load value are shown in Figure 43 and Figure 44 respectively. Some general trends seen in the cross-ply and quasi-isotropic specimens are also present in this layup: larger edge loader torque results in higher shear strain, and the isoclinics change with a change in edge loader torque. A unique aspect not seen in the previous two is that the isoclincs in the test with no applied edge load changed with increasing load whereas the isoclinic for the 40 N·m (30 lbf·ft) test did not appear to change when the load increased. Furthermore, at the higher load the isoclinics in the no edge load test appear to be similar to those in the 40 N·m (30 lbf·ft) test. This indicates that stress state in this layup, when not applying a significant torque to the edge loader, will significantly change during testing.

The $[\pm 45]_{5S}$ layup also has a larger strain gradient near the notch tip than either the cross-ply or quasi-isotropic layups. Where, in the previous two layups, the strains from the notch tip to the center of the specimen varied by only a fraction of a fringe order, the $[\pm 45]_{5S}$ varied by more than one fringe order at high loads.

The results of the photoelastic tests are consistent with the shear strength results of Section 1.5.2.1. The higher strains, induced by the torque applied to the edge loader bolts, will result in lower measured ultimate shear strength. The $[\pm 45]_{5S}$ laminates are affected by this the most, evident by the higher difference in shear strains as a result of the increased edge load.

## 1.6 Conclusion

The goal of this study was to show that the Combined Loading Shear test is suitable for determining shear properties of composite laminates. Results of the numerical

simulations predict that the location of the inner loading point affects the stress state in the V-Notched shear specimen: moving the inner loading point away from the edge of the gauge section improves the stress state.

Testing using the Combined Loading Shear test fixture developed in this investigation produced shear strength values similar to those in the literature. The shear stress-displacement curves from testing shows a high repeatability using the new fixture. The investigation into the effect of the edge load demonstrated that using a large edge load will decrease the measured shear strength in cross-ply laminates. Results from the photoelastic testing showed that both the cross-ply and quasi-isotropic laminates have a desirable stress state between the notches, indicating that this test is well suited for these laminates. Based on the strength and photoelastic testing it is recommended that a torque of 10 N·m (7.4 lbf·ft) or less be applied to the edge loader bolts as larger values may have an adverse effect on the measured shear properties.

Based on the photoelastic results, care must be taken when interpreting the results obtained from a $[\pm 45]_{ns}$ laminate tested using the new fixture. Large strain concentrations exist near the notches and the orientation of the principal strains are not oriented to provide the desired shear strain state. Increasing the load on the edge loaders will somewhat improve the orientation of the principal strains; however, the strain magnitudes were shown to significantly increase.

Care must be taken when testing thin cross-ply laminates as the mass of the test fixture may be sufficient to damage the specimen while installing the fixture into the load frame. Installation of thinner laminates, in general, may be more susceptible to misalignment issues than thicker laminates. The instability in the secondary response of the

$[0/90]_{2S}$ laminate, in addition to previous published results indicates that the current V-Notched Rail Shear test method (ASTM D 7078) is sufficient for testing these thinner, lower shear strength laminates.

# 2 DESIGN AND VALIDATION OF A SHEAR EXTENSOMETER FOR CROSS- PLY LAMINATES TESTED USING THE V-NOTCHED RAIL SHEAR TEST

## 2.1 Introduction

Many isotropic materials exhibit failure when the resolved shear stress exceeds the shear yield strength. Shear testing for isotropic materials is relatively simple compared to shear testing for orthotropic composite laminates. In most instances the shear stress-shear strain response can be formulated from a simple torsion test. Strain measurement for torsion tests of isotropic materials can be accomplished through the use of bonded strain gauges and in many instances with extensometers. Extensometers offer several advantages over strain gauges. They are reusable, and installation is relatively straight forward and quick. Extensometers are also beneficial in that they only have a one time, upfront cost, whereas the costs of bonded strain gauges are recurring.

Shear testing for composite laminates is not as direct as for isotropic materials, and often requires specific test specimen geometries and specialized test fixtures. Currently, there are several standardized tests for determining shear properties of composite laminates, each with their own specimen geometry [1]. One of the more common methods is the V-Notched Rail Shear test (ASTM D 7078). This test method was designed to measure both the shear modulus and shear strength of fiber reinforced composites [3].

This test uses a rectangular V-Notched specimen, shown in Figure 45, which is shear loaded by applying a surface traction to the specimen faces. A typical assembled V-Notched Rail Shear test fixture showing the applied load is depicted in Figure 46.

The two main material properties obtained from shear testing are the in-plane shear modulus, $G_{xy}$, and the in-plane shear strength, $S_{xy}$. The calculation of both the shear modulus and the shear strength, as defined in ASTM D 7078, requires knowledge of the average shear stress, which is defined as the applied load divided by the cross sectional area of the specimen between the notch tips [3]. Calculation of the shear modulus also requires knowledge of the shear strain for each corresponding load measurement [3]. This makes it necessary to have some method of measuring the shear strain in the specimen. Several types of bonded strain gauges have been investigated as potential candidates for this test geometry [8], however, there is currently no strain gauge that is recommended for this test geometry. Additionally, there is no commercially available extens-

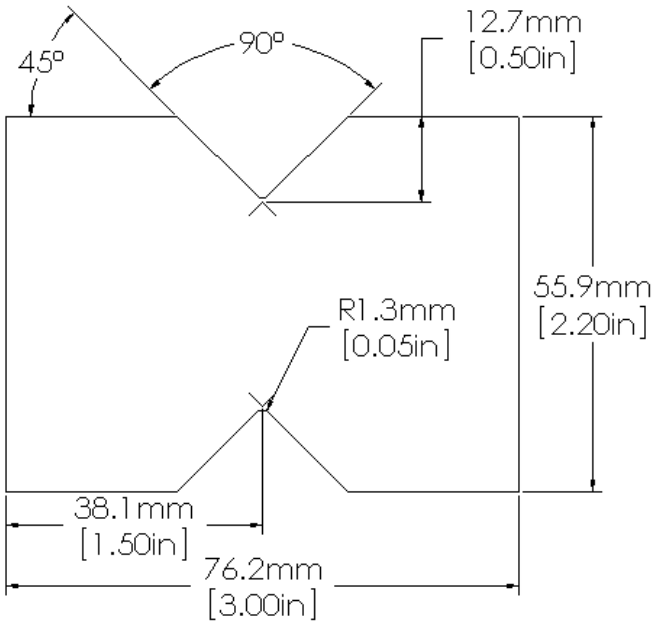


Figure 45: Dimensions of the test specimen for the ASTM D 7078 rail shear test.

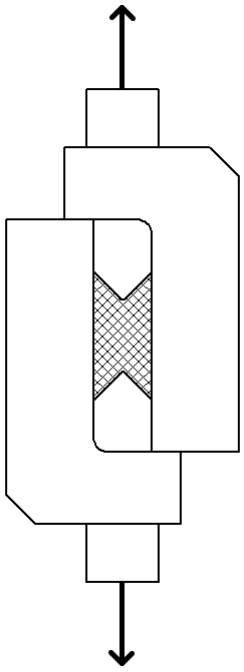

Figure 46: D 7078 test fixture and specimen showing loading direction.

ometer for this test. An extensometer, specifically designed for this shear test, would provide test engineers with a reusable alternative to bonded strain gauges.

A few attempts at making a reliable extensometer for shear testing of composite laminates have been made with varying degrees of success. One attempt was made by Walrath and Adams [4] wherein they modified an axial extensometer to attach to a V-Notched Beam Shear specimen. In their study they performed several numerical simulations of the extensometer's response; however no experimental validation was reported [4]. Their study looked at one position for the extensometer, and the shear modulus calculated from the extensometer's proposed attachment points differed from that supplied to the numerical model by approximately +15% to -8% depending on the specimen material properties and the specimen notch angle. Other attempts at building an extensometer for the V-Notched Beam Shear specimen have also been performed at the University of Utah.

In an unpublished study performed at the University of Utah [9] mechanical tests were performed on an aluminum specimen as well as specimens made from a carbon/epoxy composite material. The experimental results from this study showed some agreement with the conclusions reached by Walrath and Adams [4] in that the gauge was not able to accurately measure the shear strain and the error in shear modulus calculations between the extensometer and bonded strain gauges was dependent on the material system.

One of the difficulties in developing an extensometer for the V-Notched Beam Shear specimen is the small test region in which to measure deformation. This makes it difficult not only to attach the extensometer but also to accurately machine the device so that the attachment points are placed in the optimal location. The gauge section of the V-Notched Rail Shear specimen is almost three times larger than a V-Notched Beam Shear specimen, which should allow for easier manufacturing and installation of the device. The larger test region is also beneficial when testing laminates made from coarse textiles with large unit cells. The V-Notched Rail Shear test is also capable of testing higher strength laminates than is possible with the V-Notched Beam Shear test. The attractive properties that the V-Notched Rail Shear test has over the V-Notched Beam Shear test, and the requirement of have an accurate measure of the shear strain in order to determine fundamental material properties of orthotropic laminates is the motivation for this study.

## 2.2 Analysis

From a mechanics of materials approach, when an element is subjected to only shear stresses, as shown in Figure 47(a), the element undergoes a shear strain (Figure 47(b)) and the normal strains in the reference coordinates are zero. Opposite sides of that element remain parallel during deformation, and, if the strains are small, the change in

length of each side of the element due to the deformation can be neglected. Reorienting the deformed element with the coordinate axes, either by rotating the deformed element through an angle of +γ/2, or rotating the coordinate axis through an angle of -γ/2, the engineering shear strain, γ, can be calculated from the equation:

$$\gamma = \tan^{-1}\frac{d}{L'} \tag{5}$$

where $d$ is the relative vertical displacement of the right side of the element and $L'$ is the horizontal space between the two vertical lines (Figure 47(c)). For small values of γ, $L'$ can be approximated by the undeformed element length, $L$, and Equation (5) becomes

$$\gamma = \tan^{-1}\frac{d}{L} \tag{6}$$

From this expression it would seem reasonable that engineering shear strain could be determined by measuring the relative vertical displacement of a set of parallel vertical lines on the surface of a specimen subjected only to shear stresses. The shear modulus

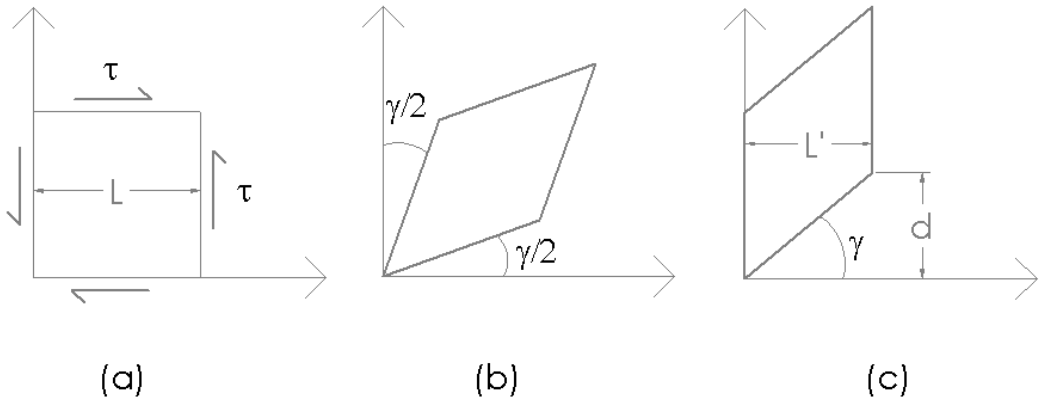


Figure 47: Depiction of the deformations of a mechanical element subjected to a shear stress.

could then be determined using a linear elastic model of Hooke's law in shear:

$$G_{xy} = \frac{\tau_{xy}}{\gamma} = \frac{\tau_{xy}}{\tan^{-1}(d/L)} \tag{7}$$

In this study it is proposed that the measurement of *d* can be accomplished by monitoring the deflections of a set of four points located at the corners of a rectangular element, like that shown in Figure 47.

The work leading up to the standardization of the V-Notched Rail Shear test has shown that the stress state in the gauge section of the specimen is one of highly uniform shear; however, it is not absent of normal stresses. The numerical analyses performed by Adams, Moriarty, Gallegos, and Adams [1] have shown that the region of uniform shear stress is affected by the degree of orthotropy. Additionally, orthotropy also influences the degree to which the normal components of stress are present in the test region [1]. The central region of the specimen is relatively free from the normal components of stress; however, near the outer regions of the gauge section these normal components become more pronounced. These results would imply that the choice of *d* and *L* cannot be chosen arbitrarily if an accurate measure of the average shear strain is desired.

When calculating the shear modulus from a V-Notched Rail Shear test, the average shear stress and average shear strain over the range of 0.002-0.006 is used. Based on the varying stress state described above, any two different choices of *d* and *L* when applying Equation (7) may yield different values for the shear modulus. Previous numerical modeling, which looked at one possible location for the attachment points, showed that the accuracy of this method of measuring shear strain in a V-Notched Rail Shear specimen is dependent on the laminate layup [10], much like the work performed on the V-

Notched Beam Shear specimen. The results from the materials used in [10] are shown in Table 9. These data would imply that there may not be a single suitable location for the attachment points that will satisfactorily provide shear strains in all possible material systems and laminates.

When calculating the shear modulus from a V-Notched Rail Shear test, the average shear stress and average shear strain over the range of 0.002-0.006 is used. Based on the varying stress state described above, any two different choices of *d* and *L* when applying Equation (7) may yield different values for the shear modulus. Previous numerical modeling, which looked at one possible location for the attachment points, showed that the accuracy of this method of measuring shear strain in a V-Notched Rail Shear specimen is dependent on the laminate layup [10], much like the work performed on the V-Notched Beam Shear specimen. The results from the materials used in [10] are shown in Table 9. These data would imply that there may not be a single suitable location for the attachment points that will satisfactorily provide shear strains in all possible material systems and laminates.

One of the most important layups to quantify is the unidirectional laminate. However, obtaining reliable shear test data from unidirectional composite materials is difficult

Table 9: Numerical results showing the shear modulus supplied to the simulation, $G_{xy,Input}$, and the shear modulus calculated from Equation (7), $G_{xy,Calc}$ [10].

| Material | $G_{xy,Input}$ [GPa] | $G_{xy,Calc}$ [GPa] | Difference [%] |
|---|---|---|---|
| Aluminum | 25.9 | 26.8 | 3.45 |
| AS4/3501 $[\pm 45]_{4S}$ | 37.6 | 36.4 | -3.24 |
| AS4/3501 $[0/\pm 45/90]_{2S}$ | 21.7 | 22.1 | 1.76 |
| AS4/3501 $[0]_{16}$ | 5.86 | 6.11 | 4.31 |

[4, 6, 7]. It has been recommended that in order to obtain the shear modulus for a unidirectional composite laminae, a $[0/90]_{ns}$ laminate be used in testing as opposed to the unidirectional layup [1,11]. For this reason it was decided to limit the scope of the current investigation to $[0/90]_{ns}$ laminates that fall within the thickness guidelines specified in ASTM D 7078: 2 mm to 5 mm (0.080 in. to 0.200 in.).

### 2.2.1 Numerical Modeling

Two separate solid models were built in SolidWorks to investigate the thinnest and thickest specimens recommended in ASTM D 7078. Each model included the fixture geometry in addition to the specimen in order to simulate an actual test. The model was then imported into ANSYS Workbench 11.0. Symmetry about the specimen mid-plane was employed. The bolts which secure the specimen in the fixture, and their corresponding fixture holes, were omitted in order to simplify the model. The entire solid model is shown in Figure 48. Frictional contact between the specimen and the fixture grips was included in the model. The clamping loads of each bolt were applied to the grip plates. The forces applied by the bolt to the grip plates were placed at the proper locations corresponding to the standardized shear fixture. The load used for each bolt was 28.9 kN (6.50 kip). The top and bottom of the grip plates were modeled as being bonded to the fixture. In work performed by Johnson, a similar finite element simulation was investigated for adequate mesh refinement using the maximum shear stress as the criteria [5]. It was determined that an element size of 1.02 mm (0.04 in.) and smaller provided adequate refinement. The element size, on the free surface of the specimen test region, was 0.762 mm (0.030 in.). A mapped mesh was used on the gauge section of the specimen in order to facilitate shear strain calculations from the displacements of a rectangular set of nodes.

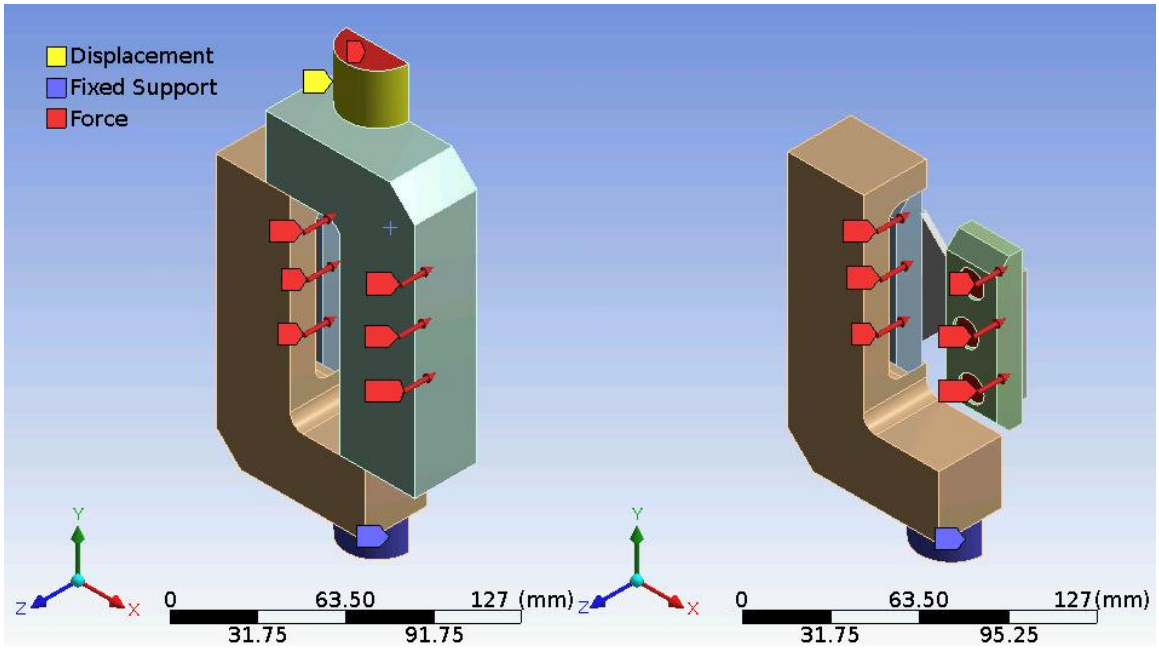


Figure 48: Boundary conditions applied to the finite element model. Left: the entire model as used in the simulations. Right: upper fixture half hidden to show the grip plates and the clamping bold loads.

The specimen mesh is shown in Figure 49.

The bottom portion of the lower fixture half was given a zero displacement boundary condition in the X, Y, and Z directions (item C in the left side of Figure 48) while the top portion of the upper fixture half was given a zero displacement boundary condition in only the X and Z directions thereby permitting the fixture to move in only the Y direction. The XY symmetry plane was constrained in the Z direction. A load was applied in the + Y direction to the upper portion of the upper fixture half (item J in the left side of Figure 48). The magnitude of the load was selected to produce an estimated shear strain of 0.006 in the test section of the specimen.

Simulations were performed for specimen thicknesses of 2 mm (0.080 in.) and 5 mm (0.200 in.). Both simulations used two load steps in the solution: the first was the clamping forces applied by the fixture bolts, and the second was the tensile load applied

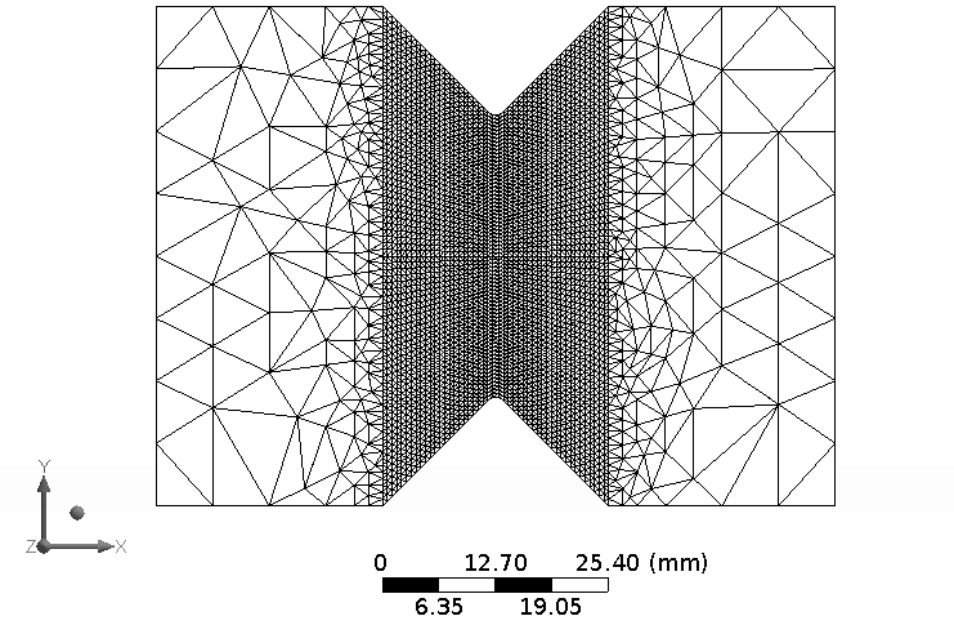


Figure 49: Mesh applied to the specimen. The notched region utilizes a mapped mesh with an element size of 0.762 mm (0.03 in.).

to the fixture.

A total of 33,933 nodes and 17,451 10 node tetrahedron elements (Solid187) were used in the 5 mm thick specimen model, with 28,513 nodes and 14,791 elements used in the specimen itself. The simulation for the 2 mm thick specimen utilized a total of 28,715 nodes and 12,847 elements with 23,268 nodes and 10,212 elements used in the specimen. Quadratic triangular contact and target elements (Conta174 and Targe170, respectively) were used to model the contact between the specimen and the grip faces as well as between the grip faces and the fixture half. A total of 762 contact elements were used in the 5 mm thick specimen model and 1092 contact elements were used in the 2 mm thick specimen model.

Validation of the numerical model was accomplished using photoelasticity. The nodal in-plane strains ($\varepsilon_x$, $\varepsilon_y$, and $\gamma_{xy)}$ on the specimen free surface were exported to a text

file and manipulated in a MATLAB program to give the maximum shear strain, $\gamma_{max}$, and the direction of the principal strains. Material properties of an $[0/90]_{4S}$ laminate of IM7/8552 carbon/epoxy, with an average cured ply thickness of 0.316 mm (0.0124 in.), were used in this simulation. A 2.0 kN (450 lbf) tensile load was applied to the fixture. This load corresponds to a 4.0 kN (900 lbf) load used in the photoelastic test.

### 2.2.2 Material Systems

As mentioned previously, material layups used in study were limited to $[0/90]_{ns}$ laminates. In order to ascertain how much variability may exist in shear strain distributions among various composite materials, several different material systems were considered following the numerical work performed by Adams and Doner [13,14]. In their work, Adams and Doner calculated the transverse tensile modulus, $E_2$, and the in-plane shear modulus, $G_{12}$, of a unidirectional fiber reinforced lamina based on the individual moduli of the fiber, $E_f$, and the matrix, $E_m$, as well as the fiber volume fraction of the composite. The fibers were modeled in a square array within the matrix. Several fiber volume fractions were modeled, and the results obtained for the transverse modulus and the in-plane shear modulus were normalized with respect to the matrix tensile modulus and shear modulus respectively. These results were used to derive the lamina properties for a range of composite materials based on their normalized constituent stiffness ratios, $E_f/E_m$. The calculation of the lamina properties assumed a fiber modulus, $E_f$, of 200, a major Poisson's ratio for the fiber, $\nu_{f12}$, of 0.200, a minor Poisson's ratio for the fiber, $\nu_{f21}$, of 0.001, and a Poisson's ratio for the matrix, $\nu_m$, of 0.38. The shear modulus for the matrix was calculated from the equation relating the tensile modulus to the shear modulus for an isotropic linear elastic material:

$$G_m = \frac{E_m}{2(1+\nu_m)} \tag{8}$$

Lastly, the out-of-plane lamina shear modulus, $G_{23}$, was calculated according to the following relation for a transversely isotropic material:

$$G_{23} = \frac{E_2}{2(1+\nu_{23})} \tag{9}$$

where $\nu_{23}$ was taken to be 0.4. The resulting lamina properties are shown in Table 10.

The material properties given in references [13,14] were unitless. As such, the material properties shown in Table 10 were given units of GPa. Using the properties listed in Table 10 and the simplifying assumption that for a and transversely isotropic lamina $E_3 = E_2$, $G_{13} = G_{12}$, $\nu_{12} = \nu_{13}$, $\nu_{21} = \nu_{31}$, and $\nu_{23} = \nu_{32}$, laminated plate theory was used to obtain the 3D material properties for a $[0/90]_{ns}$ laminate. The laminate properties

Table 10: Lamina properties used in calculating the material properties of a $[0/90]_{ns}$ laminate.

| $v_f$ | $E_m$ | $E_2$ | $E_1$* | $\nu_{12}$* | $\nu_{21}$+ | $G_{12}$ | $G_{23}$ |
|---|---|---|---|---|---|---|---|
| 0.55 | 1 | 4.64 | 110 | 0.281 | 0.012 | 1.26 | 1.68 |
| | 2 | 8.77 | 111 | 0.281 | 0.022 | 2.33 | 3.13 |
| | 5 | 19.3 | 112 | 0.281 | 0.048 | 4.83 | 6.89 |
| | 10 | 33.9 | 115 | 0.281 | 0.083 | 7.50 | 12.1 |
| | 50 | 102 | 133 | 0.281 | 0.217 | 18.0 | 36.5 |
| | 200 | 200 | 200 | 0.281 | 0.281 | 71.9 | 71.4 |
| 0.70 | 1 | 9.80 | 110 | 0.281 | 0.025 | 2.34 | 3.50 |
| | 2 | 18.1 | 111 | 0.281 | 0.046 | 4.05 | 6.48 |
| | 5 | 38.6 | 112 | 0.281 | 0.097 | 7.20 | 13.8 |
| | 10 | 60.4 | 115 | 0.281 | 0.148 | 9.82 | 21.6 |
| | 50 | 100 | 133 | 0.281 | 0.212 | 18.0 | 35.7 |
| | 200 | 200 | 200 | 0.281 | 0.281 | 71.9 | 71.4 |

*Values calculated using the rule of mixtures.
+Values calculated using reciprocity.

are shown in Table 11. The material properties of the laminate with a fiber volume fraction of 0.70 and a matrix tensile modulus equal to the fiber tensile modulus were not simulated as the resulting material properties were identical to those with a fiber volume ratio of 0.55 and equal matrix and fiber tensile moduli.

In addition to the material properties listed in Table 11, several common engineering materials, listed in Table 12, were also simulated. The properties listed are representative of an AS4/3501 and IM7/8552 $[0/90]_{ns}$ carbon/epoxy laminate as well as a 6061 aluminum alloy. For reference, the constituent stiffness ratios, $E_m/E_f$, of AS4/3501 and IM7/8552 are 54.5 and 59.1, respectively.

### 2.2.3 Postprocessing

For each material simulated, the *x* and *y* displacements were output to a text file for postprocessing. A script was written in MATLAB that read in the *x* and *y* displace

Table 11: Laminate properties for a $[0/90]_{ns}$ laminate used in the numerical simulations.

| $v_f$ | $E_m$ [GPa] | $E_x$ [GPa] | $E_y$ [GPa] | $E_z$ [GPa] | $G_{xy}$ [GPa] | $G_{xz}$ [GPa] | $G_{yz}$ [GPa] | $\nu_{xy}$ | $\nu_{yz}$ | $\nu_{xz}$ |
|---|---|---|---|---|---|---|---|---|---|---|
| 0.55 | 1 | 57.7 | 57.7 | 5.41 | 1.26 | 1.46 | 1.46 | 0.023 | 0.391 | 0.391 |
| | 2 | 60.1 | 60.1 | 10.1 | 2.33 | 2.73 | 2.73 | 0.041 | 0.386 | 0.386 |
| | 5 | 66.3 | 66.3 | 21.4 | 4.83 | 5.86 | 5.86 | 0.082 | 0.375 | 0.375 |
| | 10 | 74.8 | 74.8 | 36.4 | 7.50 | 9.81 | 9.81 | 0.128 | 0.365 | 0.365 |
| | 50 | 118 | 118 | 104 | 18.0 | 27.2 | 27.2 | 0.243 | 0.344 | 0.344 |
| | 200 | 201 | 201 | 201 | 71.9 | 71.7 | 71.7 | 0.277 | 0.342 | 0.342 |
| 0.70 | 1 | 75.4 | 75.4 | 11.3 | 2.34 | 2.92 | 2.92 | 0.037 | 0.387 | 0.387 |
| | 2 | 79.9 | 79.9 | 20.4 | 4.05 | 5.26 | 5.26 | 0.064 | 0.380 | 0.380 |
| | 5 | 90.7 | 90.7 | 41.6 | 7.20 | 10.5 | 10.5 | 0.120 | 0.366 | 0.366 |
| | 10 | 102 | 102 | 63.5 | 9.82 | 15.7 | 15.7 | 0.167 | 0.356 | 0.356 |
| | 50 | 128 | 128 | 102 | 18.0 | 26.9 | 26.9 | 0.219 | 0.347 | 0.347 |
| | 200 | 201 | 201 | 201 | 71.9 | 71.7 | 71.7 | 0.277 | 0.342 | 0.342 |

Table 12: Material properties of some common fiber/epoxy laminates and isotropic materials used in the numerical model.

| Material | $E_x$ | | $E_y$ | | $E_z$ | | $G_{xy}$ | | $G_{xz}$ | | $G_{yz}$ | | $\nu_{xy}$ | $\nu_{xz}$ | $\nu_{yz}$ |
|---|---|---|---|---|---|---|---|---|---|---|---|---|---|---|---|
| | [GPa] | [Msi] | [GPa] | [Msi] | [GPa] | [Msi] | [GPa] | [Msi] | [GPa] | [Msi] | [GPa] | [Msi] | | | |
| IM7/8552 | 88.3 | 12.80 | 88.3 | 12.80 | 13.5 | 1.960 | 4.96 | 0.719 | 4.21 | 0.611 | 4.21 | 0.611 | 0.041 | 0.410 | 0.410 |
| AS4/6501 | 77.5 | 11.2 | 77.5 | 11.2 | 11.2 | 1.62 | 5.86 | 0.85 | 4.66 | 0.68 | 4.66 | 0.68 | 0.03 | 0.37 | 0.37 |
| Al 6061 | | 68.90 | | | 9.993 | | | 25.90* | | | 3.757* | | | 0.330 | |
| Steel | | 200 | | | 29.00 | | | 75.19* | | | 11.15* | | | 0.300 | |

*Value was derived from Equation (8) and was not supplied to the model.

ments, the in-plane shear modulus, $G_{xy}$, and the average shear stress. Using Equation (7), the shear modulus was calculated based on nodal displacements, $G_{calc}$. Only nodes whose undeformed coordinate values ranged from -12.7 mm (-0.5 in.) $\leq x \leq$ 12.7 mm (0.5 in.) and -13.97 mm (-0.55 in.) $\leq y \leq$ 13.97 mm (0.55 in.) were considered. In each calculation it was required that the four nodal locations that correspond to the corners of the rectangle described in Figure 47(a) would be symmetric about the *x* and *y* axes. That is, for a given shear modulus calculation the four points would be at (-*x*, *y*), (*x*, *y*), (*x*, -*y*), and (-*x*, -*y*). Because the coordinate pairs are symmetric about x and y only one pair are used to represent the entire set. Once the shear modulus was calculated from the numerical simulation, the percent difference between the apparent value, $G_{calc}$, and the material property input, $G_{xy}$, was determined. Contour plots of the percent difference were then created for each material property set in order to show which areas in the region of interest produced the most accurate approximation of the shear modulus value supplied to the numerical model. Thus, the x, y coordinate pair was sought which minimized the percent difference across all laminates under consideration. To accomplish this, the Root Mean Square (RMS) of the percent difference values at each node was calculated and plotted.

### 2.2.4 Results

As mentioned previously, the region within the gauge section under consideration for possible points of measurement was bound by a 25.4 mm (1.00 in.) by 27.94 mm (1.10 in.) region centered at the specimen's geometric center. This region has been superimposed onto the specimen drawing in Figure 50 and is depicted by the dashed line. Because the measurement points were required to be symmetric about x and y, the contour plots showing the percent difference in shear modulus between the calculated and sup-

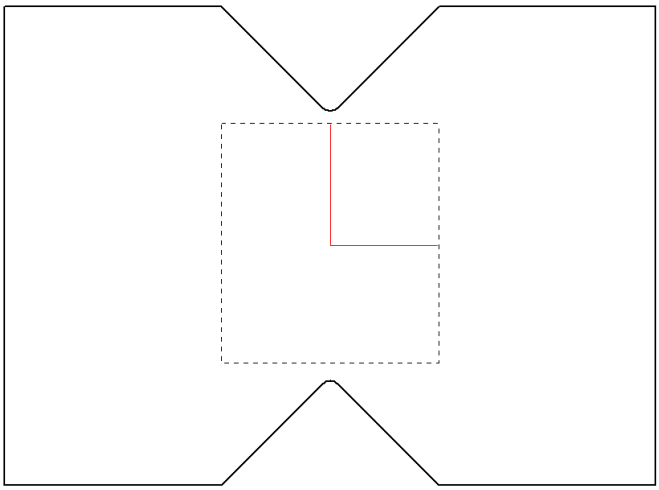

Figure 50: D 7078 specimen showing the region where Equation (7) was applied. The dashed line represents the entire region sampled and the solid line is the area which the following contour plots occupy.

plied shear modulus only occupy one quadrant of the coordinate system. All of the following contour plots reside in the region denoted by the solid red lines in the center of Figure 50.

The RMS values of the percent difference between the $G_{calc}$ and $G_{xy}$ for constituent stiffness ratios ($E_f/E_m$) ranging from 4 to 40 are shown in Figure 51. The difference data for the IM7/8552 and AS4/3501 was included when calculating the RMS values in order to weight the results toward carbon/epoxy composites with similar constituent stiffness ratios. A minimum RMS value of 0.209 % was calculated at the coordinates (1.435, 9.8425) mm ((0.0565, 0.3785) in.). This *x*, *y* coordinate pair corresponds to a notch height to vertical point separation distance of 1.59 and notch height to horizontal attachment point separation distance ratio 10.6. This vertical separation distance does not pose a manufacturing problem as it is significantly larger than that of an earlier design [10]. However, the horizontal attachment point spacing would be difficult to accommodate due to their close proximity and the size of the set screws that were used as attachment points

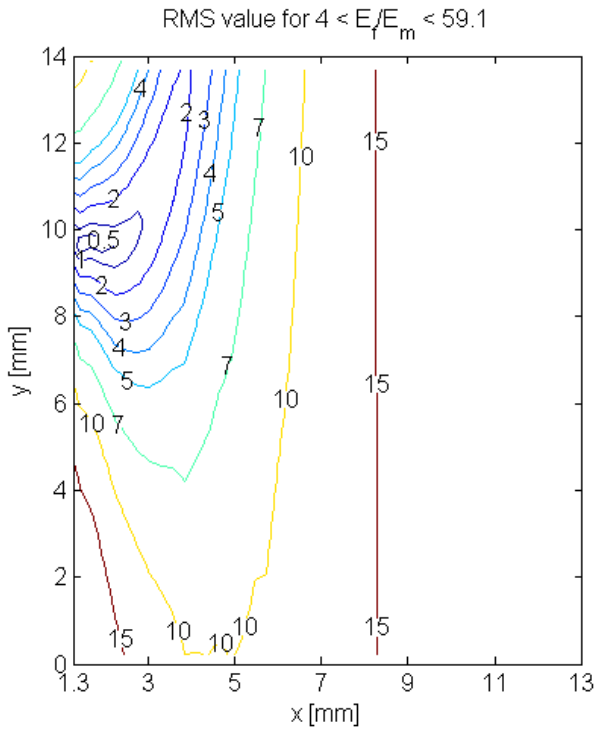


Figure 51: RMS values of the percent difference between the calculated and supplied shear modulus values using a constituent stiffness ratio range of 4-59.1.

in this study. The close spacing would also likely produce stability issues once the extensometer is installed onto the specimen. In order to alleviate the manufacturing and stability issues, a larger horizontal spacing was sought that would still maintain a reasonably small RMS value. From the results presented in Figure 51, the coordinate of (2.54, 9.83) mm ((0.100, 0.387) in.) produces a RMS value of the percent differences of 0.74%. At these coordinates the notch width to vertical and horizontal separation distance ratio is 1.55 and 6.00, respectively. This horizontal separation distance is similar to that in the earlier extensometer design [10], while the vertical separation is significantly larger and should provide greater stability than the previous design.

Contour plots showing the percent difference in shear modulus between the calculated and supplied shear modulus for the materials investigated are shown in Figure 52

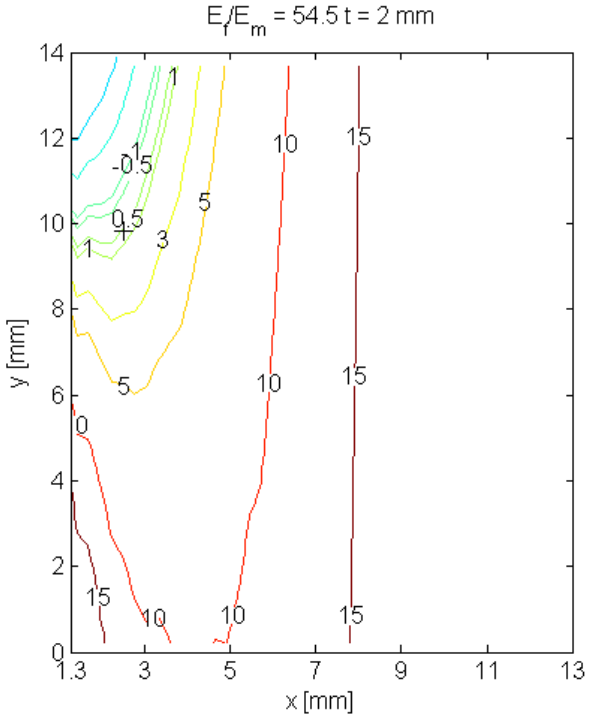


Figure 52: Shear modulus percent difference for AS4/3501.

through Figure 59. In order to visualize the expected error for this set of attachment points this position has been indicated by a + sign in each contour plot.

Referring to Figure 54 to Figure 59, it is seen that increasing the modulus of the matrix relative to the fiber modulus has the effect of moving the region bounded by the +1% and -1% error contours toward the x axis and away from the y axis. The numerical results predict that the proposed attachment points will result in errors in shear modulus measurement no greater than approximately ±1% for constituent stiffness ratios ranging from 4 to 59. The contours for materials with a constituent ratio of 20, shown in Figure 56 and Figure 57, predict that the error in the calculated shear modulus is within ±0.5%. Based on these results, it was concluded that a set of attachment points with a 5.1 mm (0.200 in.) horizontal and 19.7 mm (0.774 in.) vertical separation distance should provide acceptably accurate shear modulus measurements. For reference, the percent difference

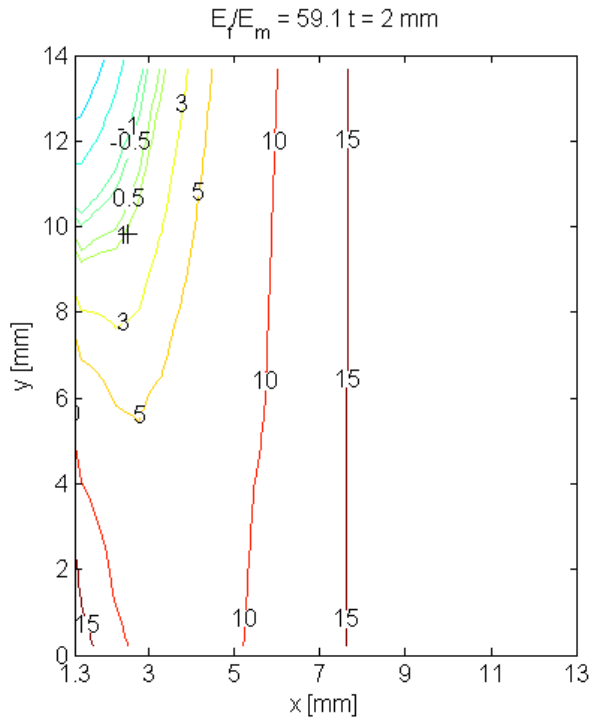


Figure 53: Shear modulus percent difference for IM7/8552.

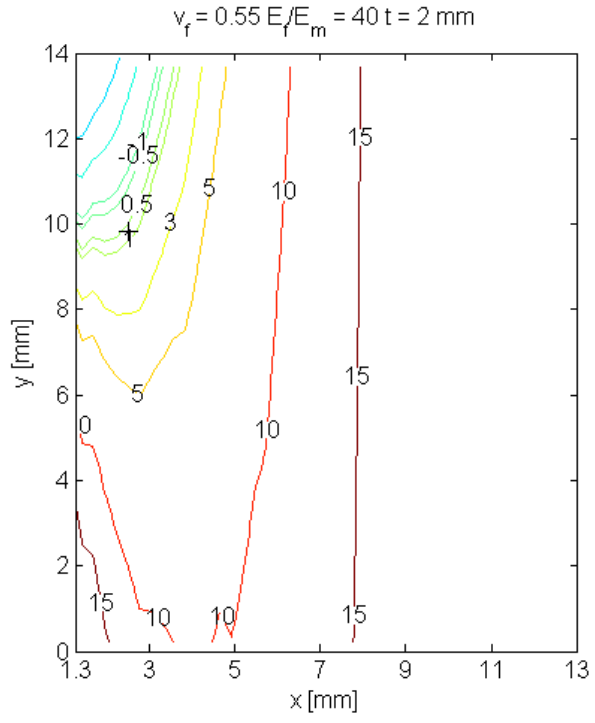


Figure 54: Shear modulus percent difference for a fiber volume fraction of 0.55 and a constituent stiffness ratio of 40.

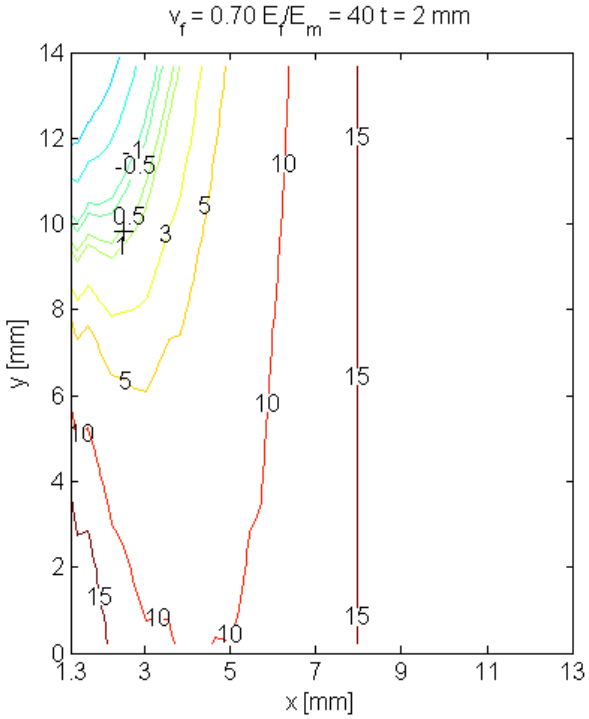


Figure 55: Shear modulus percent difference for a fiber volume fraction of 0.70 and a constituent stiffness ratio of 40.

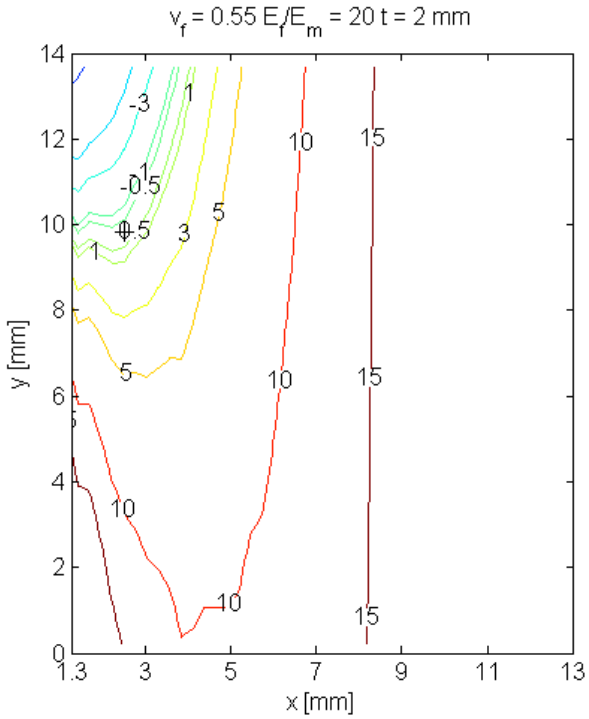


Figure 56: Shear modulus percent difference for a fiber volume fraction of 0.55 and a constituent stiffness ratio of 20.

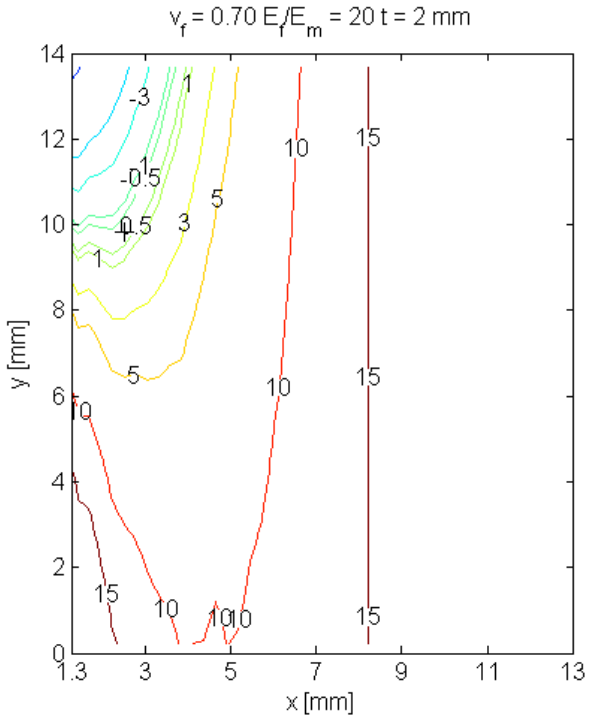


Figure 57: Shear modulus percent difference for a fiber volume fraction of 0.70 and a constituent stiffness ratio of 20.

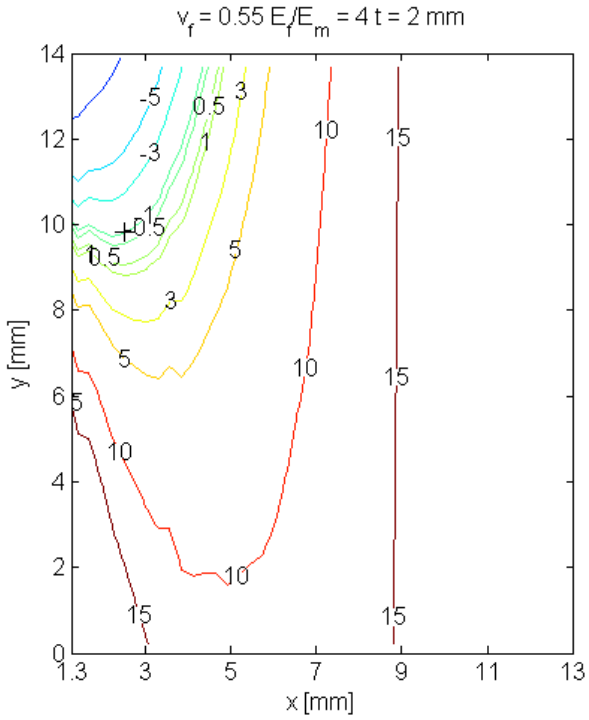


Figure 58: Shear modulus percent difference for a fiber volume fraction of 0.55 and a constituent stiffness ratio of 4.

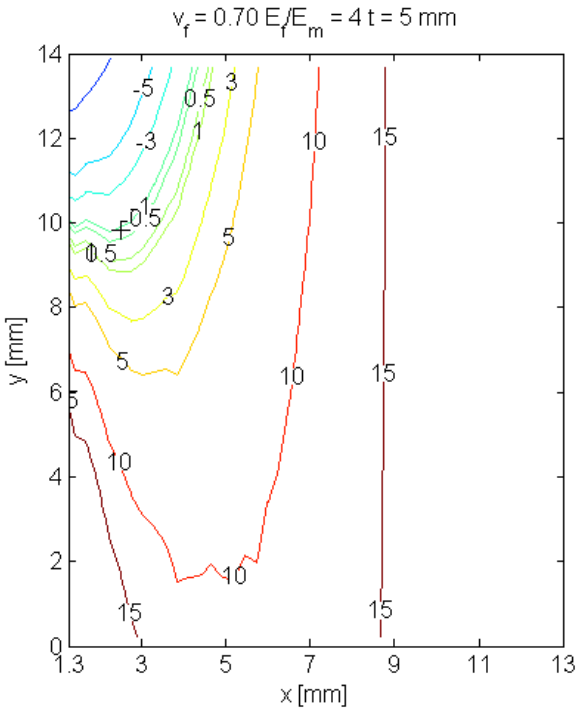


Figure 59: Shear modulus percent difference for a fiber volume fraction of 0.70 and a constituent stiffness ratio of 4.

contours for an isotropic aluminum alloy are shown in Figure 60.

## 2.3 Mechanical Testing

### 2.3.1 Shear Strain Extensometers

Two extensometers were manufactured for experimental testing. A diagram of the extensometer detailing its major components is shown in Figure 61. The extensometer halves used for testing are shown in Figure 62. Each device is assembled in a double fixed cantilevered beam configuration. Two sensing elements are used in each extensometer half in order for the attachment points to remain planar to the specimen face during deflection. Each sensing element is instrumented with two single grid strain gauges and together the beams of each extensometer are wired in a full Wheatstone bridge circuit. The sensing elements were made from steel shim stock while the remaining components,

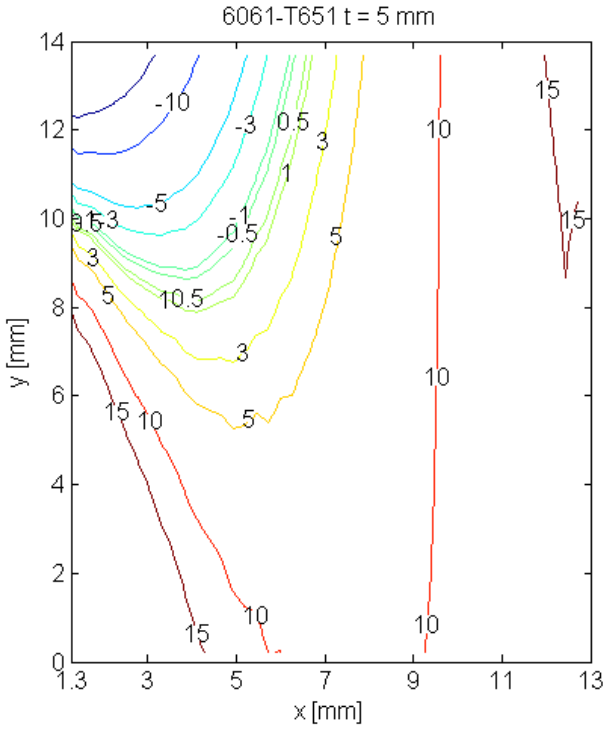


Figure 60: Shear modulus percent difference for an isotropic 6061 aluminum alloy.

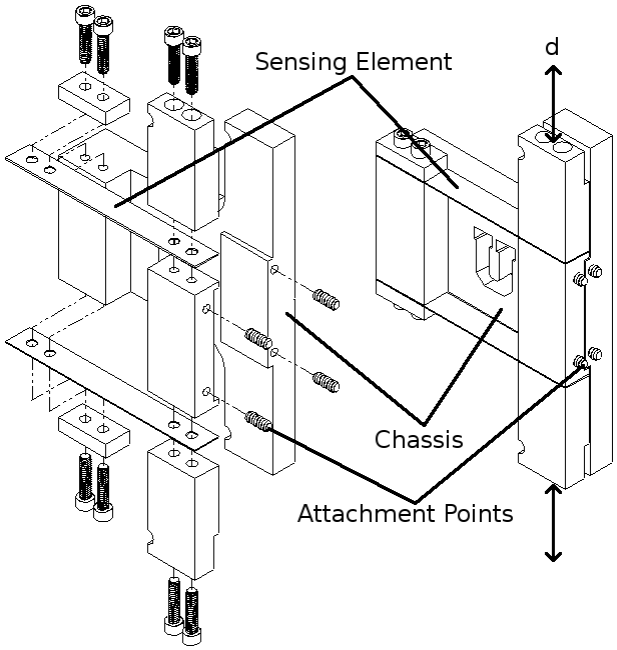


Figure 61: Exploded view of the shear extensometer. The left set of attachment points move through a vertical displacement d during a test.

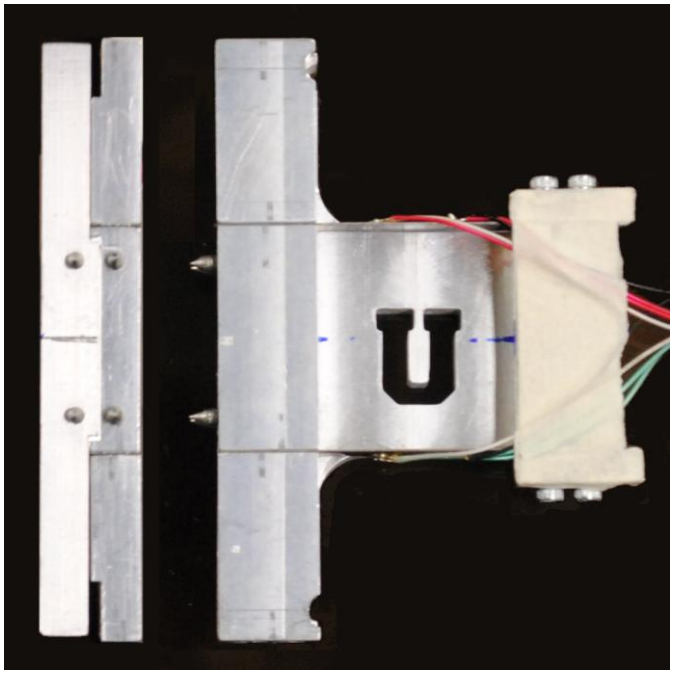

Figure 62: Front and side view of one extensometer used for testing.

apart from the cap screws and attachment points, were made from 6061 aluminum. As seen in Figure 61 the attachment points are located on the front face of the extensometer. The left set of attachment points are permitted to move vertically, relative to the right set of attachment points on the chassis. The relative displacement is measured via the strain gauges bonded to the steel strip.

A calibration factor was determined for each extensometer half that related the strain measured by the bridge circuit to the displacement imparted on the extensometer. This was accomplished experimentally by securing the extensometer in a vice and positioning a dial indicator to measure the displacement of the free end. The free end was moved to each of its extreme positions and returned to its nominal position while measuring the strain output from the device. A National Instruments SCXI-1520 data acquisition system, along with a LabView interface, was used to measure the strains. The displace-

ments measured by the dial indicator were manually recorded and a least squares fit of the displacement versus strain data was used to obtain the conversion factor for each device. Previous work with this extensometer design has shown this type of measurement device to by highly linear in terms of the displacement versus strain response, which makes taking intermediary data points unnecessary.

Once the device was assembled, the positions of the attachment points were measured using a machinists rule and digital photography. The measured vertical and horizontal separation distances for both extensometers are listed in Table 13. It is seen that the separation distance between the upper and lower set of attachment points were not equal for either extensometer half. As such, when using Equation (6) to calculate the shear strains, the average separation distance was used for *d*. In order to minimize the error due to the specimen twisting during a test, the shear strain measured by both extensometers was averaged before being used to calculate the shear modulus.

### 2.3.2 Specimen Preparation

Test specimens were manufactured from three different unidirectional pre-preg materials: IM7/8552 carbon/epoxy from Hexcel, Kevlar-49/AR251, and glass/AF254 from Aldila Composite Materials. Two different laminate thicknesses were prepared for each material. The carbon/epoxy laminates were $[0/90]_{2S}$ and $[0/90]_{4S}$ and had an aver-

Table 13: Measured extensometer point separation lengths.

| Extensometer | Vertical Separation | | | | Horizontal Separation | | | |
|---|---|---|---|---|---|---|---|---|
| | 1 | | 2 | | 1 | | 2 | |
| | [mm] | [in.] | [mm] | [in.] | [mm] | [in.] | [mm] | [in.] |
| 1 | 20.00 | 0.7875 | 19.86 | 0.7820 | 5.11 | 0.2014 | 5.23 | 0.2061 |
| 2 | 19.88 | 0.7828 | 19.92 | 0.7844 | 5.12 | 0.2017 | 5.14 | 0.2023 |

age cured ply thickness of 0.312 mm (0.0123 in.). The Kevlar/epoxy laminates were $[0/90]_{4S}$ and $[0/90]_{12S}$ and had an average cured ply thickness of 0.105 mm (0.00414 in.). The glass/epoxy laminates were $[0/90]_{5S}$ and $[0/90]_{9S}$ and had an average cured ply thickness of 0.146 mm (0.00573 in.). Strain gauges were applied to two of the thicker specimens from each material group. The strain gauges were prototype gauges from Vishay Micro-Mesurements which utilized overlapping ±45° grids, wired in a half bridge circuit, that spanned the entire region between the notches. The Vishay part number for the gauges was A2A-00-C170A-500. The gauges had a grid width of 4.32 mm (0.170 in.) and each grid had a resistance of 500 Ω. The strain gauges are similar to shear gauges used when testing V-notched Beam Shear specimens. A gauge factor of 2.0 was assumed, as one was not provided by Vishay. Guidelines were drawn on specimens that were to be tested with the extensometers to aid in positioning the extensometers properly within the gauge section.

One carbon/epoxy $[0/90]_{4S}$ specimen was analyzed using photoelastic methods. A PS-1D photoelastic sheet and PC-1 two part adhesive from Measurements Group were used. The sheet had a nominal thickness of 0.53 mm (0.021 in.), a K factor of 0.15, and a fringe value of 3600. Each full fringe order is expressed as a red-blue color transition. A rectangular strip, nominally 23 mm (0.9 in.) wide, was cut from the sheet. Notches were then cut into each strip to roughly match those of the specimen, with a 2-3 mm (0.8 -0.12 in.) overhang. After bonding the photoelastic sheets to each specimen, and allowing the adhesive to fully cure, the excess photoelastic material was removed using small files until it matched the contour of the specimen notch.

### 2.3.3 Testing

Testing preceded in general accordance with ASTM D-7078. The specimens were installed into the test fixture and then inserted into a 222 kN (50 kip) load frame. Data acquisition was handled by the same National Instruments SCXI-1520 unit used when calibrating the extensometer, and was controlled through LabView. Specimens with bonded strain gauges were connected to the National Instruments strain module and calibrated using National Instruments' Measurement and Automation software. For the remaining specimens, the extensometers were attached to both specimen faces and were held together with elastic bands. The cross head speed was 1.27 mm/min (0.05 in./min). Testing proceeded until one of the follow criteria occurred: significant plastic deformation occurred, the bonded strain gauges debonded, or the extensometers slipped. After the tests were complete the shear modulus was calculated using both a least squares fit and a secant fit over the strain range of approximately 0.002 to 0.006. The shear stress versus shear strain response for each material group were plotted using MATLAB.

The photoelastic test was performed using a United 89 kN (20 kip) load cell to measure the loads. Datum 3.0 was used to control the load frame. The testing speed was 1.27 mm/min (0.050 in./min). Datum was programed to stop at specific loads in order to photograph the isoclinic and isochromatic fringes. The load stops used were 2.0 kN (450 lbf), 4.0 kN (900 lbf), and 6.0 kN (1350 lbf). Only the ±45° isoclinics, along with the isochromatic fringes were recorded as they are of primary interest in shear testing.

A Measurements Group 031-A polariscope was used to view the photoelastic fringes. A Nikon D3000 digital camera and a Sigma EX 105 mm DG Macro lens were used to photograph the resulting fringe contours. The camera settings used were: aper-

ture $f$2.8, shutter speed 1/10 s, ISO 800, and incandescent white balance. The images were opened in UFRaw and edited in GIMP before saving in an uncompressed Windows Bitmap format. The exposure values, EV, of the isoclinic images were increased to +3.25 in UFRaw in order to differentiate the isoclinics from low exposure areas. This was not done to the isochromatic images as this would generally overexpose the images of the strain contours. Both the polariscope and the camera were mounted to a tripod. An angle gauge was used to ensure the alignment of the tripod mounting boss.

### 2.3.4 Results

#### 2.3.4.1 Photoelastic Results.

The numerical simulations of the photoelastic measurements are shown in Figure 63, while the experimental photoelastic results are shown in Figure 64. It is believed that the contour in the upper left corner of the photoelastic specimen (Figure 64) is due to im-

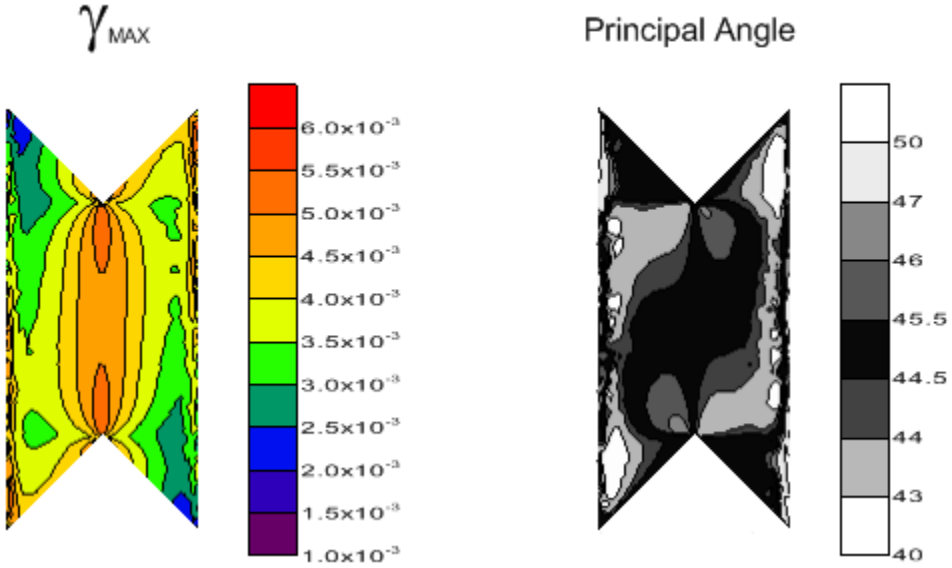


Figure 63: Maximum shear strain and principal strain direction from numerical modeling of the $[0/90]_{4S}$ carbon/epoxy specimen.

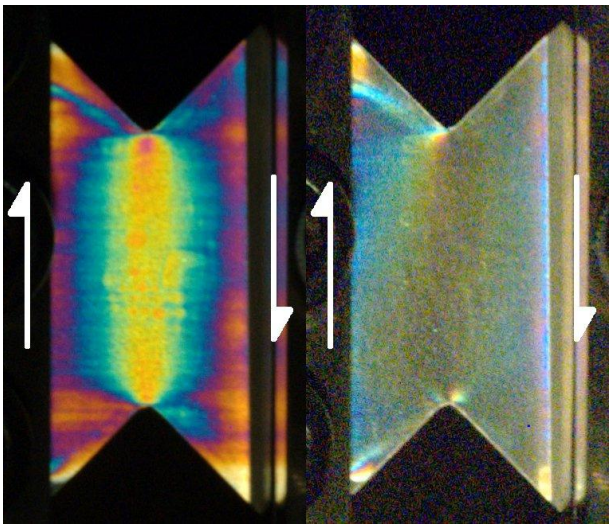

Figure 64: Photoelastic results from the carbon/epoxy $[0/90]_{4S}$ laminate. The isochromatics are shown on the left and the isoclinics on the right.

proper bonding of the film, and is not representative of the strain state in the specimen. In general similar features are observed in the predicted and experimental isochromatic and isoclinic contour plots, suggesting that the numerical model is a proper representation of the experimental setup.

2.3.4.2 Extensometer Results

The shear modulus results for the IM7/8552 carbon/epoxy cross-ply laminate are summarized in Table 14 and the shear stress versus shear strain response for both the extensometer and strain gauge measurement methods are shown in Figure 65. Similarly, results for the Kevlar/AR251 laminate are shown in Table 15 and Figure 66, and the glass/AF254 results are shown in Table 16 and Figure 67. In addition to the shear modulus values, each table shows the percent difference in the average shear modulus between the two different strain measurement methods. In Figure 65, Figure 66, and Figure 67 the curves generated from the strain gauge data is depicted in red, while the data from the

Table 14: Shear modulus results for the IM7/8552 cross-ply laminate.

| Strain Measurement Method | Specimen | Gxy Secant [GPa] | Gxy Secant [Msi] | Gxy Least Squares [GPa] | Gxy Least Squares [Msi] | $R^2$ | % Difference Secant | % Difference Least Squares |
|---|---|---|---|---|---|---|---|---|
| Extensometer | CN-04 | 4.88 | 0.708 | 4.90 | 0.711 | 0.9997 | | |
| | CN-08 | 4.69 | 0.680 | 4.72 | 0.685 | 0.9995 | | |
| | CN-10 | 4.89 | 0.710 | 4.91 | 0.712 | 0.9994 | | |
| | CT-04 | 4.84 | 0.702 | 4.85 | 0.704 | 0.9995 | | |
| | CT-05 | 4.76 | 0.690 | 4.77 | 0.692 | 0.9997 | | |
| | **Average** | **4.81** | **0.698** | **4.83** | **0.701** | | 1.16 | 1.22 |
| | **COV** | **2.37** | | **2.44** | | | | |
| Strain Gauge | CT-01 | 4.81 | 0.698 | 4.82 | 0.699 | 0.9996 | | |
| | CT-02 | 4.70 | 0.682 | 4.72 | 0.685 | 0.9997 | | |
| | **Average** | **4.76** | **0.690** | **4.77** | **0.692** | | | |
| | **COV** | **1.69** | | **1.45** | | | | |

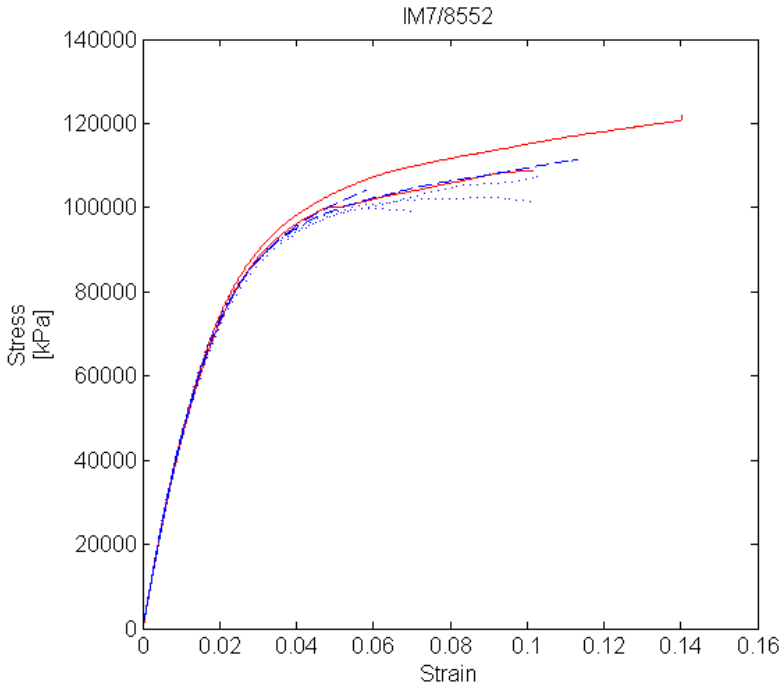


Figure 65: Shear stress versus shear strain response for the carbon/epoxy laminates. The red curves are from strain gauges, and the blue curves are from the extensometer. The dotted lines are from the thinner specimens.

Table 15: Shear modulus results for the Kevlar/AR251 cross-ply laminates.

| Strain Measurement Method | Specimen | Gxy Secant [GPa] | Gxy Secant [Msi] | Gxy Least Squares [GPa] | Gxy Least Squares [Msi] | $R^2$ | % Difference Secant | % Difference Least Squares |
|---|---|---|---|---|---|---|---|---|
| Extensometer | KN-01 | 1.97 | 0.286 | 1.94 | 0.281 | 0.9990 | | |
| | KN-02 | 1.96 | 0.284 | 1.94 | 0.281 | 0.9994 | | |
| | KN-03 | 1.87 | 0.272 | 2.03 | 0.295 | 0.9960 | | |
| | KT-04 | 1.98 | 0.287 | 1.98 | 0.287 | 0.9999 | | |
| | KT-06 | 1.97 | 0.286 | 1.97 | 0.286 | 1.0000 | | |
| | **Average** | **1.95** | **0.283** | **1.97** | **0.286** | | -1.25 | 0.05 |
| | **COV** | **2.26** | | **1.95** | | | | |
| Strain Gauge | KT-01 | 2.01 | 0.292 | 2.01 | 0.292 | 0.9999 | | |
| | KT-02 | 1.94 | 0.281 | 1.93 | 0.280 | 0.9999 | | |
| | **Average** | **1.98** | **0.286** | **1.97** | **0.286** | | | |
| | **COV** | **2.65** | | **3.07** | | | | |

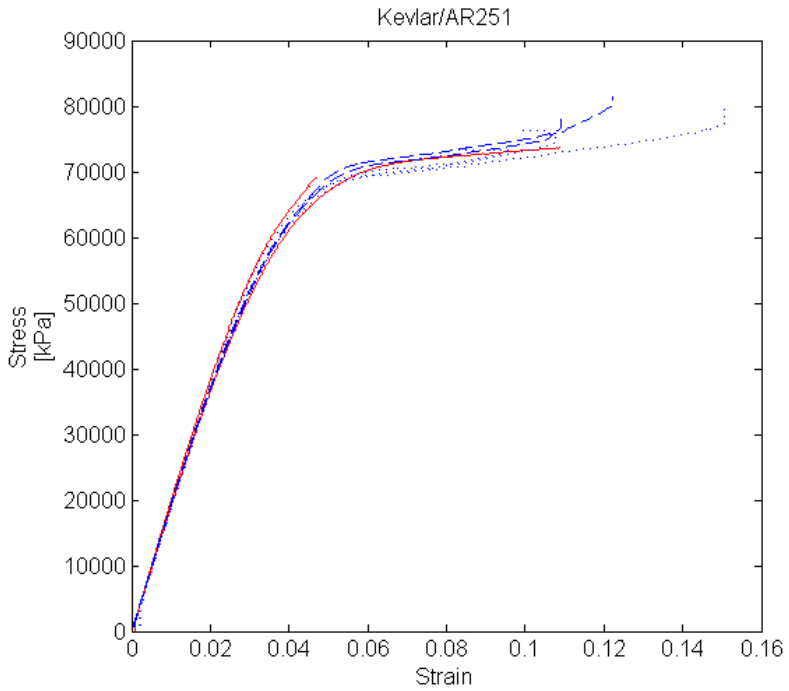


Figure 66: Shear stress versus shear strain response for the Kevlar/epoxy laminates. The red curves are from strain gauges, and the blue curves are from the extensometer. The dotted lines are from the thinner specimens.

Table 16: Shear modulus results for the Glass/AF254 cross-ply laminates.

| Strain Measurement Method | Specimen | Gxy Secant [GPa] | Gxy Secant [Msi] | Gxy Least Squares [GPa] | Gxy Least Squares [Msi] | $R^2$ | % Difference Secant | % Difference Least Squares |
|---|---|---|---|---|---|---|---|---|
| Extensometer | GN-01 | 3.63 | 0.526 | 3.61 | 0.524 | 0.9980 | | |
| | GN-02 | 3.70 | 0.537 | 3.71 | 0.538 | 0.9978 | | |
| | GN-03 | 3.78 | 0.548 | 3.77 | 0.547 | 0.9980 | | |
| | GT-05 | 3.63 | 0.527 | 3.63 | 0.527 | 0.9982 | | |
| | GT-06 | 3.53 | 0.512 | 3.54 | 0.514 | 0.9990 | | |
| | **Average** | **3.65** | **0.530** | **3.65** | **0.530** | | 0.62 | 0.34 |
| | **COV** | **2.55** | | **2.39** | | | | |
| Strain Gauge | GT-01 | 3.65 | 0.529 | 3.65 | 0.529 | 0.9984 | | |
| | GT-02 | 3.62 | 0.525 | 3.63 | 0.527 | 0.9985 | | |
| | **Average** | **3.63** | **0.527** | **3.64** | **0.528** | | | |
| | **COV** | **0.56** | | **0.27** | | | | |

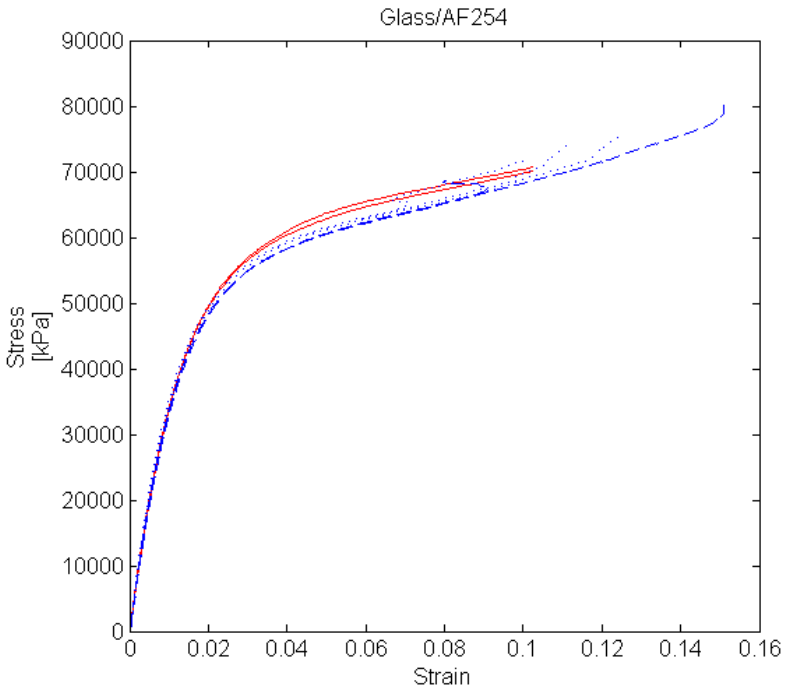


Figure 67: Shear stress versus shear strain response for the glass/epoxy laminates. The red curves are from strain gauges, and the blue curves are from the extensometer. The dotted lines are from the thinner specimens.

extensometers is in blue. The thinner specimens are differentiated from the thicker specimens by use of a dotted line.

Results from the carbon/epoxy specimen show that the extensometer produces a shear modulus that is approximately 1.2% higher than the value obtained using strain gauges and approximately 3% higher than the results reported in [18]. It is noted, however, that the results presented in [18] were obtained using ASTM D3518-94 [19] and the material used had a thinner cured ply thickness as well as a different fiber volume fraction than the material used in the present study. As such, some discrepancy between the results may be unavoidable, as even the shear modulus obtained from the bonded strain gauges differs by 2% between the two test methods. Additionally, the strain gauges used in this study were supplied without a gauge factor, and while a gauge factor similar to those for the smaller shear gauges was used (2.0) the actual gauge factor for these gauges will affect all the results reported in this study.

The coefficient of variation in the measured shear modulus for the extensometers is low, indicating that the device is sufficiently precise so long as it is properly placed on the specimen. Additionally, the shear stress versus shear strain response obtained from the extensometer generally follows that obtained from the bonded strain gauges, as seen in Figure 65.

The Kevlar/epoxy results show a closer agreement between shear modulus calculations using the two strain measurement methods. Depending on the calculation method used, the extensometer was shown to provide comparable shear modulus values to the bonded strain gauges. Similar to the results of the carbon/epoxy laminate, the variation in the calculated shear moduli was low.

The shear stress versus shear strain response of the Kevlar/epoxy laminate using the extensometer is similar to that of the bonded strain gauges. Both the initial linear region as well as the nonlinear region show the same trends and follow the same general path. It should be noted that while testing specimen KT-01 one strain gauge debonded near the notch tip before reaching 5% shear strain, and the test was stopped. This is depicted in Figure 66 as the shorter red curve. The curves for the thicker specimens tested with the extensometer look as though they would fall between the curves from the strain gauged specimens had the strain gauges not separated while testing specimen KT-01.

The glass/epoxy results show good agreement between the two strain measurement methods, with a percent difference less than 1% using either the secant or least squares method. Similar to the carbon/epoxy and Kevlar/epoxy laminates, the variation in modulus calculations using the extensometer is low. While the coefficient of variation in the shear modulus determined using the bonded strain gauges is below 1%, this may be due to the small sample size.

The shear stress versus shear strain response for the glass/epoxy laminate is generally the same for both strain measurement methods. While the inelastic portion of the curves from the extensometer are below those of the strain gauges, the curves follow the same trends and have the same overall shape. Note that the extensometers did slip during testing, as indicated by the drop in measured shear strain with an increase in shear stress; however, the device is capable of measuring large shear strains, evident by the long dashed blue line in Figure 67.

## 2.4 Conclusions

The goal of this study was to develop an extensometer that would accurately measure the shear strains in a cross-ply fiber reinforced composite V-notched rail shear test specimen. The numerical study focused on the predicted displacements of various fiber/matrix combinations in order to investigate how the use of different constituent materials would affect the accuracy of the device. The nodal displacements were used to investigate the accuracy of the shear strains calculated from the movement of a rectangular set of points centered about the specimen center. From these results a set of points were chosen which minimized the difference between the calculated and supplied shear modulus. A carbon/epoxy specimen with a photoelastic film was tested to validate the results from the numerical study. The results of the photoelastic test were in general agreement with the numerical results.

Based on the numerical study, a shear extensometer was developed to measure the relative displacement of a set of points on the specimen surface. Three different material systems were tested using the extensometer as well as bonded strain gauges. The results of these tests showed excellent agreement between the two strain measurement methods in the carbon/epoxy, Kevlar/epoxy, and glass/epoxy specimens. Each material system showed similar trends in the shear stress – shear strain response, and the measured shear modulus differed by approximately ±1% between the two measurement methods.

Based on the experimental results, the shear extensometer is capable of accurately measuring the shear strain in a cross-ply laminate tested using the V-Notched Rail Shear test method. The extensometer may be used to accurately measure the shear modulus as well as the shear strain well beyond the initial linear region. The extensometer was also

found to be usable with a variety of constituent materials and within a relatively wide range of shear moduli.

# 3 DETERMINATION OF CLAMPING FORCES IN THE V-NOTCHED RAIL SHEAR AND V-NOTCHED COMBINED LOADING SHEAR TEST FIXTURES

## 3.1 Introduction

Previous work by Johnson [5] determined a static friction coefficient between the grip faces of the V-Notched Rail Shear test fixture and an IM7/8552 carbon epoxy laminate for use in numerical analysis. The experimental data used to determine this friction coefficient were obtained by using different torque values applied to the clamping bolts and then loading the test fixture until the test coupon slipped in the fixture. During the analysis there was some uncertainty as to the amount of force being applied by the clamping bolts of this fixture. The analysis performed by Johnson utilized an equation modified from Shigley's Mechanical Engineering Design [15] that approximates the force applied by the bolt as a function of the applied torque ($T_r$), thread pitch ($l$), mean bolt diameter ($d_m$), the friction between the bolt and the plate ($f$), and the thread angle ($2\alpha$), as shown in Equation (10).

$$T_r = \frac{F d_m}{2}\left[\frac{l + \pi f d_m sec(\alpha)}{\pi d_m - f l sec(\alpha)}\right] \tag{10}$$

The assumption in the analysis was that the force in the bolt, $F$, was applied to the face loaders of the rail shear fixture. In order to determine the validity of these assump-

tions an experiment was performed to measure the actual load being applied by the clamping bolts for a given applied torque.

## 3.2 Load Cell Design and Fabrication

### 3.2.1 Design

In order to obtain in situ measurements of the force applied by the clamping bolts a load cell was specifically designed and built to fit within the cavity of the V-Notched Rail Shear test fixture. The dimensions of the cavity measured 38.1 mm (1.5 in.) wide, 76.2 mm (3.0 in.) high, and 27.23 mm (1.072 in.) deep on the fixture used for this test. In experimental tests performed by Johnson the applied torque values were 45 Nm (33.2 lbf·ft), 55 Nm (40.6 lbf·ft), and 65 Nm (47.9 lbf·ft) [5]. Using the largest of these torque values, along with the required bolt dimensions and a value of 0.15 for $f$, in Equation (10) results in a bolt force value, $F$, of approximately 52 kN (11.7 kip). For the current investigation it was believed that the space limitation would prohibit manufacturing a load cell that would be capable of measuring 52 kN so, a capacity of 22.2 kN (5.00 kip) was set as the design target.

A binocular type load cell design was used and SolidWorks SimulationXpress was used to assess the adequacy of the initial design. The design was revised until the maximum Von Mises stress in the model for a 22.2 kN (5.00 kip) load, with an applied factor of safety of 2, was within an acceptable value for steel. The final as designed dimensions of the load cell are shown in Figure 68. Using these dimensions and a load of 22.2 kN (5.00 kip) the maximum von Mises stress in the model was 651 MPa (93.2 ksi). The load cell was manufactured from A2 tool steel due to its ability to be hardened to the point that its yield strength was at least twice the magnitude of the maximum expected stress for the

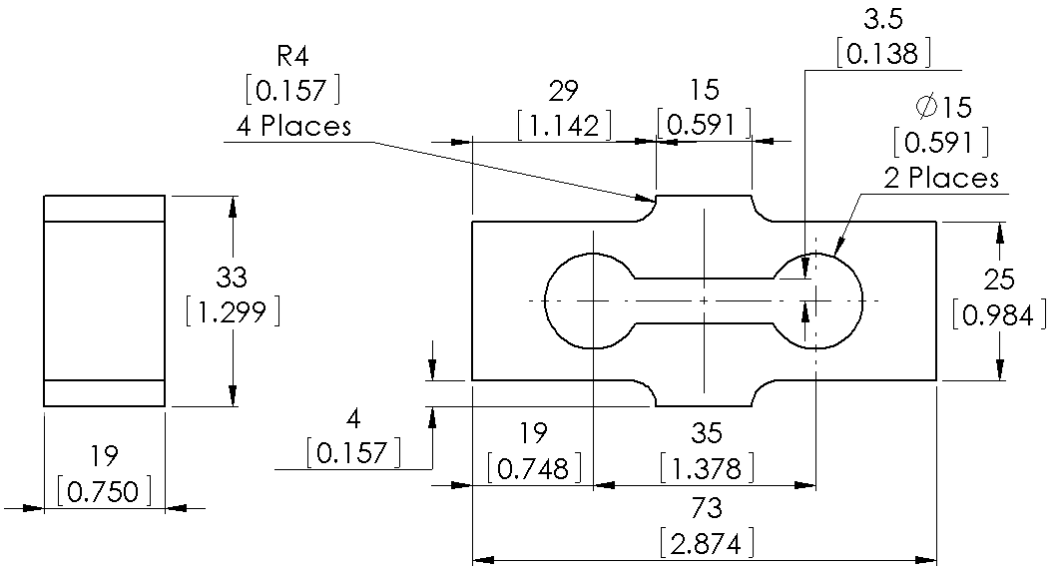


Figure 68: As designed drawing of the load cell used to determine the clamping loads. Dimensions are in mm [in.].

design load.

### 3.2.2 Fabrication

The load cell was machined from a 19 mm (0.75 inch) plate of A2 steel using an OMAX waterjet machine. The machine settings for the interior portion of the load cell were set so as to minimize the amount of through thickness taper. The final machined dimensions of the load cell are shown in Figure 69. The piece was then heat treated using a Thermolyne Type 10500 furnace. The load cell was wrapped in a paper towel then inserted into a cast iron pipe before being inserted into the furnace at 926.7 °C (1700 °F). The paper towel was used to prevent decarburization during heat treatment and the pipe was used to prevent rapid cooling of the load cell by coming into contact with the tongs used to remove it from the furnace. The load cell remained in the furnace for 74 minutes. Upon being removed from the furnace it was quenched using used crankcase oil.

After a the temperature of the load cell had reached ambient conditions the sur-

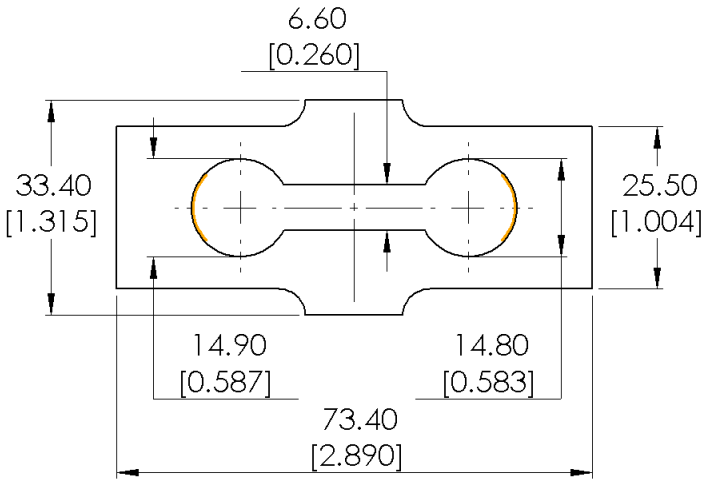


Figure 69: As machined dimensions of the load cell after heat treatment. The orange regions indicate where the strain gauges were applied. Dimensions are in mm [in.].

face hardness was measured at 10 different locations using the Rockwell C scale on a Wilson Mechanical Instrument Co. Model R3 Rockwell hardness testing machine. The average hardness was HRC 60.4 with a coefficient of variation of 0.985 %. The load cell was then tempered in the same furnace at a temperature of 232.2 °C (450 °F) for approximately 150 minutes. The surface temperature of the load cell after 150 minutes was 182.2 °C (360 °F). The load cell was then removed from the furnace and allowed to cool in ambient air. After tempering the load cell the surface hardness was again tested at 10 different locations using the previously mentioned hardness testing machine. An average hardness of HRC 57.7 was measured with a coefficient of variation of 1.10 %.

The hardness of low alloy steel can be related to its yield strength. In order to determine the yield strength of the load cell after heat treatment test data for yield strength and hardness for this alloy was obtained. Using data from a material data sheet published by Bohler-Uddeholm [16] a curve fit was obtained to determine an approximation of the

load cell's yield strength. The data and regression line are shown in Figure 70. The equation for the regression line is

$$\sigma_y = 72.33 \cdot HRC - 2230 \tag{11}$$

where $\sigma_y$ is in MPa. The coefficient of determination for the linear regression is 0.9814. For a hardness of HRC = 57.7 Equation (11) yields $\sigma_y$ = 1943 MPa (281.9 ksi) which gives a factor of safety of 3.0, with respect to the design load.

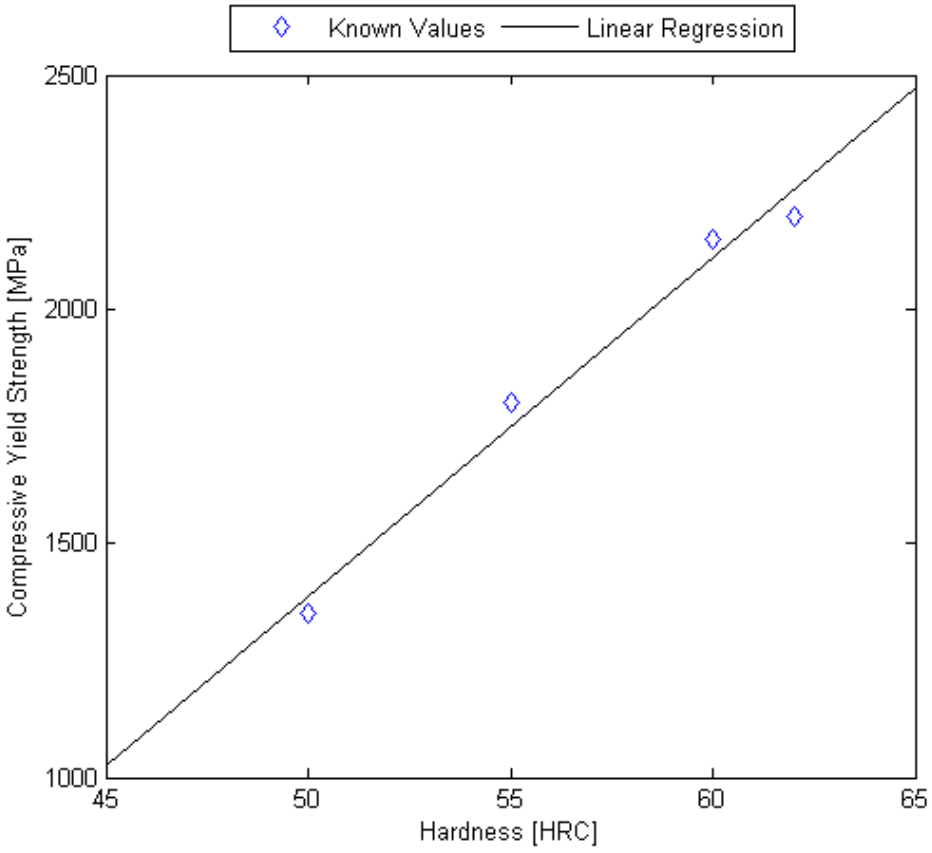


Figure 70: Data for the Rockwell hardness and compressive yield strength of AISI A2 tool steel [16].

## 3.3 Calibration and Testing

### 3.3.1 Calibration

The load cell was placed into a 222 kN (50 kip) load frame and loaded to 22.2 kN (5.00 kip) to ensure that the load cell would meet the design load. After the capacity of the load cell had been verified single-grid strain gauges were applied to the circumference of the round cavity as shown in Figure 69 so that when the load cell was in compression the strain gauges would likewise be in compression. The Vishay Micro-Mesurements CEA-06-125UN-350 gauges were wired into a full Wheatstone bridge configuration using two Micro-Mesurements S-350-01 precision resistors as the bridge completion resistors. The completed circuit was then connected to a Vishay 2120A strain gauge conditioner amplifier with a Vishay 2110 power source and a Vishay 2131 digital readout.

A calibration factor relating the load applied to the load cell to the output of the bridge circuit was determined by placing the specialized load cell in the 222 kN (50 kip) load frame and recording the conditioned output voltage as the load frame applied a load. A National Instruments SCXI-1520 strain gauge input module was used to monitor the load frame output and the specialized load cell's conditioned voltage output. A LabView program was used to record the data during the test. Five tests were performed and a linear regression was performed on each data set resulting in an average conversion factor of 3125 N/V (703 lbf/V) with a coefficient of variation of 0.11 %. After the first set of clamping force tests with the load cell the bridge circuit had to be rebuilt due to a loose connection. The tests for determining the calibration factor were repeated resulting in an average conversion factor of 3109 N/V (699 lbf/V) and a coefficient of variation of 0.03

%. The linear regression performed on each data set had a coefficient of determination value ($R^2$) of at least 0.9999, with the second set of tests having values closer to 1 than the first set of tests. A plot of the first five calibration tests is shown in Figure 71.

### 3.3.2 Testing

#### 3.3.2.1 V-Notched Rail Shear Test Fixture

In order to obtain the most accurate value of the load applied by the test fixture's clamping bolts one half of the fixture was clamped in a table vice and the load cell was inserted into the fixture cavity. A picture of the setup outside of the vice is shown in Figure 72. The center bolts on the fixture half were then hand tightened until they made contact with the load cell. A Snap-on TESI 125 torque wrench was used to tighten one of the two bolts in contact with the load cell. The torque wrench has a stated accuracy of ±2 % above 25% of its maximum range. At a 125 Nm (92.2 lb·ft) maximum torque the low value for accuracy would be 31.2 Nm (23.0 lb·ft). Because of this limitation in accuracy below the threshold value, tests performed with this torque wrench were limited to values above 35 Nm (25.8 lb·ft). The torque was applied increasingly in stages starting from values of 35 Nm (25.8 lb·ft) up to 55 Nm (40.6 lb·ft). At each torque stage the output voltage from the Vishay 2131 digital readout was recorded along with the applied torque. Once a value of 55 Nm (40.6 lb·ft ) had been reached and the voltage recorded the clamping bolts were loosened and the test repeated. Five sets of tests were performed using this torque wrench after which the load cell recalibrated and another five sets of tests were performed. The tests were repeated using a Craftsman Microtork torque wrench; however, the values were similar to those obtained with Snap-on wrench.

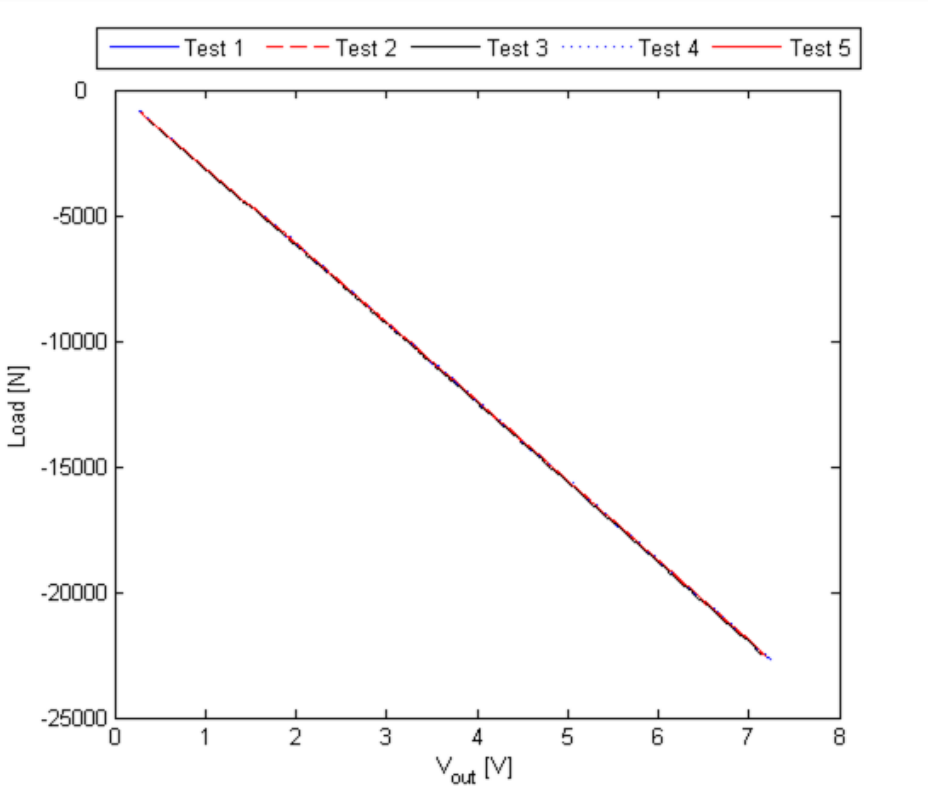


Figure 71: Load cell bridge circuit response to an applied compressive load.

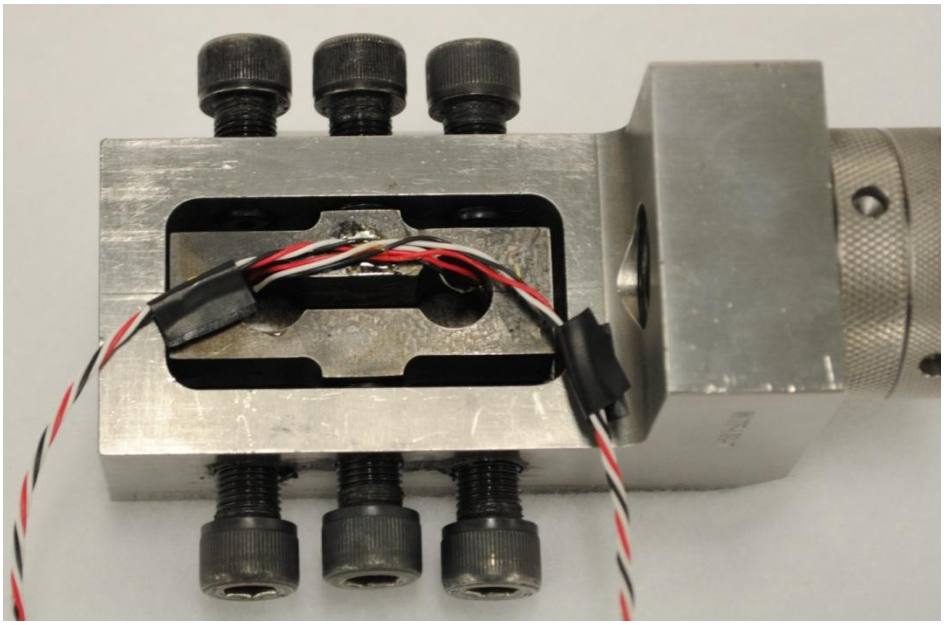

Figure 72: The load cell placed in the fixture half as used in testing. The vice has been omitted for clarity.

3.3.2.2 V-Notched Combined Loading Shear Fixture

Testing methods for the V-Notched Combined Loading Shear fixture were generally the same as those for the V-Notched Rail Shear fixture. The same load cell and data acquisition method were used. The installed position of the load cell differed from that of the V-Notched Rail Shear fixture due to differences in geometry between the two fixtures. The load cell, as it was installed in the Combined Loading Shear fixture is shown in Figure 73. The fixture was secured in a vice during testing. The thread size for the new fixture's clamping bolts is 5/8 inch x 18 tpi.

A new conversion factor of 3163 N/V (711 lbf/V) was used based on the load cell quantification testing for use in the new fixture. Two sets of tests were performed. The first used set screws with a thread length shorter than the thread length of the fixture, and the second used the supplied fixture bolts with a threaded length greater than the threaded length of the fixture. The Craftsman Microtork torque wrench used in the previous tests was used to apply the torque to the bolts/screws. The fasteners were coated with Molykote Gn assembly paste prior to testing. The range of applied torque using the set screws was 20 – 33 Nm (15 – 27 lbf·ft), while the range of torques used with the bolts supplied with the fixture was 20 – 75 Nm (15 -55 lbf·ft). These tests were performed prior to specimen testing.

### 3.3.3 Results

3.3.3.1 V-Notched Rail Shear Fixture

The data for the clamping bolt tests with the V-Notched Rail Shear fixture are shown in Figure 74. The equation for the best fit line for the data in Figure 74 using a least squares regression is:

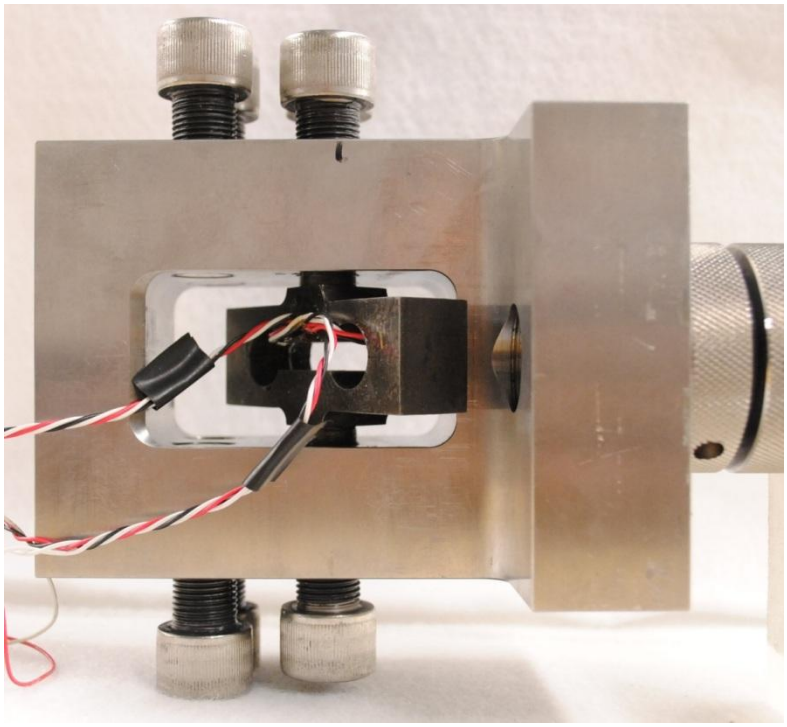

Figure 73: Load cell installed in the V-Notched Combined Loading Shear fixture.

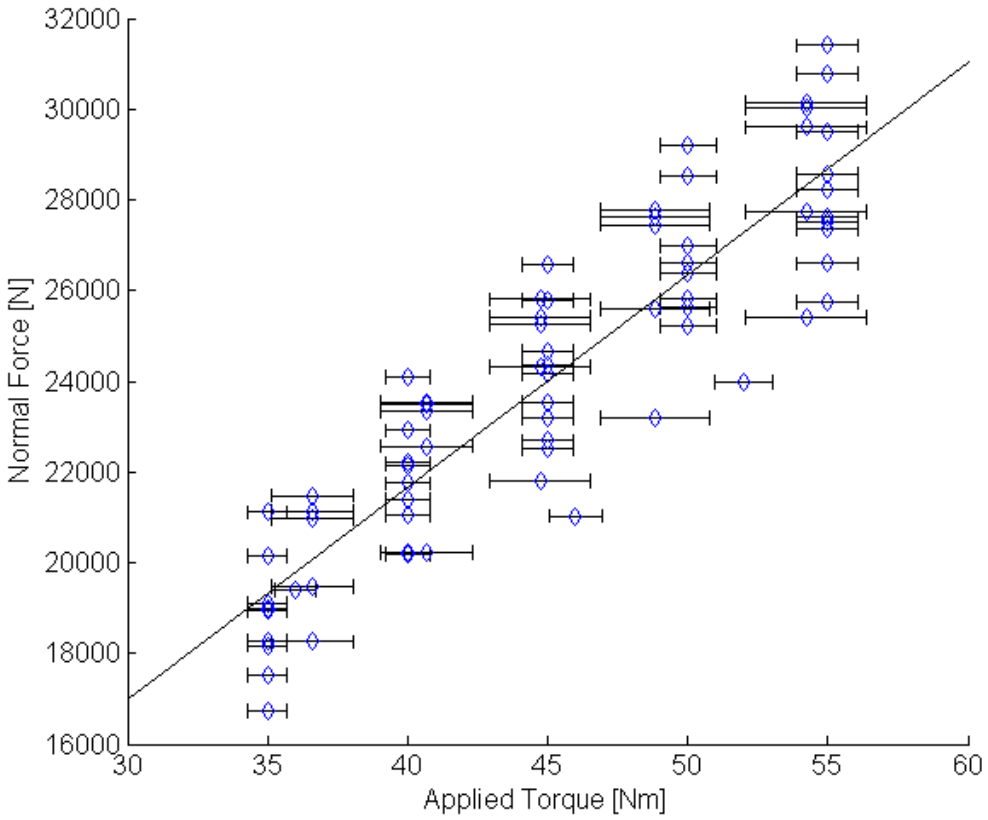


Figure 74: Results for the clamping bolt tests of the V-Notched Rail Shear test fixture. The line through the data is the best fit line found using a least squares regression. The error bars represent the uncertainty in the measured torque as stated by the manufacturer.

$$P = 468.64T + 2938.1 \tag{12}$$

where $P$ is the normal force applied by the bolt in N, and $T$ is the applied torque in Nm. The coefficient of determination for Equation (12) was 0.8089. Using the torque values used from Johnson in his slipping experiments [5] with Equation (12) results in the applied normal force values listed in Table 17. For reference, the normal force per bolt calculated from Equation (10) in [5] has also been listed in Table 17. The experimental values are approximately 50% smaller than the calculated values. Using similar methods

Table 17: Results showing the applied normal force, P, of a bolt for a given applied torque, T.

| T | | P* | | P+ | | Difference |
|---|---|---|---|---|---|---|
| [N·m] | [lbf·ft] | [N] | [lbf] | [N] | [lbf] | [%] |
| 45 | 33.2 | 24027 | 5401.5 | 35719 | 8030.0 | 48.7 |
| 55 | 40.6 | 28713 | 6454.9 | 43657 | 9814.5 | 52.0 |
| 65 | 48.0 | 33400 | 7508.6 | 51594 | 11598.8 | 54.5 |

* Values obtained from Equation (12).
+Values obtained from [5].

outlined in [5] the coefficient of friction between the grip faces of a V-Notched Rail Shear fixture and an IM7/8552 specimen is approximately 0.423.

3.3.3.2 V-Notched Combined Loading Shear Fixture

A similar data spread was observed in the new Combined Loading Shear fixture; however, a least squares fit of the data shows that the relationship between applied torque and clamping load differs in this new fixture and also differs between the two bolts tested. Because the bolts supplied with the fixture are more likely the ones to be used in testing, only data obtained using those bolts are shown. A plot of the normal force – applied torque is shown in Figure 75. The equation relating the clamping load as a function of the applied torque for the set screws is shown in Equation (13), while the same equation for the supplied fixture bolts is shown in Equation (14), with $P$ and $T$ having units of N and Nm, respectively. Comparing the two equations at an applied torque of 50-70 Nm (36.9-51.6 lb·ft) the set screws apply a clamping load that is approximately 80% higher than the supplied fixture bolts.

$$P = 698.35\,T + 5224.9 \tag{13}$$

$$P = 397.01\,T + 2192.7 \tag{14}$$

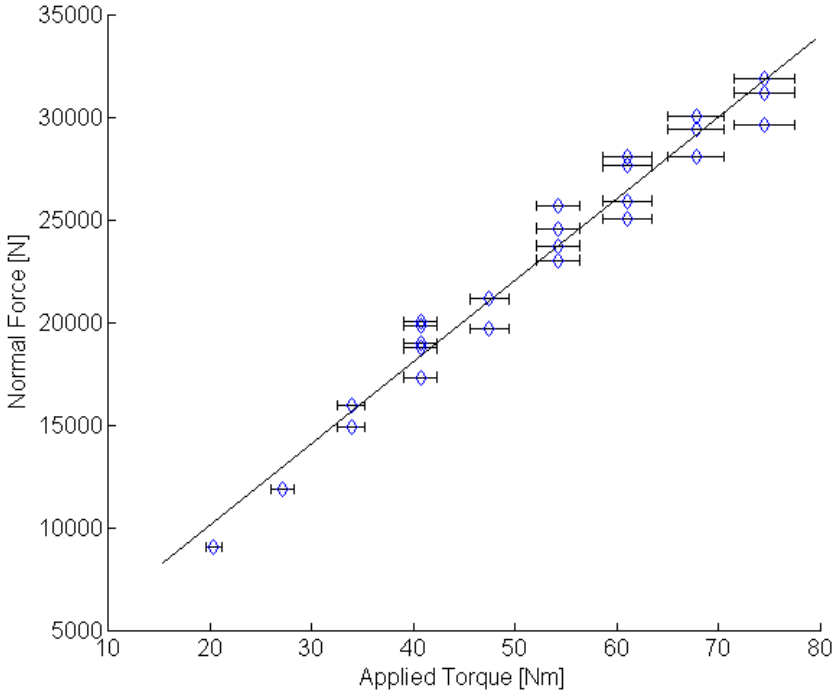


Figure 75: Data from the Combined Loading Shear fixture clamping bolt test using the supplied fixture bolts. The solid line is the least squares linear regression of the data. The error bars represent the uncertainty in the measured torque as stated by the manufacturer.

Where the current V-Notched Rail Shear test standard recommends a torque of 55 Nm (40.6 lb·ft ) [3], a torque of 65 Nm (47.9 lb·ft ) is required in the Combined Loading fixture in order to obtain a similar clamping load per bolt as the current fixture.

## 3.4 Conclusions

The results of this study showed that the torque applied to the clamping bolts in the V-Notched Rail Shear and Combined Loading Shear test fixtures is linearly proportional to the amount of force produced by the bolt. This relationship is similar to the bolt tension-bolt torque relationship in bolted connections published in [15], however, the modified equation in [15] used by Johnson [5] results in torque values that are signifi-

cantly larger than experimental values.

The results from bolt torque testing both test fixtures show a significant amount of scatter in the data, and the equations derived in Section 3.3.3 relating the bolt torque to the applied force will only provide rough estimates on the average normal force applied by the fixture bolts. Based on the results obtained using the Combined Loading Shear fixture, a larger bolt torque is required to attain a similar normal force per bolt than for the V-Notched Rail Shear test fixture. The lower normal forces determined as a result of this study suggest that a larger static friction coefficient is present than that used by Johnson [5].

# 4 THESIS CONCLUSIONS

The conclusions of each study within this thesis were placed at the end of their respective chapters. However, the results of each study will be briefly summarized here for easy reference.

The clamping loads for the current V-Notched Rail Shear test fixture, as well as the proposed V-Notched Combined Loading Shear test fixture were determined experimentally using a specially designed load cell. The results revealed that the in situ normal loads due to bolt torque are significantly smaller than those used by Johnson [5]. Based on these results, a new static friction coefficient was determined and used in all relevant numerical modeling. The results also showed that a larger bolt torque is required in the Combined Loading Shear test fixture in order to attain the same normal force per bolt as the V-Notched Rail Shear test fixture.

For the Combined Loading Shear test fixture, a face loader bolt torque of 65 Nm (47.9 lb·ft) was used during testing. This value proved to be sufficient at securing most of the laminates tested. Testing of higher shear strength laminates, specifically those with most plies oriented at ±45°, may benefit from a larger torque value as slipping can still occur. Due to the Combined Loading Shear test fixture's increased side wall thickness, it should be possible to sustain a larger bolt torque than is possible with the V-Notched Rail Shear fixture.

Numerical models were analyzed using the Combined Loading Shear test fixture

geometry to investigate the state of stress in the specimen using various orthotropic material properties. Several different edge loading configurations were modeled as well. Validation of the numerical models was performed by replicating the measurements possible through photoelastic methods. These numerical results showed good correlation with experimental photoelastic results, indicating that the model is adequate.

Mechanical testing with the new fixture showed that measured shear strengths are consistent with results published previously in the literature. It was also shown that the apparent shear strength is dependent on the amount of load applied by the edge loader. By increasing the torque applied to the edge loader bolts to 65 Nm (47.9 lb·ft), the measured shear strength in a $[0/90]_{4S}$ laminate differed by almost 10%. The measured shear strength of a cross-ply laminate at several edge loads were shown to decrease with an increase in edge load beyond 10 Nm (7.4 lb·ft ) bolt torque applied to the edge loader bolts. Photoelastic experiments further reinforced this observation by showing that the principal strains on the specimen face increase when tested at higher edge loads.

Based on the photoelastic results, care must be taken when interpreting the results obtained from a $[\pm 45]_{ns}$ laminate tested using the new fixture. Significant strain gradients exist near the notches, and the orientation of the principal strains are not oriented to provide the desired shear strain state. Increasing the load on the edge loaders will somewhat improve the orientation of the principal strains; however, the strain magnitudes were shown to increase as well. Both the cross-ply and quasi-isotropic laminates; however, display desirable shear strain states.

The shear strain extensometer was shown to accurately measure the shear strain in cross-ply composite specimens tested with the V-Notched Rail Shear test fixture. The

extensometers performed well with several constituent materials, providing accurate values for the shear modulus. The shear strain response of the extensometers was comparable to the bonded strain gauges over a large range of shear strain.

# APPENDIX A

## PHOTOELASTIC RESULTS FROM THE V-NOTCHED RAIL SHEAR TEST

The images contained in this section are the results of photoelastic testing performed on a $[0/90]_{4S}$, $[0/\pm45/90]_{4S}$, and $[\pm45]_{5S}$ laminate using the V-Notched Rail Shear test fixture. The loads used in these tests are the same as used in testing with the Combined Loading Shear test fixture and are listed in Table 3. The same load steps were used to facilitate direct comparison of the two test methods. Images of the cross-ply laminate are shown in Figure 76 and Figure 77. Images of the quasi-isotropic laminate are shown in Figure 78 and Figure 79. Images of the $[\pm45]_{5S}$ laminate are shown in Figure 80 and Figure 81.

Some visible blemishes in the photoelastic images, which are not indicative of the specimen response, were observed for both the cross-ply and quasi-isotropic specimen. In Figure 76 and Figure 77, the top left notch flank has a line of high shear strain. This is likely due to a poor bond, or a disbond of the photoelastic coating in that area and is not representative of the expected maximum shear strain magnitude. In the isochromatic images of the quasi-isotropic laminate (Figure 78 and Figure 79), near the center of the specimen, there is a region where the maximum shear strain has a discontinuous gradient. This artifact was not present in the results of the Combined Loading Shear test of the same laminate and may be due to an air bubble in the adhesive.

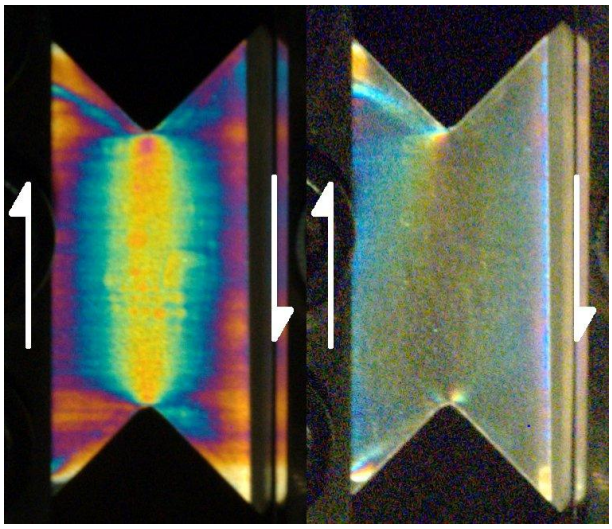

Figure 76: Isochromatic contours (left) and 45° isoclinic (right) for the $[0/90]_{4S}$ laminate at 4.00 kN (900 lbf) tensile load.

The results for the $[\pm 45]_{5S}$ laminate tested using the V-Notched Rail Shear test fixture do not show the same level of symmetry seen during the Combined Loading Shear test of the same laminate. This is likely due to the fixture halves not being identical. One fixture half used for these tests has a groove machined in the bottom of the cavity which houses the grips. This design feature was included to expedite installation and removal of the specimen during testing, as it allows the specimen to be removed without removing the fixture from the load frame. The left side of the specimen is attached to the fixture half with the groove, and is the area of the test region which shows a different maximum shear strain contour than the tests performed using the Combined Loading Shear test fixture.

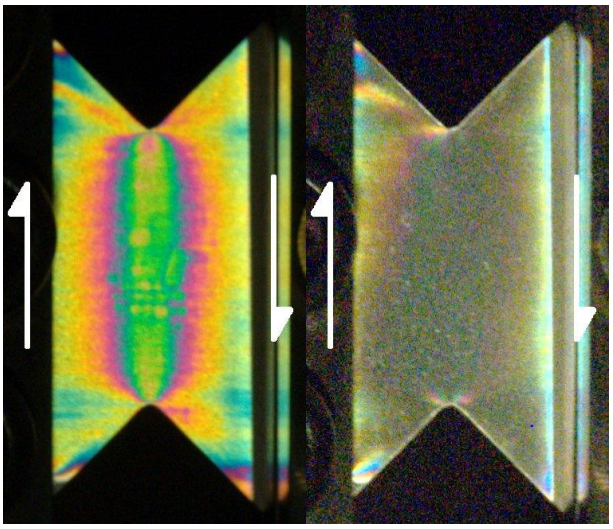

Figure 77: Isochromatic contours (left) and 45° isoclinic (right) for the $[0/90]_{4S}$ laminate at 6.01 kN (1350 lbf) tensile load.

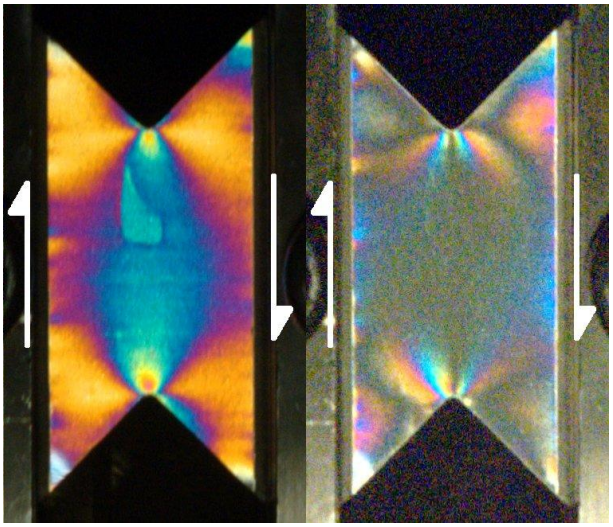

Figure 78: Isochromatic contours (left) and 45° isoclinic (right) for the $[0/\pm45/90]_{4S}$ laminate at 25.8 kN (5800 lbf) tensile load.

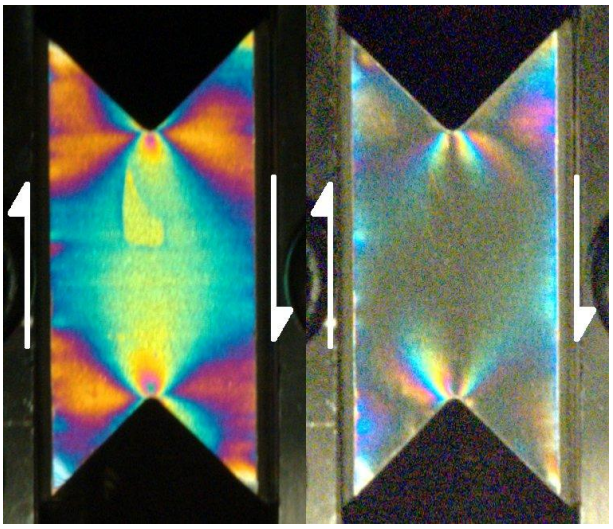

Figure 79: Isochromatic contours (left) and 45° isoclinic (right) for the $[0/\pm45/90]_{4S}$ laminate at 32.0 kN (7200 lbf) tensile load.

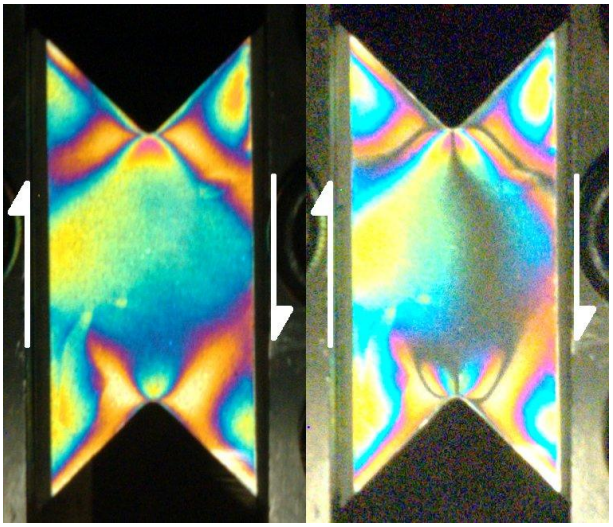

Figure 80: Isochromatic contours (left) and 45° isoclinic (right) for the $[\pm45]_{5S}$ laminate at 28.9 kN (6000 lbf) tensile load.

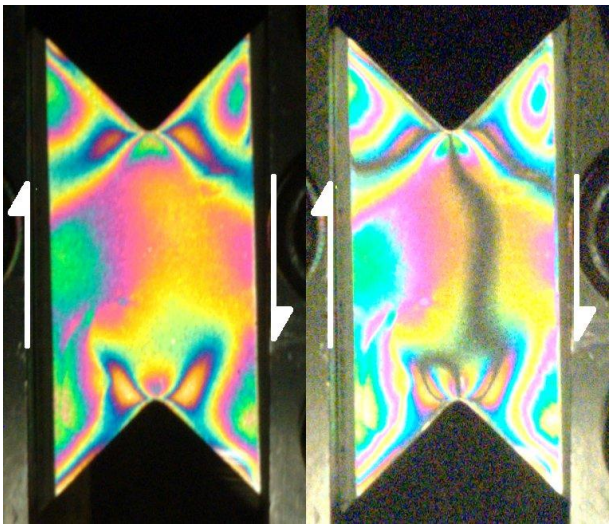

Figure 81: Isochromatic contours (left) and 45° isoclinic (right) for the $[\pm 45]_{5S}$ laminate at 40.0 kN (9000 lbf) tensile load.

# APPENDIX B

## COMBINED LOADING SHEAR FIXTURE DRAWINGS

The dimensional drawings of the components of the Combined Loading Shear test fixture are provided in this section. Unless otherwise noted, all dimensions are in inches. A front view of the fixture half is shown in Figure 82, while a side and sectional view are shown in Figure 83. The face loading grip is shown in Figure 84. The edge loader is shown in Figure 85.

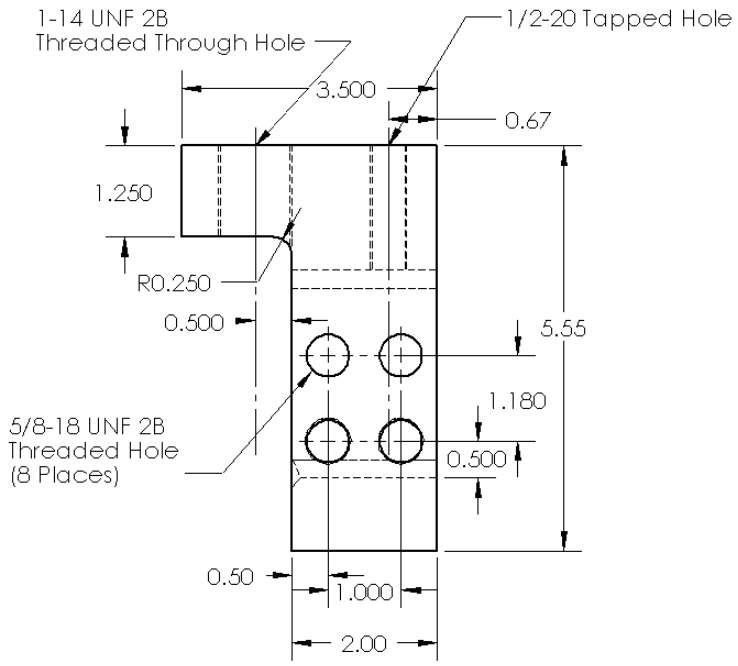


Figure 82: Front view of the Combined Loading Shear test fixture. All dimensions are in inches.

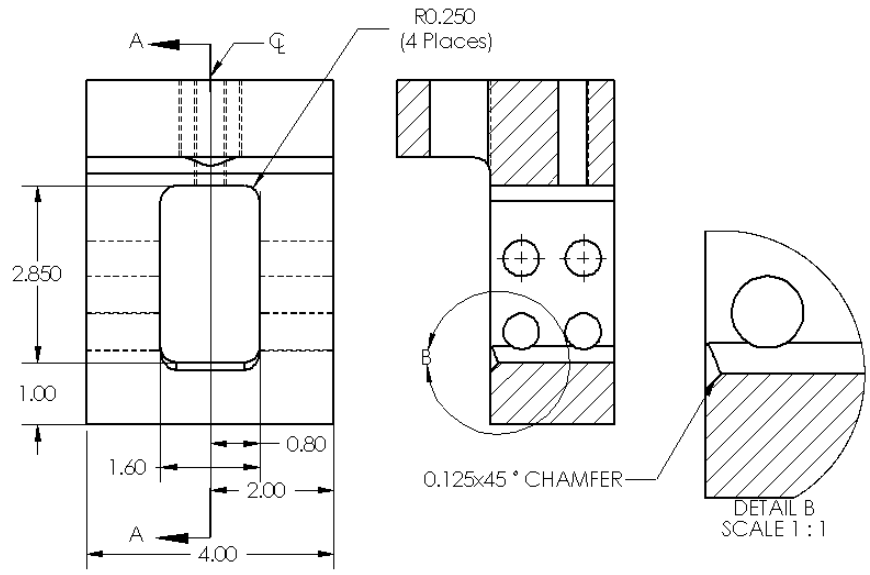


Figure 83: Side and sectional view of the Combined Loading Shear test fixture. Dimensions are in inches.

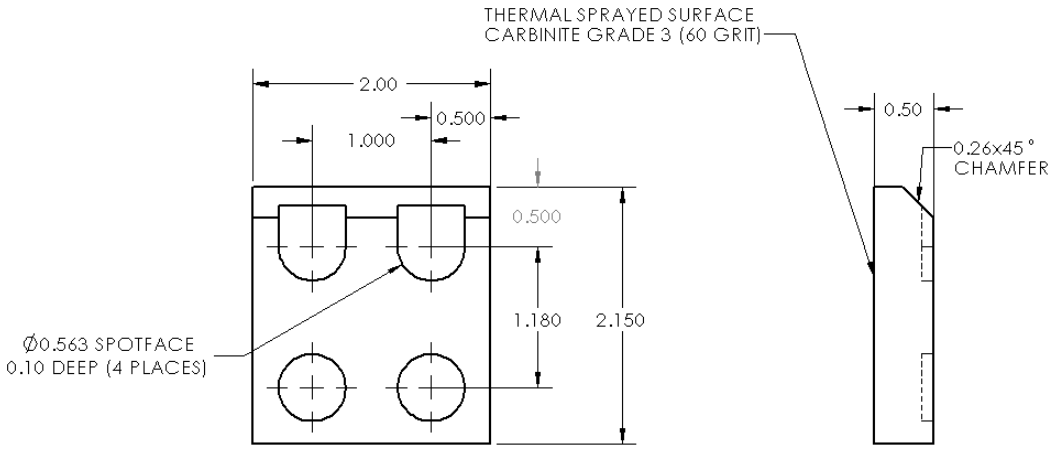


Figure 84: Face loading grip for the Combined Loading Shear test fixture. All dimensions are in inches.

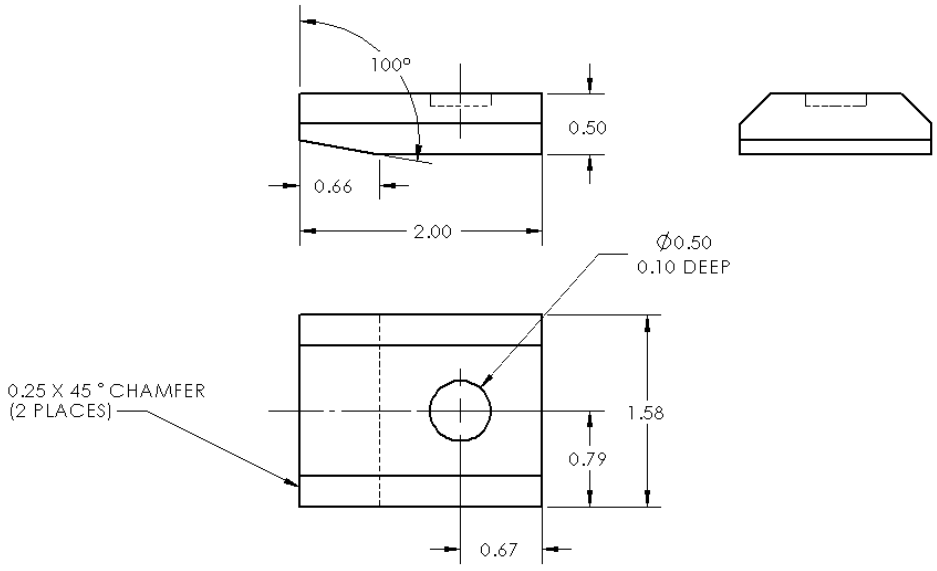


Figure 85: Edge loader for the Combined Loading Shear test fixture. All dimensions are in inches.

# APPENDIX C

## SHEAR STRAIN EXTENSOMETER DRAWINGS

This section contains the detailed drawings of the shear strain extensometer components. Unless otherwise noted, all dimensions are in inches. The chassis is shown in Figure 86. The center attachment block is shown in Figure 87. The outer attachment blocks are shown in Figure 88 and Figure 89. The sensing element is shown in Figure 90. The sensing element attachment block is shown in Figure 91.

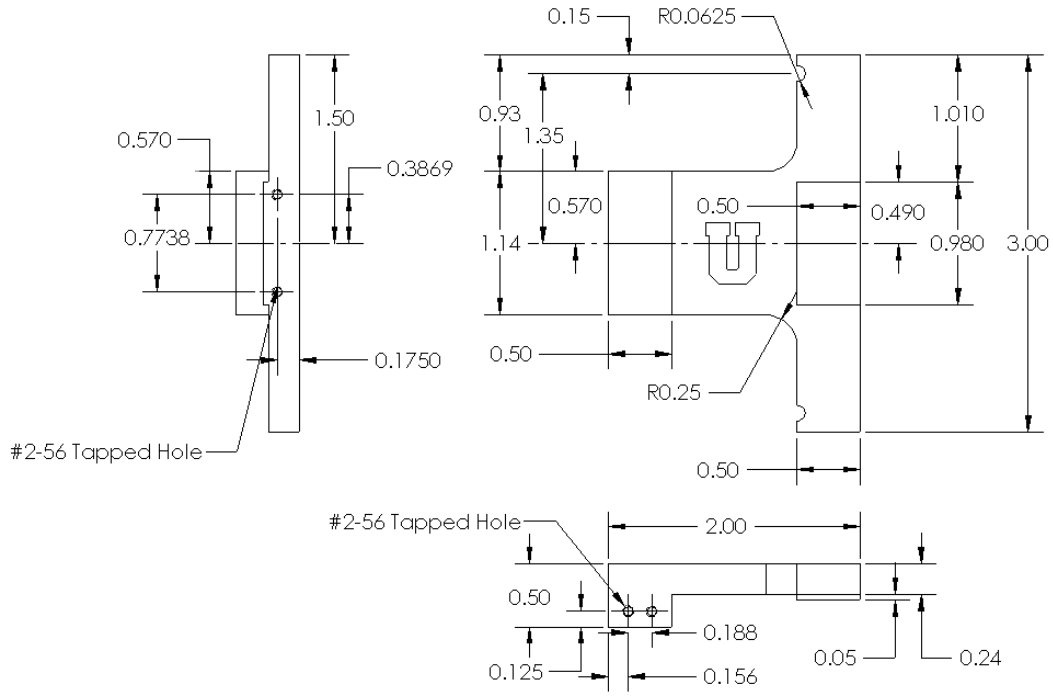


Figure 86: Dimensions of the chassis of the shear strain extensometer. All dimensions are in inches.

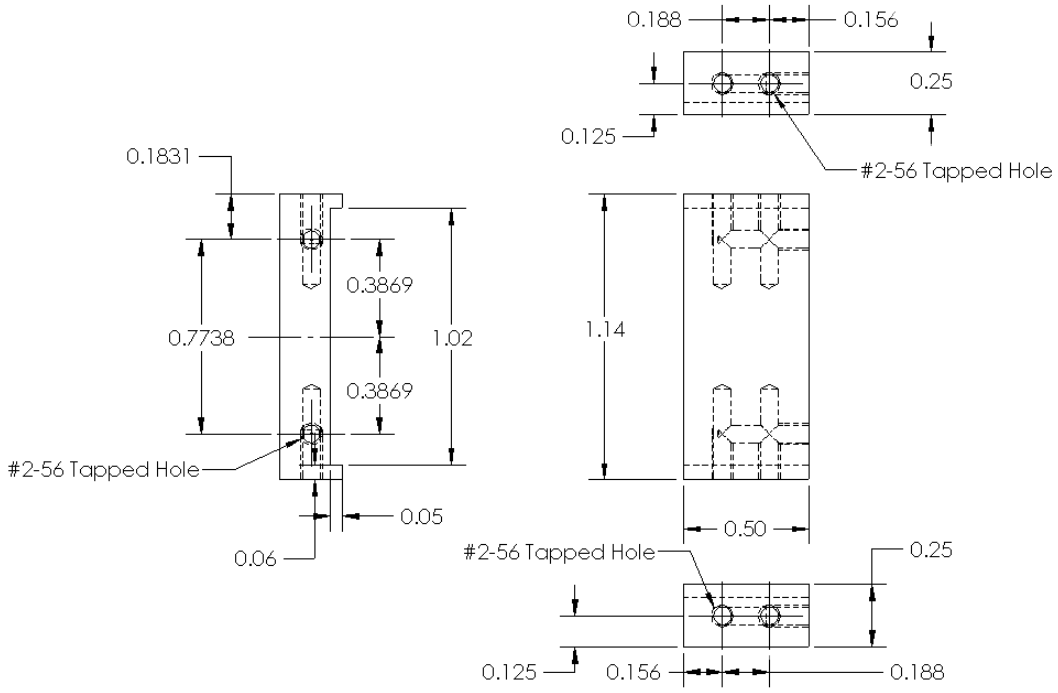


Figure 87: Dimensions of the center attachment block of the shear strain extensometer. All dimensions are in inches.

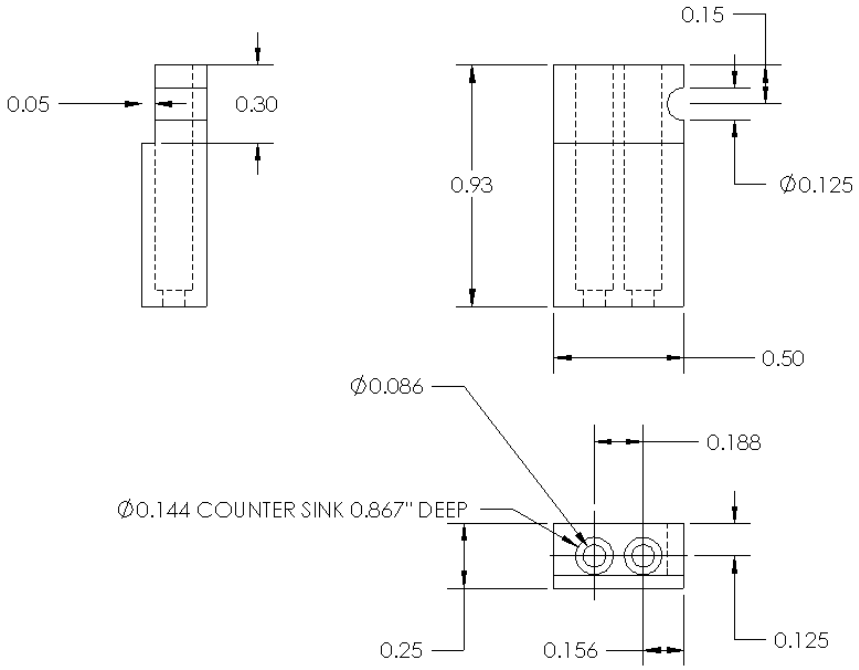


Figure 88: Dimensions of the first of two outer attachment blocks of the shear strain extensometer. All dimensions are in inches.

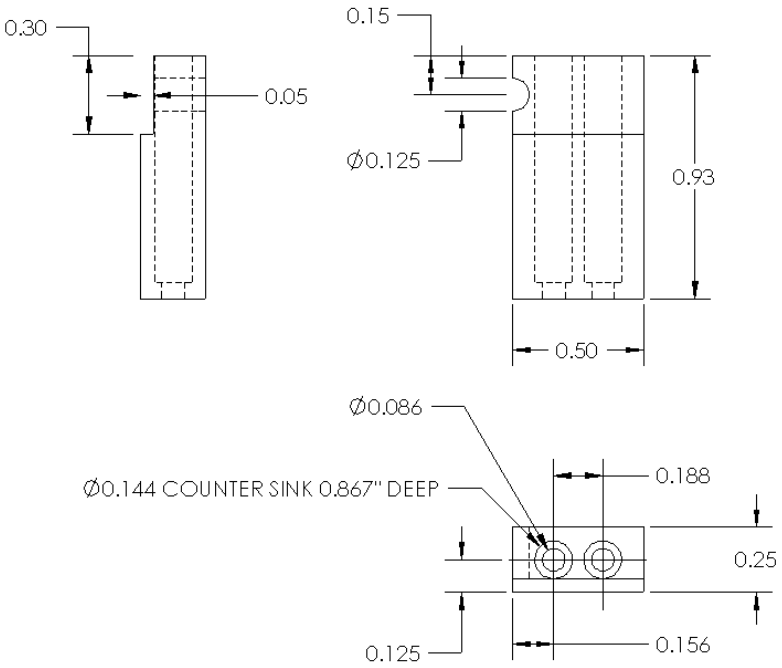


Figure 89: Dimensions of the second of two outer attachment blocks of the shear strain extensometer. All dimensions are in inches.

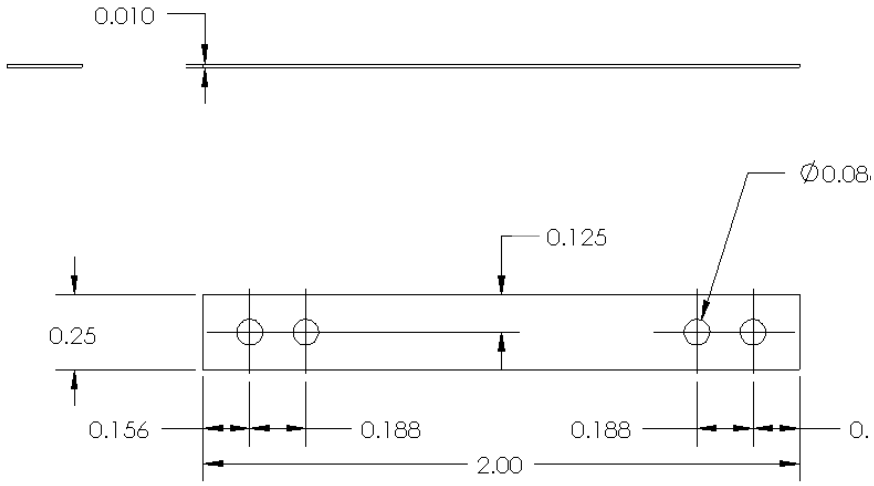


Figure 90: Dimensions of the sensing element in the shear strain extensometer. All dimensions are in inches.

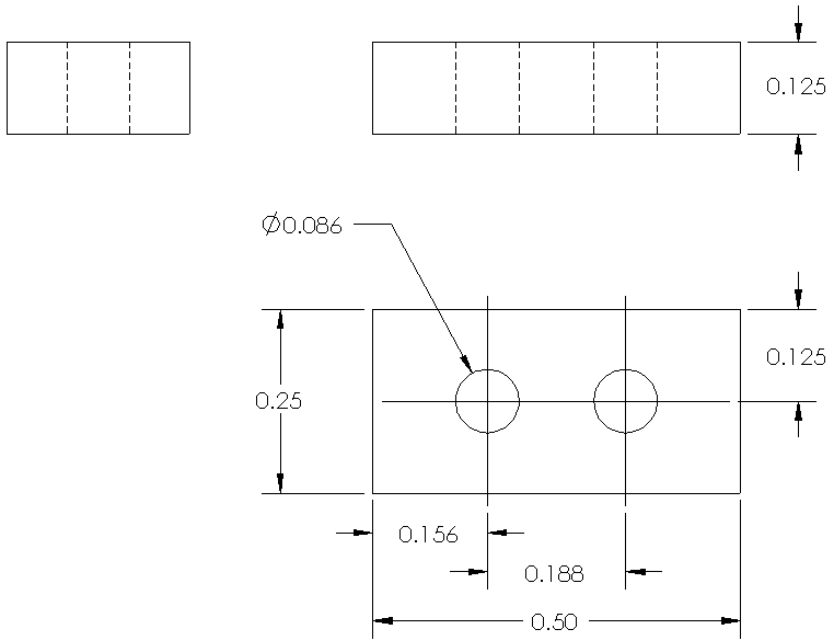


Figure 91: Dimensions of the sensing element mounting plate of the shear strain extensometer. All dimensions are in inches.

## REFERENCES


[1] "Development and Evaluation of the V-Notched Rail Shear Test for Composite Laminates." United States. Federal Aviation Administration Office of Aviation Research Report DOT/FAA/AR-03/63, Washington, DC, 2003.

[2] ASTM D 5379, "Standard Test Method for Shear Properties of Composite Materials by the V-Notched Beam Method," ASTM International, West Conshohocken, PA, 2005

[3] ASTM D 7078, "Standard Test Method for Shear Properties of Composite Materials by the V-Notched Rail Shear Method," ASTM International, West Conshohocken, PA, 2005

[4] Department Report UWME-DR-401-103-1, "Verification and Application of the Iosipescu Shear Test Method," University of Wyoming, Composite Materials Research Group, Department of Mechanical Engineering, Laramie, WY, 1984.

[5] Johnson, J. D., 2010, "Development and Evaluation of the Combined Loading Modification to the V-Notched Rail Shear Test Method for Composite Laminates," M.S. Thesis, University of Utah, Department of Mechanical Engineering, Salt Lake City, UT.

[6] Abdallah, M. G., Gascoigne H. E., 1989, "The Influence of Test Fixture Design on the Iosipescu Shear Test for Fiber Composite Materials", *Test Methods and Design Allowables for Fibrous Composites*, C. C. Chamis eds., ASTM, Philadelphia, PA., Vol. 2, pp. 231-260.

[7] Department Report UWME-DR-301-102-1, "Analysis of the Stress State in an Iosipescu Shear Test Specimen," University of Wyoming, Composite Materials Research Group, Department of Mechanical Engineering , Laramie, WY, 1983.

[8] Nielsen, M. K., "Evaluation of the V-Notched Rail Shear Test for Use With Coarse Textile Composites," M.S. Thesis, University of Utah, Department of Mechanical Engineering, Salt Lake City, UT, 2006.

[9] Campbell, D., Ng, P. K. H, O'Connell, S. K., Thornton, P., 1998, "Iosipescu Shear Strain Extensometer Design," Senior Design Report, Unpublished, University of Utah, Department of Mechanical Engineering, Salt Lake City, UT.

[10] Litz, D. J. et al. "Development of a Shear Strain Extensomter for V-Notched Rail Shear Testing of Composite Laminates," *SAMPE Fall Technical Conference Pro-*

*cedings: Advanced Materials and Processes: Enabling the Future,* Salt Lake City, UT, October 11-14, 2010. Society for the Advancement of Material and Process Engineering, CD-ROM-10 pp.

[11] Adams, D. O., Moriarty, J. M., Gallegos, A. M., and Adams, D. F., "The V-Notched Rail Shear Test," *Journal of Composite Materials*, February 2007, vol 41, 3: pp 281-297.

[12] Totry, E., Molina-Alderaguia, J. M., González, C., LLorca, J., "Effect of Fiber, Matrix and Interface Properties on the In-Plane Shear Deformation of Carbon-Fiber Reinforced Composites," *Composites Science and Technology*, February 2010, Vol. 70, : pp 970-980.

[13] Adams, D. F., Doner, D. R., "Transverse Normal Loading of a Unidirectional Composite," *Journal of Composite Materials,* January 1967, Vol 1, 1: pp 4-17.

[14] Adams, D. F., Doner, D. R., "Longitudinal Shear Loading of a Unidirectional Composite," *Journal of Composite Materials,* April 1967, Vol 1, 2: pp 152-164.

[15] Budynas, R.G. and Nisbett, J.K, 2008, *Shigley's Mechanical Engineering Design,* 8th. ed.,McGraw-Hill Science/Engineering/Math, pp. 396-408.

[16] Bohler-Uddeholm North America, 2003, "AISI A2 Cold Work Tool Steel Data Sheet," Material Data Sheet, http://www.bucorp.com/files/aisi_a2.pdf

[17] The Technical Staff of Measurements Group, Inc., 1988, *Strain Gauge Based Transducers: Their Design and Construction*, 2nd. ed., Measurements Group, Inc., Publishing, Raleigh, NC

[18] "Hexcel 8552 IM7 Unidirectional Prepreg 190 gsm & 35%RC Qualification Material Property Data Sheet." National Institute for Aviation Research, NCAMP Test Report No. CAM-RP-2009-015 Revision A, Wichita State University, Wichita, KS, 2011.

[19] ASTM D 3518, "Standard Test Method for In-Plane Shear Response of Polymer Matrix Composite Materials by Tensile Test of a ±45° Laminate," ASTM International, West Conshohocken, PA, 2007

[20] ANSYS Simulation, Version 11.0, 2007, ANSYS, Inc., Canonsburg, PA.

[21] MATLAB, Version R2010a, © 2011 The MathWorks, Inc. MATLAB and Simulink are registered trademarks of The MathWorks, Inc. See www.mathworks.com/trademarks for a list of additional trademarks. Other product or brand names may be trademarks or registered trademarks of their respective holders.